Aus der

Medizinischen Klinik und Poliklinik I

Klinikum der Ludwig-Maximilians-Universität München

The effect of physiological treadmill training on myocardial hypertrophy in the mouse model

Dissertation

zum Erwerb des Doktorgrades der Medizin

an der Medizinischen Fakultät

der Ludwig-Maximilians-Universität München

vorgelegt von

Agus Simahendra

aus

Singaraja (Bali) - Indonesien

Jahr

2024

Mit Genehmigung der Medizinischen Fakultät der

Ludwig-Maximilians-Universität München

Erstes Gutachten:	Prof. Dr. med. Stefan Brunner
Zweites Gutachten:	Prof. Dr. Konstantinos Dimitriadis
Drittes Gutachten:	Prof. Dr. Martin Halle
weitere Gutachten:	
Promovierter Mitbetreuer:	Prof. Dr. Ulrich Grabmaier
Dekan:	Prof. Dr. med. Thomas Gudermann

Tag der mündlichen Prüfung: 20.09.2024

Table of content

Zusammenfassung (Deutsch):

Hintergrund. Ausdauertraining ist mit einer geringeren Inzidenz und Prävalenz von kardiovaskulär bedingter Morbidität und Mortalität assoziiert. Die Herzhypertrophie ist eine Folge der trainingsinduzierten chronischen Volumen- und Druckbelastung. Dennoch sind das Trainingsprofil, der genaue Zeitpunkt der beobachteten Herzhypertrophie, und weitere wissenschaftliche Daten zur Morphometrie, Histologie, Herzfunktion sowie molekularen Veränderungen noch nicht vollständig erforscht. Zur Charakterisierung der Herzhypertrophie wurde ein intensitätsgesteuertes Tiertrainingsmodell unter Verwendung einer multimodalen Analyse durchgeführt.

Material und Methodik. Männliche Wild Typ C57BL/6-Mäuse im Alter zwischen 5–8 Wochen wurden gleichmäßig entweder in Training- oder Kontroll-Gruppen zu fünf verschiedenen Messpunkten (0-, 2-, 4-, 8 und 12 Wochen) zugeordnet. Nach einer Woche Akklimatisierung liefen die Mäuse 120 Minuten/Tag mit einer Geschwindigkeit von 15 m/min und einer Neigung von 5°. Jede Trainingskohorte wurde mit einem ^{18}F-FDG-PET/CT-Scan untersucht, um kardiale metabolische und volumetrische Parameter zu bewerten. Die morphometrische Analyse wurde jeweils nach den PET-Scans durchgeführt. Die Herz- und Skelettmuskelproben wurden histologisch vorbereitet, um die Querschnittsfläche, die Infiltration von Entzündungszellen und Fibröse zu untersuchen. Die Ribonukleinsäure (RNS) von Trainingsherzen nach 8 Wochen wurde isoliert, verarbeitet und unter Verwendung einer RNS-Sequenzierungstechnik analysiert.

Ergebnisse. Wir konnten zeigen, dass Ausdauertraining bei Trainingsmäusen einen signifikanten Körpergewichtsverlust erzeugt, unabhängig von einer Zunahme des Skelettmuskelgewichts. Nach 8- und 12-wöchigem Training war das Herzgewicht und das Verhältnis von Herzgewicht zu Schienbeinlänge in den Trainingsgruppen signifikant höher. Die *Gastrocnemius*-Muskelgewichte waren nach der 12-Wochen Trainings signifikant höher. Die Querschnittsflächen der Kardiomyozyten und Skelettmyozyten waren histologisch um das 1,8- bzw. 1,3-fache vergrößert und in der 8-wöchigen Trainingsgruppe. Die Kardiomyozytengröße war dennoch nach 8 Wochen Training auf einem Plateau. Darüber hinaus zeigten wir keine begleitende Entzündung oder Fibröse bei Trainingsherz- und Skelettmuskelproben. Die kardialen Herzfunktionsparameter zeigten bei schon vormals gesunden Tieren keine signifikanten Änderungen, welches die physiologische Antwort des Trainings unterstreicht. Die RNS-Expressionsanalyse zeigte, dass die Gene, die an der Verankerung der Proteinsynthese, Zellzyklus, Apoptose, der kontraktilen Proteinexpression und des TGF-β-vermittelten Organwachstums beteiligt sind, zu den am stärksten differentiell exprimierten Genen in den 8-Wochen-Trainingsherzen gehörten.

Fazit. Unsere Studie bestätigte, dass forciertes intensitätskontrolliertes Ausdauertraining die physiologische Herzhypertrophie bei Mäusen förderte. Nach 8 Wochen zeigt sich ein Plateau der Hypertrophie-Antwort. Die Ergebnisse unserer Studie könnten als Grundlage für weitere Studien dienen, um die Auswirkungen von Ausdauertraining auf die Herzfunktion und die Herzhypertrophie mit gentechnisch veränderten Versuchstieren oder in Kombination mit Krankheitsmodellen zu analysieren.

Abstract (English):

Background. Endurance training is generally associated with a lower incidence and prevalence of cardiovascular-related morbidity and mortality. Cardiac hypertrophy is one of the adaptive results of training induced volume and pressure alterations. Nonetheless, the training duration, frequency, intensity, and additional scientific data regarding phenotyping, histology, cardiac function as well as molecular analysis are still under debate. Animal forced intensity-controlled training model using treadmill was conducted to characterize the cardiac hypertrophy utilizing multimodal analysis.

Material and method. Wild type male adult C57BL/6 mice age between 5-8 weeks old were equally assigned to chronic forced endurance training using treadmill divided into five different measurement points (0-, 2-, 4-, 8-, and 12-weeks). After one week of acclimatization, mice ran for 120 minutes/day, with the speed of 15 m/min and 5^{o} inclination. After each training duration, the animals were scanned using ^{18}F-FDG PET/CT to evaluate cardiac metabolic and volumetric parameters. The morphometric analysis was performed after each scan. The heart and skeletal muscles samples were then prepared histologically to measure cross-sectional area and to investigate inflammatory cell infiltration and fibrosis. The RNA of 8-week training whole hearts were isolated, processed and analyzed using high-throughput bulk RNA sequencing technique.

Results. We showed that endurance training promoted significant body weight loss in training mice irrespective of augmentation of skeletal muscle weight. After 8- and 12-weeks of training, heart weight and heart weight/tibia length ratio were significantly higher in the training groups compared to the sedentary groups. Moreover, the *gastrocnemius* muscle weights were recorded significantly higher in the 12-weeks training group. The cardiomyocytes and skeletal myocytes cross-sectional areas histologically were enlarged 1.8- and 1.3-fold respectively, as well as shifted proportionally to the larger surface area after 8-weeks training. The cardiomyocytes size was nevertheless plateaued after 8 weeks of training. Moreover, we showed no accompanying inflammation or fibrosis in training heart and skeletal muscle specimens. There were no significant alterations in cardiac function in these healthy mice, which was in line with the histology assessment. The mRNA expression analysis showed several genes involve in proteins synthesis, cell cycle, apoptosis, contractile protein expression, and TGF-β-mediated organ growth were among the topmost differentially expressed genes in the 8-weeks training hearts.

Conclusion. Our study confirmed that forced intensity-controlled endurance training promoted physiological cardiac hypertrophy in mice. After 8 weeks of training the hypertrophic response reached a plateau. This could serve as a basis for further studies to dissect the effects of endurance training on the heart function and cardiac hypertrophy using genetically modified experimental animals or disease models.

List of figures

List of tables

List of abbreviations

%IA/g	Percentage of injected radioactivity per gram myocardium
^{18}F-FDG	2-deoxy-2-[^{18}F]fluoro-D-glucose
ANP	Atrial natriuretic peptide
ANS	Autonomic nervous system
AKT/PKB	A serine-threonine protein kinase/protein kinase B pathway
ATP	Adenosine triphosphate
AV	Atrioventricular
AV-O_2	Arterio-venous oxygen gradient difference
Bcl-2	B-cell lymphoma 2
BMC	Biomedical Center
BMP	Bone morphogenic protein
BNP	B-type natriuretic peptide
Bp	Base pairs
BSA	Bovine serum albumin
Bq	Becquerel
Ca^{2+}	Calcium ion
CAM	Core facility of animal model
CaMK	Ca^{2+}/calmodulin-dependent protein kinase
CD	Cluster of differentiation
CDK	Cyclin dependent kinase
cGMP	Cyclic guanosine monophosphate
CO	Cardiac output
CI	Cardiac index
ECG	Electrocardiogram
EDV	End-diastolic volume
EF	Ejection fraction
EICR	Exercise induced cardiac remodeling
eIF2B	Eukaryotic initiation factor 2B
ERK	Extracellular signal regulated kinases
ESV	End-systolic volume
FDR	False Discovery Rate
FFA	Free fatty acid
FGF	Fibroblast growth factor

GLUT	Glucose transporter
GPCR	G-protein coupled receptor
GSEA	Gene set enrichment analysis
GSK3β	Glycogen synthase kinase-3 beta
HBSS	Hank's balanced salt solution
HDAC	Histone deacetylase
HE	Hematoxylin-Eosin
HSP70	Heart shock protein 70
IGF-1	Insulin growth factor-1
JAK-2/STAT	Janus kinase-2/signal transducer and activator of transcription
JNK	c-Jun N-Terminal kinase
KEGG	Kyoto encyclopedia of genes and genomes
LAD	Left anterior descending coronary artery.
LMU	Ludwig-Maximilian University Munich
LTCC	L-type calcium channel
LVEDD	Left ventricular end-diastolic volume
LVEF	Left ventricular ejection fraction
LVMV	Left ventricular metabolic volume
LVOT	Left ventricular outflow tract
LVWT	Left ventricular wall thickness
MAPK	Mitogen activated protein kinase
MBq	Mega Becquerel
MEF-2	Myocyte enhancer factor
MET	Metabolic equivalent in training
MRI	Magnetic resonance imaging
MSB	Multispecies barrier
mTOR	Mammalian target of rapamycin
NCX	Sodium-calcium exchanger
NFAT	Nuclear factor of activated T-cells
NO	Nitric oxide
PBS	Phosphate buffer saline
PDK	Phosphoinositide-dependent kinase
PET/CT	Positron emission tomography/computed tomography
PFA	Paraformaldehyde

PI3K	Phosphatidylinositol 3-kinase
PIGF	Placental-induced growth factor
PKC	Protein kinase C
PKG1	Protein kinase G-1
QPS®	Quantitative Perfusion SPECT
QGS®	Quantitative Gated SPECT
RAAS	Renin-Angiotensin-Aldosteron-system
RNA	Ribonucleic acid
RNA-Seq	Ribonucleic acid sequencing
ROS	Reactive oxygen species
rpm	Rotation per minute
RVD1	Basal right ventricle diameter
RVOT	Right ventricular outflow tract
RyR2	Ryanodine receptor type 2
SERCA2a	Sarcoplasmic/reticulum endoplasmic Ca^{2+}-ATPase
SPECT	Single photon emission computed tomography
SA	Sinoatrial
SD	Standard deviation
SV	Stroke volume
TGA	Triglyceric acid
TGF-β	Transforming growth factor beta
VEGF	Vascular endothelial growth factor
VO_2	Oxygen consumption
VO_{2max}	Maximum oxygen consumption
VOI	Volume of interest
WGA	Wheat germ agglutinin

1. Introduction

1.1 Basics of cardiovascular system

1.1.1 Cardiac function and adaptive response to physiological challenges

The heart is the main pump organ to provide the body with oxygen and nutrients. The heart is a hollow structure which contains four distinct chambers. Each of the heart's four functional chambers varies in their form, muscle fibers orientation, and wall-thickness depending on the volume received, workload, and pressure to be generated to propel the blood against forward vascular resistance. The right atrium receives unoxygenated blood from the body and allows it to flow through tricuspid valve to the right ventricle during the diastolic phase. The right ventricle pumps the blood further during the systolic phase to the lower resistance lungs' capillary bed through pulmonary valve for gas exchange. The left side of the heart develops a thicker wall by default due to the higher pressure in the systemic circulation. The freshly oxygenated blood from the lungs is accepted by the left atrium and delivered through mitral valve to the left ventricle during the diastole and finally pumped forward to the aorta through aortic valve during systole and finally to the vascularized organs of the body (1).

The cardiac cycle consists of two important phases: The systole and diastole. The relaxation of cardiac chambers occurs during the diastole, where they are filled with blood. The elasticity of muscle fibers and compliance of the heart wall are the major contributing factors that influence the diastolic relaxation phase. Certain pathological conditions affect the ability of heart muscle to relax eliciting heart failure as terminal consequence. Systole on the other hand is the ejection phase to empty the blood to the vessels of circulation system. Any cardiac diseases affecting the strength of systolic contractions such as coronary artery disease or cardiomyopathy also produce heart failure symptoms (1, 2).

Preload occurs at the end of diastole is described as the volume when the heart relaxed and most filled with blood, therefore the values is equivalent to end-diastolic volume (EDV). End systolic volume (ESV) in contrast is defined as the remaining ventricular volume after systole. The ventricles need to build up pressure against closed semilunar valves to overcome the pressure in the aorta and eject blood to the systemic circulation. This pressure is determined as afterload. Stroke volume (SV) is the volume of blood that has been ejected from the ventricle during systole and can be easily measured by subtracting ESV from EDV. The ejection fraction of left ventricle (LVEF) is defined as the volumetric fraction of total blood ejected from the left ventricle during each systole. The value indicates the effectiveness of left ventricle to pump blood into systemic circulation and is measured by dividing the SV to EDV as a percentage. The cardiac output is then interpreted as a multiplication result of heart rate/minute and SV. The cardiac index (CI) in the other hand involves a more complex calculation by adding the body surface area (Ideal body weight in relation to height) to the formula for a better and more objective evaluation of heart function based on individual's size (2, 3).

The heart as a pump and its blood vessels tributaries works in coordination with other organ systems and are tightly regulated by numerous interconnected physiological neuroendocrine pathways such as: The Renin-Angiotensin-Aldosterone system (RAAS), autonomic nervous system (ANS) mainly through α-, β-adrenergic and muscarinic receptors, and neurohumoral activation pathways involving Atrial and Brain Natriuretic Peptides (4). In the certain situation, the body

metabolic demands for oxygen and nutrients need to be fulfilled by the working heart by modifying this interplaying physiological feedback mechanism. This adaptive mechanism is triggered and harmoniously regulated due to shift of physiological, mechanical, metabolic demands during certain situations such as exercise, emotional stress, and changing of environmental conditions. To maintain the body homeostasis, cardiac cells are prepared with the ability to grow (hypertrophy), sprout newly form vasculature (angiogenesis) and switch effectively their energy substrates (metabolic plasticity) (5). The physiological cardiomyocytes growth alongside with their supporting stromal environment in response to beneficial stimuli takes place generally in the growing children to meet the nutritional demands of maturing organs and expanding muscle mass. This reflects the plasticity of the cardiac cells to adapt in the constantly changing demands. A classic example of cardiac morphological and physiological adaptation to external stress is the exercising heart. The regular exercise has been proclaimed as a major protective measure to avoid cardiovascular ischemia, injury, and mortality. The training hearts undergo adaptive modifications in their mass, volume, and metabolism against the mechanical or afterload challenges of working skeletal musculature which lead to physiological alterations on the cardiac cellular biochemistry profile as well as morphology without dramatically altering their functionality. Similar physiological hypertrophic adjustments also occurs in pregnancy, but as opposite to exercise training, pregnant hearts adapt mainly to the increasing preload challenge as a result of expanding blood volume to provide nutrients to the developing fetus (6, 7).

Unfortunately, these physiological changes can also be chronically overwhelmed and lead to maladaptive response in certain pathological conditions such as decompensated heart failure or ischemic heart disease, where the over-activation of neuro-humoral as well as inflammatory and remodeling responses take place (4, 8, 9). Furthermore, pathologically enlarged cardiomyocytes associated with interstitial fibrosis and myocytes disarray could also be occurred as a result of genetic mutations, which are inherited according to Mendelian's law with certain degrees of penetrance, such as storage disease, mitochondrial disease, and triple repeat syndromes (10). Familial hypertrophic cardiomyopathy is one of the classical examples of this derangement, which could affect both younger and ageing individuals. Although both physiological cardiac hypertrophy and pathological familial hypertrophic cardiomyopathy are characterized with enlarged cardiomyocytes, this disease is classically characterized by concentric cardiac hypertrophy with asymmetrical left ventricular hypertrophy predominantly of the interventricular septum. The serious manifestations of this disease encompass a wide variety of clinical manifestations including heart failure, malignant arrhythmia, and sudden cardiac death. Thus, the key features between physiological and pathological cardiac hypertrophy should be disputed carefully and separated accordingly (11).

1.1.2 The histology of cardiomyocytes

The organization of heart's cellular architecture can be comprehensively visualized by two-dimensionally microscopical imaging (12). The heart histologically comprises mainly of the cardiomyocytes, fibroblasts, extracellular matrix components, endothelial cells, vascular smooth muscles, and clusters of cells that exert specific functions such as inflammatory cells, adipocytes, myofibroblasts, and electrically conductive cells (13). The histological and cytological examination of heart samples are performed since many years ago to visualize several cardiovascular physiology and pathologies including heart hypertrophy (14). This can be achieved by cardiac biopsy and tissue processing followed by both regular and special staining techniques.

Hematoxylin-Eosin (HE) staining serves as basic stain of most tissues for visualization under the light microscope. The heart comprises of three layers namely endocardium, myocardium, and epicardium. The outer epicardium contains loose connective tissues and merges with visceral pericardium to provide protection and ensure smooth cardiac movability during contraction. Most of the cardiac tissue is formed by thick myocardium. Most of the cardiomyocytes are rich of glycogen granules and organized transversally, longitudinally, and tangentially in this layer to provide tensile strength and coordinate contraction to eject blood against peripheral vascular resistance. Unlike skeletal muscles, the cardiomyocytes are branched, intercalated with disks, rich in mitochondria, centrally mononucleated, equipped with sarcoplasmic reticulum and t-tubules which are essential in excitation-contraction coupling process. The striated appearance is caused by arrangement of contractile proteins troponin, myosin, and other supportive filaments as heart's smallest contractile units. The single cell layer endocardium lines the innermost part of heart chamber and can be occasionally equipped with a thin layer of smooth muscle cells. Between endocardium and myocardium lies subendocardial space which contains fine collagen fibers, loose elastic connective tissues, nerve endings, and capillaries (15).

Certain advanced staining techniques are performed to visualize several pathologies which are not easily be revealed by regular light microscopy. The immunofluorescence and immunohistochemistry techniques take advantage of using antibodies coupled with fluorescent dyes and other chemical compounds respectively to detect the presence of specific antigens. These antigen-antibody complexes aid as a powerful tool to diagnose acute transplantation rejection reaction, infiltrative tumors, cardiomyopathies, and other inflammatory diseases. **Figure 1** depicts normal cardiomyocytes stained using immunofluorescence technique.

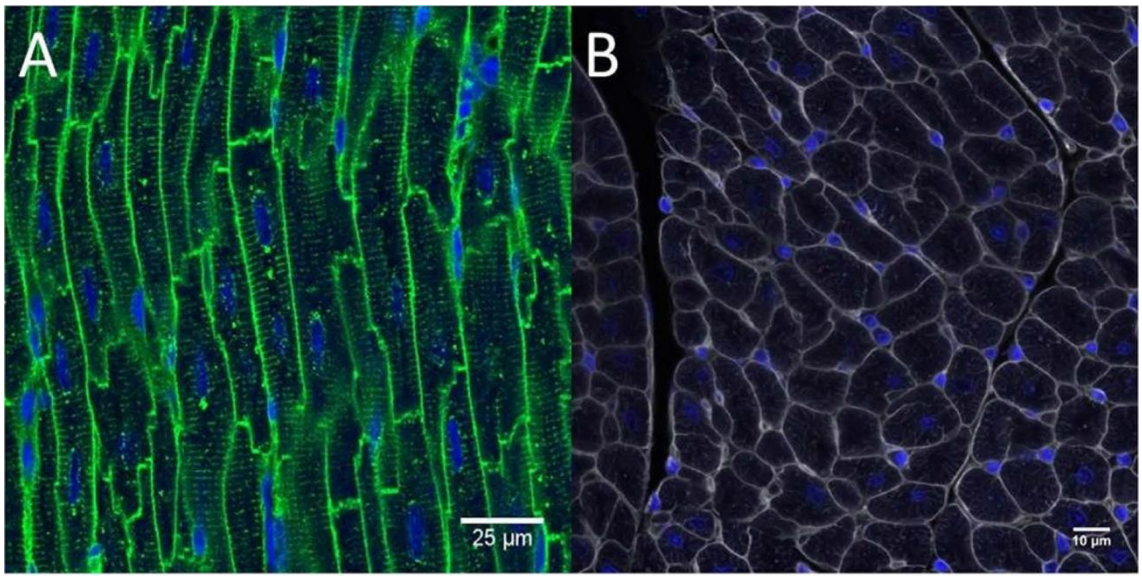

Figure 1. (A) Sagittal/coronal section of cardiomyocytes. DAPI stains nuclei shown in blue, WGA conjugated with Alexa Fluor® 488 stains cell membrane appears in green. (B) Cross-sectional cut of cardiomyocytes, DAPI appears in blue, WGA-AF488 here stained as grey (16).

Moreover, special staining procedures such as Congo red, Prussian blue, Masson's trichrome or Picrosirius red are well-established to detect amyloidosis, iron deposition, and fibrosis in cardiac tissues respectively (17, 18). In pre-clinical research, immunofluorescence technique using wheat germ agglutinin (WGA) to stain cell membrane is commonly used as a basic approach to measure fibrosis after myocardial infarction and to quantify cardiac cross-sectional area in hypertrophic

hearts model following certain micro-RNA administration as an inhibitor signal of cardiac hypertrophy (19, 20). Nevertheless, the application of this technique to calculate cardiac hypertrophy after intensity-controlled endurance training in animal model is not yet well-established and systematically validated.

1.2 Physiological and biochemical changes during endurance training

1.2.1 Basic sport physiology

Muscle fibers change their structural and biochemical properties in response to the increased force applied during sport. Physical exercise can be distinguished by the degree of dynamic (endurance, isovolumetric) or static (resistance, isotonic) components. During static muscle action, the muscle fibers produce force by crosslinking the sarcomeric proteins without altering their length as well as moving the corresponding joints. A typical example of this type of muscle action is weight-lifting performance. On the other hand, dynamic exercise generates force by creating sliding movements between the sarcomeric proteins resulting in shortening of muscle fiber and joint movement. Endurance trainings such as long distance running, swimming, and cycling are classical examples of dynamic exercise (21).

As previously described in the literature, the physiologic ability of cardiac muscle to eject blood is changing depends on metabolic requirement. Demography profile, genetic components, cardiopulmonary functional reserve, and the existence of cardiac or pulmonary diseases govern a significant role in influencing individual's response against stress including exertion during endurance training. Furthermore, endurance training requires an integrated enhancement of respiratory, cardiovascular and integument systems function as an acute response to meet the sudden increase on energy and oxygen demand (22).

The main response of cardiovascular system during acute aerobic exercise is the augmentation of CO as a principal element of maximal oxygen consumption (VO_2). The CO is varied from one individual to another depending on the degree of activity and could range from 5 L/min in untrained healthy resting human to 40 L/min in athletes who perform extensive chronic regular physical activity (23). During aerobic performance, the increase of EDV (Preload), myocardial contractility, and heart rate due to activation of sympathetic nervous system are responsible for incrementing the SV and CO respectively to divert more than 80% circulating blood volume to exercising muscles (22).

The peak VO_2 on the other hand reflects the ability to uptake, transport, utilize and assimilate oxygen at the maximum level. These serves as surrogate parameter to determine aerobic capacity, skeletal muscle metabolic function, and cardiopulmonary fitness. VO_2 can be calculated using Fick equation by multiplying CO and the difference between arterial and venous oxygen concentration ($AV\text{-}O_2$). During aerobic exertion, the skeletal muscle typically extracts more oxygen in the periphery, therefore the $AV\text{-}O_2$ discrepancies broaden resulting in increasing VO_2 in addition to CO enhancement. The absolute peak VO_2 values are expressed either in liters per minute (L/min) or milliliters per minute (mL/min), which range physiologically from 3.6-5.8 L/min. It is very essential to point out that the larger muscle and lean body mass correspond linearly with higher peak VO_2 values. Moreover, age and sex should be also put into the equation, as along with the aging process, the VO_2 max decreases steadily 5-20% per decade and women normally have higher

fat composition, lower lean body mass, and lower CO compared to their male counterparts (22, 24).

On the steady-state condition, the resting metabolic rate of around 3.5 mL/min/kg is maintained to supply energy to brain, kidneys and liver which is equivalent to 1 MET ‘’Metabolic Equivalent’’. During aerobic exercise however, this number could reach 4-6 times higher than the value at rest or even greater in elite athletes due to activation of neurohumoral pathways and CO increase to meet the exercise demand on working skeletal muscles. There are certain parameters that could be monitored during exercise such as perceived exertion, ventilatory threshold, peak respiratory exchange ratio, minute volume-carbon dioxide output, blood pressure response, heart rate response, and recovery time (24).

1.2.2 Excitation-contraction coupling mechanism.

Calcium ions (Ca^{2+}) play a significant role in initiating cardiac contraction. The specials cells in right atrial SA node are capable in generating their own action potential through opening of atypical sodium channel. This automatic depolarization wave is propagated and able to open L-type Ca^{2+} channels (LTCC) which are located along the t-tubules in the neighboring cardiomyocytes. This initial calcium influx triggers further accumulation of Ca^{2+} intracellularly known as Ca^{2+} induced Ca^{2+} release which can be increased efficiently under the influence of adrenergic nervous system stimulation during sport (25).

The increase availability of Ca^{2+} during excitation-contraction coupling contributes to strengthen cardiomyocytes contractility during physical exertion. This has been a consequence of more efficient type 2 ryanodine receptors (RyR2) activation which allow Ca^{2+} flux from sarcoplasmic reticulum as calcium ions storage into the cytosol, where they exert their action by enhancing the binding with troponin C within the sarcomere. This troponin C-Ca^{2+} complex allows conformational change of tropomyosin filaments which opens the troponin attachment sites to myosin’s head leading to contraction. After each systole, the free cytosolic Ca^{2+} ions are required to be transported back into the sarcoplasmic reticulum or extracellular space through SERCA2a (Sarco/endoplasmic reticulum Ca^{2+} -ATPase) or Na^{2+}/Ca^{2+} exchanger (NCX) respectively to allow the heart to relax during diastole (26).

1.2.3 Cardiac energy utilization during exercise

During low intensity endurance training, steady supply of oxygen can be secured to generate energy through cellular respiratory chain reaction in the mitochondria. This aerobic metabolism yields much more adenosine triphosphates (ATP) per mmol of glucose through Krebs cycle and oxidative phosphorylation compared to anaerobic glycolysis. Meanwhile, during high-intensity exercise, the ability of the heart to provide oxygen to the active organs is limited. The oxidative phosphorylation cannot be efficiently used to generate energy due to lack of oxygen molecules. The anaerobic glycolytic pathway is activated by rapidly breaking down the stored glycogen in the muscle into glucose once the ATP storage is exhausted. This catabolic process promotes not only a lower yield of energy production but also accumulation of lactic acid, which lead to skeletal muscle acidification and fatigue. Albeit, this might be beneficial to the exercising cardiomyocytes which are able to utilize this metabolic byproduct as a quick energy substrate (27).

In every contraction cycle in sarcomeric troponin-myosin complex, ATPs are required as primary energy substrate. A physiologically exercising heart generate its own ATPs primarily (60-90%) through β-oxidation of free fatty acids in cardiomyocytes’ mitochondria and the rest minimum of

10-40% is provided by catabolism of glucose, amino acids, and lactate. However, this balance in heart metabolism could be shifted towards glucose usage as the consequence of maladaptive response during pathological process or rigorous physical exertion. This metabolic substrate switch is believed to be influential in sending certain atypical signaling pathways or messengers leading to pathological enlargement of cardiac chamber. Furthermore, the healthy trained heart is also capable more efficiently to store the unused FFA by esterification process into TAGs (Triacylglycerol) in the lipid droplets of the pericardial fat tissue as endogenous energy depot that can be readily available to replenish ATPs supply to avoid excessive glucose utilization (28).

1.2.4 Endurance training in maintaining health state.

Cardiovascular disease and degenerative diseases are the major cause of morbidity and mortality in industry nations as well as developing countries. Exercise training has been established as one of the most important cornerstones to increase cardiorespiratory fitness and to prevent as well as to treat major cardiovascular and metabolic diseases such as diabetes mellitus. Physical exercise generates several physiological, biochemical, and molecular alterations, which work positively in maintaining body homeostasis and improving mental health. Chronically, a properly performed training activities may lead to positive adaptive adjustments in both organ morphology and functionality, especially the cardiovascular and skeletal muscle systems, which may contribute to the reduction of major cardiovascular adverse events (29).

Aerobic endurance exercise typically concentrates on enormous augmentation of CO and large recruitment of skeletal muscles type I, which are more resistant to fatigue due to higher content of myoglobin, mitochondria for oxidative phosphorylation, and capillary density (30). Chronic repetitive aerobic endurance training produces a pleiotropic positive physiological adaptation in heart and vasculature such as reducing arterial stiffness, increasing the endothelial *de-novo* production of natural vasodilator such as nitric oxide (NO), improving the lipid profile in blood, and offering protection against insulin resistance, systemic oxidative stress, and inflammation. These lead to better control of several important cardiovascular pathologies such as hypertension, heart failure, and ischemic heart diseases, as well as autoimmune disorders and cancer (31).

1.3 Cardiac hypertrophy as a response against pressure and volume overload

1.3.1 Physiological cardiac hypertrophy in athlete’s heart

Aerobic exercise training when performed regularly and chronically leads to numerous hemodynamic adaptive changes. These can be translated roughly to an increase of cardiac performance and described as exercise induced cardiac remodeling (EICR) (32). The four heart chambers including their cavity enlarge homogenously, and the ventricular wall thickens eccentrically to accommodate the higher metabolic requirements, preload, and afterload attributable to increasing skeletal muscle mass and circulating volume in elite athletes. The enlargement of the cardiac dimension can be easily detected by means of echocardiography or more subjectively by using cardiac MRI or PET imaging technique showing increase of left ventricular end diastolic diameter (LVEDD), left ventricular wall thickness (LVWT), left atrial diameter (LAD), right ventricular internal basal diameter (RVD1), right ventricular outflow tract (RVOT), left ventricular outflow tract (LVOT), and aortic root diameter (33).

The size augmentation of individual cardiomyocytes (hypertrophy), increase the width of the cell (surface area), muscle fiber elongation and capillary density can further be observed histologically in the animal's heart which performed swimming as chronic endurance training of 90 min/day, 5 days a week for 60 days (34). Although hypertrophied, the cardiac mass in athletes is expected to be more receptive for the incoming blood volume (preload) by virtue of improvement in relaxation ability and diastolic cardiac filling. The improvement in diastolic function can be subjectively measured using Doppler echocardiography showing a longer isovolumetric-relaxation times and increase in trans-mitral inflow velocity indicating more rapid diastolic ventricular filling (35, 36). The athlete's hearts are also capable to amplify stroke volume despite of training induced tachycardic response without significantly altering the left ventricular ejection fraction (LVEF). The long-term effect of uninterrupted aerobic exercise observed in rigorously trained young Olympic athletes showed no significant changes in cardiac morphology, detrimental effects on the LV function or incidence of major cardiovascular adverse events (37). Several cellular processes contribute to the remodeling in cardiac hypertrophy (**figure 2**). Furthermore, several cardiac parameter modifications in EICR are also described in previous studies such as augmentation in oxidative phosphorylation capacity and skeletal muscle arteriole-capillary conductivity which led to decrease in peripheral vascular resistance and higher peak of oxygen consumption (VO_2 max) (38).

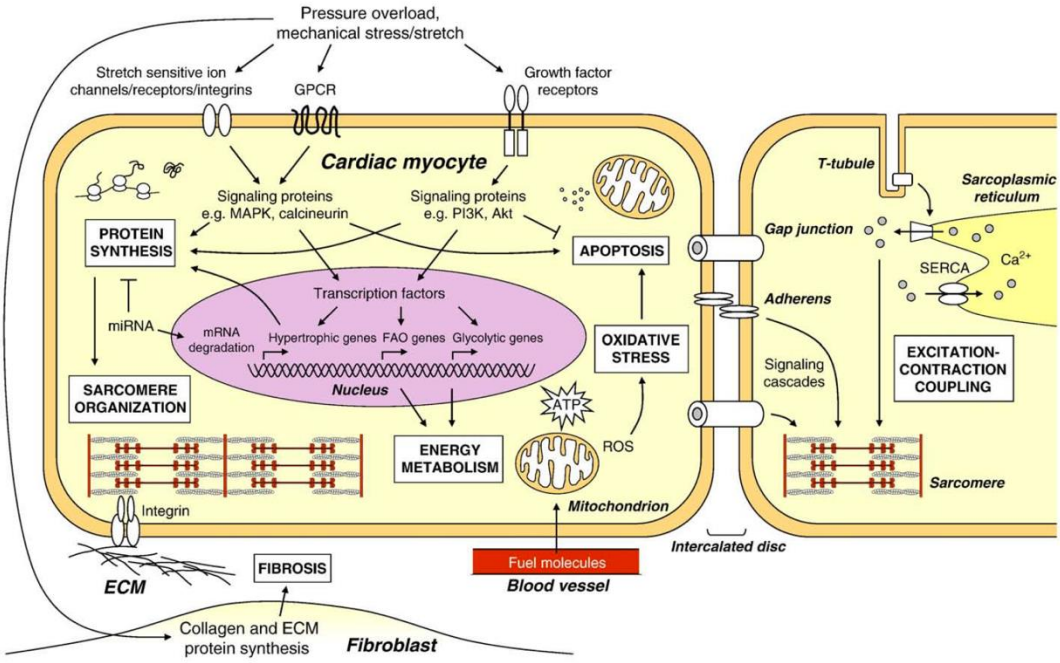

Figure 2. The physiological cellular and metabolic processes involve in cardiac hypertrophy remodeling during endurance training (39).

Exercise induced remodeling affects not only the heart anatomy and physiology, but also alters the electrical conduction system due to increase of vagal tone. Several recorded ECG changes have been observed in both elite athletes and marathon rats associated with EICR, such as sinus bradycardia, sinus arrhythmia, lower degree AV block, bundle branches block, and left and right ventricular strain pattern indicating chamber hypertrophy due to electrical substrates alteration which may lead to the arrhythmia induction and occurrence of sudden cardiac death (40, 41). Furthermore, based on current emerging animal data also showed that rigorously training individ-

uals are having a higher susceptibility in developing atrial fibrillation compared to a normal sedentary population assignable to structural alterations of training heart, fibrosis, and autonomic nervous system imbalance (42).

Though endurance training is associated with a lower incidence of cardiovascular-related diseases, the intensity and frequency of aerobic exercise training to create these desirable positive effects remain scientifically unknown. Recently there has been also scientific reports suggesting that vigorous endurance exercise training in rodents might promote cardiac collagen deposition, fibrosis marker elevation, deleterious electrical remodeling, and create substrate for cumbersome cardiac arrhythmias particularly atrial fibrillation and ventricular tachycardia (41). Moreover, both adaptive structural and functional remodeling are expected to occur in training athletes after several weeks of moderately intense regular endurance training, nevertheless, the exact time point, training intensity, and additional scientific data on myocardial performance and possible deleterious effects of intense exercise are remained to be elucidated (35).

Due to the limitation of study approaches to explore these observed changes in human, several animal models are available to give more understanding on the biological process involved in physiological cardiac hypertrophy. Several experimental strategies have been developed to mimic the endurance training in human such as forced running exercise using treadmill machine for small animals. Voluntary wheel running and swimming exercise with certain training protocols as well as exercise conditions were also widely used in rodents as alternative, which provided reliable and promising results. Moreover, several studies indicated that experimental exercise training on cardiovascular functions in larger animals such as dogs, rabbits, and swine were more favorable due to the resemblance of anatomy and structure to human heart and vasculatures (43-45). Nevertheless, ethical clearance, limitation in genetic manipulation, and higher cost are the major obstacles to perform such studies. Furthermore, the results interpretation should be translated carefully due to fundamental differences and limitations among these experimental techniques (46).

1.3.2 Cardiac hypertrophy as maladaptive response

Cardiac hypertrophy is one of the adaptive results of chronic volume and pressure overload. Meanwhile long-term appropriately regimen of endurance training leads to eccentric cardiac hypertrophy and improving cardiovascular fitness without affecting natural left ventricular pump function. Several pathological conditions such as chronic arterial hypertension and valvular heart diseases on the contrary produce maladaptive cardiac enlargement, increase cardiac stiffness, and augmentation of left ventricular wall thickness without compensatory increase in LVEDD known as concentric hypertrophy. Moreover, chronic concentric cardiac hypertrophy can lead to eccentric hypertrophy with hallmarks of chamber dilatation, mitochondrial dysfunction, and cell deaths if the source of pathological stimuli are not managed appropriately (47) (**figure 3**). Pathological cardiac hypertrophy associated with robust inflammatory process, programmed cell death, necrosis, inefficient calcium utilization, rarefaction of vascular density, and interstitial fibrotic changes leading to hypoxia, cardiomyocytes disarray, heart geometrical disorganization, systolic failure, and disturbances in relaxation phase (5, 47).

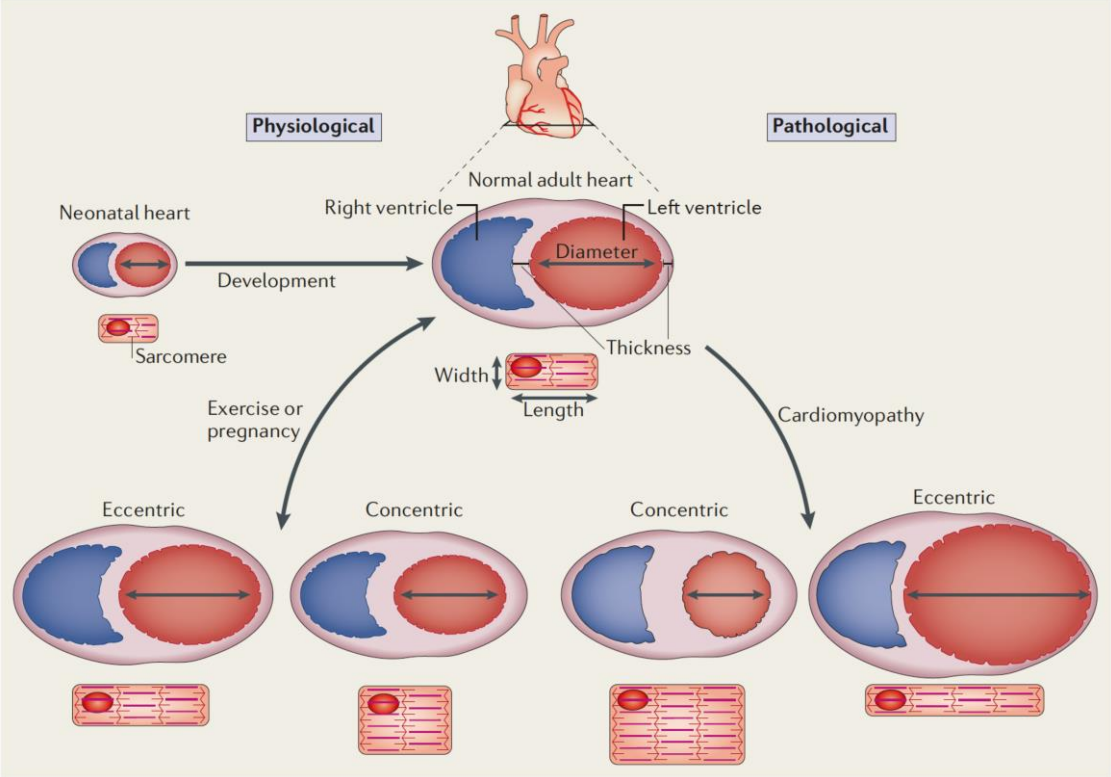

Figure 3. Distinct triggering factors generating different type cardiac hypertrophy. Both physiological and pathological stimuli produce eccentric and concentric cardiac hypertrophy. The main difference of the phenotype between health and disease is on the degree of the occurring anatomical and physiological changes. Physiological stimuli such as endurance training or pregnancy produce adaptive concentric and eccentric cardiac hypertrophy by maintaining heart function while fulfilling the body's increasing demand of nutrients and oxygen supply. Pathological situations in the other hand elicits maladaptive response and more prominent eccentric and concentric cardiac hypertrophy resulting in pump function failure and fibrotic tissue remodeling (48).

Concentric hypertrophy exhibits a pronounce increase of wall and interventricular septum thickness and reduced left ventricular cavity as the consequence. A raise in cardiomyocyte thickness and width without compensatory elongation of muscle fiber can be histologically observed in cardiomyocytes specimens with pathological hypertrophy caused by increased afterload *in vitro (49)*. According to the Laplace Law, the ventricular wall stress increases proportionally with both intraventricular pressure and cavity radius, however inversely related to the thickness of ventricle wall. In pathological concentric cardiac hypertrophy, the wall stress increases significantly due to buildup of intracardiac pressure and cavity radius enlargement leading to an exponential rise in oxygen demand and transformation of heart geometry (50).

Robust distinctive signaling cascades drive the differentiation between physiological and pathological cardiac hypertrophy. Moreover, modulatory alterations of various molecular processes such as cellular metabolism switch to glucose, energy substrate utilization, excessive ROS (Reactive oxygen species) production, inflammation, gene expressions, protein translation and sarcomere organization arise due to stress-induced profuse neurohumoral and sympathetic nervous activation leading to propagation of negative cardiac remodeling (51). In the long run, concentric cardiac hypertrophy elicits significant LVEF reduction, diastolic dysfunction, and correlated with development of end-stage decompensated heart failure symptoms associated with increase cardiovascular morbidity and mortality. The distinctive differentiation between physiological and

pathological cardiac hypertrophy especially their biochemical, molecular, and pathophysiological aspects, however, is currently still under meticulous debate, thus more research are deemed to be necessary for a better understanding of the underlying process (39).

1.4 Molecular signaling pathways involved in cardiac hypertrophy

1.4.1 The classical hypertrophic signaling circuits

Distinct pathways and target effectors are dynamically regulated in both physiological cardiac conditioning during exertion and heart diseases. Although initial functional, gross anatomy, and histology of hypertrophic heart are often indistinguishable, the gene expression and signaling pathways activation of both situations diverge in the opposite direction. The main initial stimuli to promote cardiac hypertrophy mediated by neurohumoral activation and biomechanical stretch-sensitive receptors due to volume and pressure overload. These stimulating ligands comprise of cytokines, chemokines, peptide growth factors, and hormones that attach normally to membrane-bound G-protein-coupled receptors (GPCR) which activate subsequently intracellular tyrosine kinase and serine/threonine kinase domains. This initial activation promotes a cascade of second messenger production and signal transduction pathways which is propagating downstream into the nucleus, modifying gene expression, increasing protein translation, and diminishing protein degradation (**figure 4**) (47, 52).

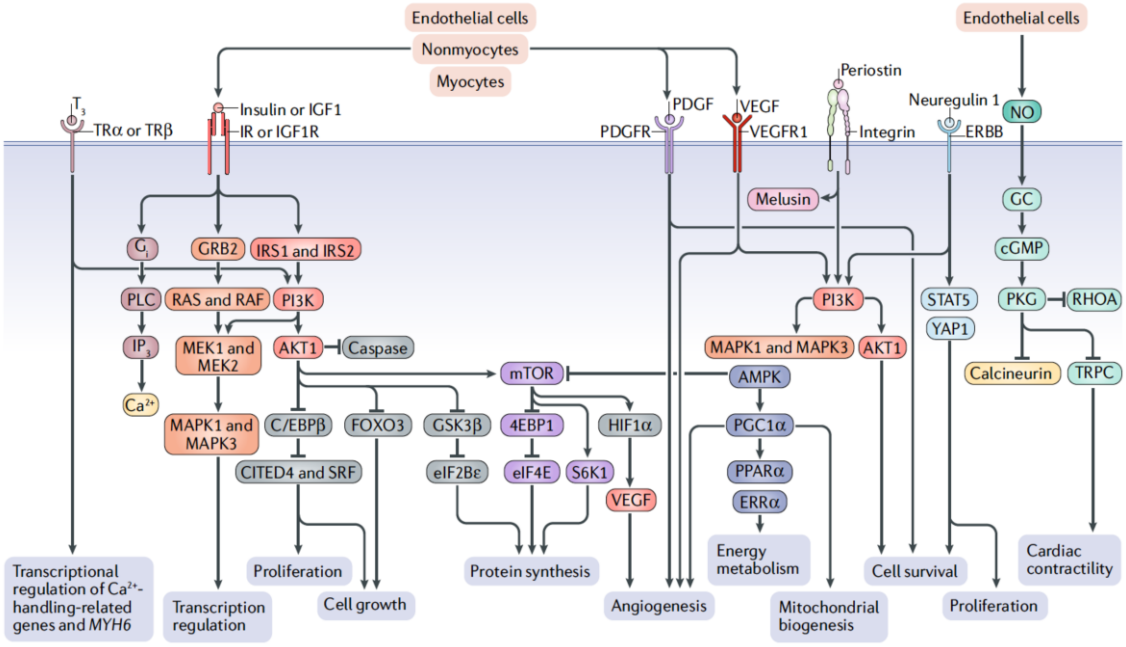

Figure 4. The important molecular pathways involved in physiological cardiac hypertrophy (47).

Several basic sciences research using animal models have shown complex interactions of intracellular proteins and crucial classical signaling pathways that propel eccentric cardiac hypertrophic response during training such as MAPK (Mitogen-activated protein kinase), calcineurin-NFAT (Nuclear Factor of activated T Cells), IGF-I-PI3K-AKT/PKB-mTOR (Insulin-like growth fac-

tor I, phosphatidylinositol 3-kinase, protein kinase B, mammalian target of rapamycin), transcription factors involved in cell cycle (cyclin-dependent kinase-7 and -9, CDKs), and epigenetic regulations (Histone deacetylases/HDAC class II in chromatin remodeling) (53). A moderate-high intensity aerobic exercise using treadmill in rodents for 60 min/day, 5 days/week for 8-12 weeks led to 17-32% augmentation of cardiomyocytes size by activating concurrently several of these pathways, promoted neo-angiogenesis, improved cardiac performance, and increased cardiac expression of both Bcl-2 and heat shock protein 70 (HSP70) as markers of apoptosis inhibition (54).

Several classical ligands are known to propagate hypertrophy signals in response to both volume and pressure overload such as catecholamines through their α-receptors, angiotensin II, IGF-I, and endothelin-I. The circuits involved as downstream processes are also already well characterized in the experimental animal models. The IGF-I signaling is pivotal for physiological cardiac hypertrophy and proper heart growth during embryological development. The binding of IGF-I to their $G_{\alpha q/\alpha 11}$ proteins-coupled transmembrane receptors induce phospholipase C production that catalyzes the generation of activated protein kinase C (PKC). The activated PKC promotes subsequently the PI3K (Phosphatidylinositol 3-Kinase) and phosphatidylinositol-1,4,5-triphosphate accumulation which liberates Ca^{2+} from smooth endoplasmic reticulum into the cytosol (55, 56). The raising cytosolic calcium concentration and alteration of calcium handling mediate further the hypertrophic signal cascades through serine/threonine protein phosphatase calcineurin, nuclear pro-hypertrophic transcription factor NFAT activation, and inactivation of CaMK (Calmodulin-dependent kinase)-HDAC (57). The HDACs promote chromatin condensation, which subsequently prevents DNA transcription, thus promote protein synthesis via transcription factor MEF-2 (Myocyte enhancer factor-2) when HDACs inhibition ensue (58).

Moreover, the activation of PI3K recruits synergistically the AKT/PKB (Protein kinase B)/PDK1 (Phosphoinositide-dependent kinase-1) sarcolemma complex which is also crucial in regulating physiological cardiac growth. The acute expression of myocardial AKT/PKB in experimental animals results in coordinated cardiac hypertrophy by inhibiting GSK3β (Glycogen synthase kinase-3β) and inducing angiogenesis, meanwhile chronic activation for at least 6 weeks leads to decompensated cardiac chamber dilatation (52, 54). The downstream end-target of AKT/PKB are convinced to be in the nucleus and contributes directly to gene expression involved in hypertrophic process such as GATA-4, β-catenin, c-Myc, NFAT, and protein translation elongation factor *eIF2B* which involves in protein synthesis enhancement by activating mTOR (59). Besides, mTOR regulates synthesis of protein by increasing biosynthesis pathway by ribosomes and serves as initiator of protein translation. In fact, rapamycin, a classical inhibitor of mTOR attenuated both physiological and pathological cardiac weight augmentation up to 68% in acute pressure overload rodents model inflicted by ascending aortic banding (60).

Cardiomyocytes MAPK-MEK-ERK pathway is activated by the same G protein subclass and other stimuli such as FGF (Fibroblast growth factor) and IGF-I via tyrosine kinase receptors, TGF-β (Transforming growth factor-β)/BMP/SMAD through serine/threonine kinase receptors, and cardiothrophin-1 on the gp130 receptor. The MAPK-MEK circuit does the crosstalk with calcineurin-NFAT pathways and subsequently phosphorylates and activates p38, JNK (c-Jun N-terminal kinases), and ERK1/2 (Extracellular signal regulated kinase), which brings the necessary second messengers into the nucleus to modify certain transcription factors and reprogram gene expression involving in compensated cardiac hypertrophy (61). Transgenic mice which constitutively activate cardiomyocytes MEK and ERK1/2 develop signs of cardiac fibrosis at the age up to 6 months and 25-30% increase of heart-body weight ratio indicating cardiac hypertrophy (54).

1.4.2 Brief overview of molecular hallmarks in pathological cardiac hypertrophy

Several biological processes mark the transition from physiological into pathological cardiac hypertrophy such as reduction of capillary density, calcium overload, apoptosis, oxidative stress, and cardiomyocytes inflammation. The dominant feature of pathological cardiac hypertrophy is the reactivation of several fetal gene expressions such as MHC-β (myosin heavy chain-β), skeletal alpha actin and atrial natriuretic factor (ANF). The increase production of transcription p53 which inhibits the activity of HIF-1 is associated with reduction of capillary density in pathological hypertrophy. The excessive concentration of reactive oxygen species (ROS) in pathological response creates NO imbalance state and activates the pro-hypertrophic signaling kinases such as extracellular signal-regulated kinase, c-jun N-terminal protein kinase, p38 mitogen-activated protein kinase (MAPK), as well as NFκβ. The declining compensatory adaptation in calcium handling by reduction of SERCA2a gene expression highlight the transition from adaptive to maladaptive hypertrophic response. This may lead to intracellular calcium accumulation which activates calmodulin and modulate the pro-hypertrophic pathways of Ca^{2+}/CaM/CaMKII/MEF-2 as well as Ca^{2+}/CaM/CaMKII/calcineurin/NFAT (47, 62)

Production of inflammatory cytokines such as interleukins 1 (IL-1) and 6 (IL-6) is also associated with progression of pathological cardiac hypertrophy. Elevated TNF-α and TGF-β involved in development of heart failure, cardiac remodeling, and fibrosis. Furthermore, increase concentration of TGF-β triggers p38 MAPK which further activation of downstream signaling cascades leading to pathological cardiac remodeling and fibrosis. Under stress circumstances, the cardiomyocytes upregulate several hypoxias induced mitogen factor and growth differentiation factor-15 (GDF-15) which might serve as a prognostic biomarker of pathological cardiac hypertrophy. Apoptosis serves also as a major hallmark of cellular damage caused by disease including in pathological cardiac hypertrophy. The angiotensin II as hypertrophic agonist activates mitochondrial caspases, a group of cysteine proteases, which finally induce apoptotic signaling cascades leading to DNA fragmentation and cellular death (63).

1.4.3 Other signaling pathways of cardiac hypertrophy

Additionally, alternative signaling pathways involving fetal gene expressions are also associated with cardiac hypertrophy and cell renewal stimulation in pathological pressure overload, but more prominent observed in endurance training. Recent animal studies using multi-isotope imaging mass spectrophotometry in aged mice and lineage tracing approaches showed that voluntary endurance training and intensity controlled swimming in rodents promote cardiomyogenesis, the formation, and differentiation of endogenous cardiac progenitor stem cells by activating stem cell factor receptor *c-kit* (64, 65).

Alternatively, biomechanical stress signals during physical exercise mediate activation of several cardiac signaling molecules including melusin through β-integrins involvement which anchor extracellular matrix to intracellular cytoskeleton within each sarcomere. Melusin interconnects with calcineurin-NFAT pathways, AKT/PKB/GSK3β, and might work independently through JAK-2/STAT (Janus kinase-2/signal transducer and activator of transcription) to translocate G proteins into the cytosol upon activation by stretching. This leads to cardiac hypertrophy mediated by ERK regulation (66).

The ANP (atrial natriuretic peptide), BNP (B-type natriuretic peptide), and NO (Nitric oxide) are generated upon pressure challenge in the heart and activate various guanylate cyclases which

produce cGMP (cyclic guanosine monophosphate) leading to PKGI (Protein kinase G-1) accumulation as inhibitor of calcineurin-NFAT, PI3K-AKT/PKB, and ERK1/2 circuits (53). Furthermore, experimental endurance exercise in rodents´ aging hearts may also lead to balanced neovascularization by means of endothelial and vascular smooth muscle proliferation via VEGF (Vascular endothelial growth factor), PIGF (Placental induced Growth Factor), and FGF-2 (Fibroblast growth factor-2) signaling activation due to relative ischemia state during physical training (67, 68). Additionally, transcriptional DNA modifications by microRNA and long non-coding RNA have also been reported in several animal studies to be involved in cardiac hypertrophy, however the evidence if the contribute positively or negatively is still scarce (69-71). Although recent studies exert robust information regarding the interconnecting molecular signaling pathways of both adaptive and maladaptive cardiac hypertrophy induction (**figure 5**), the exact mechanisms of each signaling pathway and their interactions are yet to be determined.

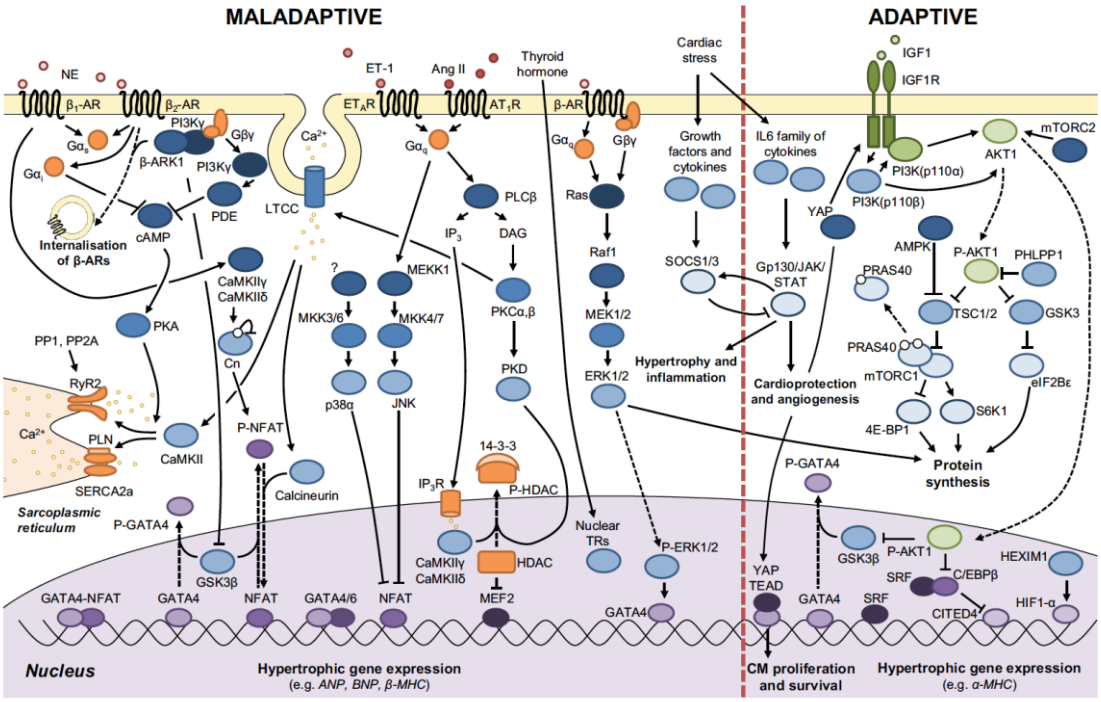

Figure 5. The interconnecting molecular pathways participated in adaptive and maladaptive cardiac hypertrophies (58).

1.5 The controlled forced endurance training protocol using treadmill machine in murine model to elicit cardiac hypertrophy

The animals can provide valuable information to fathom the underlying mechanisms of cardiovascular physiological changes during physical exertion and their phenotypic consequences down until molecular levels which are almost impossible to be performed in human due to ethical grounds. The performed animal training regimens also show high reliability, reproducibility, and technically have been improved in recent years to mimic the real situation in human allowing possibility of translational application and discovering therapeutic targets (72).

Cardiac hypertrophy in pathological model can be achieved surgically by ligating the aorta to increase the cardiac afterload or performing aorto-caval fistula mimicking volume overload. Administration of chemical substance to activate the RAAS or sympathetic nervous activity as well as several transgenic mice with mutation in important growth signaling pathways are also available (73). However, the murine model to analyze the physiological cardiac hypertrophy is not yet readily available. Treadmill training in rodents involves protocol which encompasses periodic changing of velocity, total distance run, running duration, and inclination angle with possible simultaneously recording of metabolic rate, heart rate and maximal oxygen uptake (VO_{2max}), which resembles closely to exercise testing equivalent in human. Nonetheless, the standard tools to objectively quantify the exercise capacity during endurance training are still in ongoing debate. Total mechanical work completed (measured in Joules) and peak power output in constant velocity are the examples of energy-based metrics that can be utilized to calculate training capacity, yet their application in animal research or human studies is rather complicated and mostly cumbersome (74).

Endurance training using commercially available treadmill machine (**figure 6**) encompasses a forced and intensity-controlled exercise conditioning. It also allows the addition of velocity, training duration, and inclination to control energy expenditure and working performance. Other advantages of using this method are simpler work calculation and the possibility of metabolic rate determination utilizing a specific metabolic chamber. However, endurance training using treadmill poses some disadvantages to the animals such as cortisol release due to stressful forced nature of the training protocols, more expensive to purchase and maintain, the need of constant supervision to avoid injury risk, and potentially affecting the circadian cycle of the experimental animal (75).

Figure 6. The treadmill machine dedicated to small animals. The machine consists of five divided lanes which are intended concurrently to train the same number of animals.

An acclimatization period on the first week of training is often implemented to familiarize the animal to the machine, avoid unwanted injuries, and allow consistency in training performance. This process can be done only in limited time by introducing a lower starting speed of 5-10 m/min on the first 2-5 days of training and escalating the velocity 1 m/min per day. (72, 75). Table 1 summarizes the available forced running protocols on the treadmill for rodents on the literatures which has been used successfully to produce cardiac hypertrophy.

Table 1. The selected treadmill machine protocol used in rodent models of forced exercise training-induced cardiac hypertrophy (74).

Species and Sex	Treadmill forced running protocol	Results and reference
Rat, adult female	Five times/week, 60 min/day, 11 weeks, 10-26 m/min, 10-20% grade inclination, graded increase velocity and duration	Increased in ratio of LV mass/Body weight (76).
Rat, adult female	Five times/week, 60 min/day, 20-30 weeks, 31 m/min, 10% grade inclination, constant protocol	Increased in ratio of LV mass/Body weight and increased cardiomyocytes dimensions (77)
Rat, adult male	Five times/week, 30 min/day, 6-12 weeks, 0.8 km/h, 0% grade inclination, constant protocol	Increased in ratio of LV mass/Body weight (78)
Rat, adult male and female	Five times/week, 60 mins/day, 4-13 weeks, interval 8 min 85-90% of VO_{2max} and 2 min 50-60% of VO_{2max}, 47% grade inclination, high intensity protocol	Increased in ratio of LV mass/Body weight, RV mass/Body weight, heart weight/Body weight, and increased in cardiomyocytes dimensions (79)
Mice, adult male and female	Five times/week, 120 mins/day, 8 weeks, interval 8 min 85-90% of VO_{2max} and 2 min 50-60%, 47% grade inclination, high-intensity protocol	Increased in ratio of LV mass/Body weight, RV mass/Body weight, heart weight/Body weight, and increased in cardiomyocytes dimensions (80)

Recent protocol suggests that training can be performed 4-5 days/week for 15-60 minutes duration with total intervention time of 4-13 weeks. The speed and inclination can be easily adjusted to produce 50-60% VO_{2max} for low and up to 90% VO_{2max} for high intensity. Several cardiac phenotypes as outcome parameter have been observed in various experimental pre-clinical research using this well-established protocol such as increased VO_{2max}, cardiac index and left ventricular mass, augmented cardiomyocytes size, increased proliferation markers and angiogenesis, decreased peripheral vascular resistance, and activation of genes controlling growth without showing any indication of cell death, apoptosis, or fibrosis (74, 80).

1.6 Assessment of cardiac hypertrophy using imaging modality – Overview of nuclear medicine approach on cardiac function analysis

1.6.1 Cardiac PET basics

In pre-clinical application and human research, the exercise testing has been integrated with more subjective assessment of cardiac function including the application of electrocardiography, echo-

cardiography, left ventriculography, invasive cardiac monitoring, cardiac magnetic resonance imaging, and more recently nuclear scintigraphy using radiotracer-based PET (Positron emission tomography)-Scan. The PET technology has been recently combined with computed tomography (CT) imaging modality to facilitate a more comprehensive hybrid assessment of both anatomical and functional parameter in certain medical disciplines including in oncology, clinical immunology, neurology, and cardiology (81-83). Cardiac PET/CT facilitates serial, non-invasive, and simultaneously multiparameter recording of cardiac morphology and function assessment in vivo using intravenously administered radionuclide as tracer.

There are several types of radiotracers which have been used in cardiology depending on the aim of the investigation such as evaluation of myocardial perfusion, cardiac metabolism, innervation, and determination of inflammatory component of atherosclerosis in vascular imaging (84). Even though the diverse applications, the radiotracer administration shares a common principle. The radionuclide tracers used in metabolic evaluation are need first to be distributed to the whole body and taken up metabolically by the intended target organ. During the distribution process after injection, positrons are discharged and collide with an electron resulting in annihilation of positron due to the opposite direction of two photons emission. In the organ, these tracers decay further and emit two 511 -keV γ-rays that can be detected with several specialized stationary rings of scintillating 360^0 detectors which converts this newly formed energy into an electrical signal in all directions or in each plane to allow 3-dimension (3D) or 2-dimension (2D) visualization and quantification respectively. The two photons are recorded simultaneously due to a narrow coincidence timing-window of 6-12 ns detection by the scanner. By this real-time detection, an algorithm of image reconstruction can be performed based on the annihilation of two photon pairs and the position of distributed positron-emitting radionuclides in the body. In a combined cardiac PET/CT, the CT component is used to attenuate the photons and configure the scatter correction of PET data to allow accurate and valid interpretation of myocardial metabolic perfusion, gross morphology, and function (85, 86).

The major advantage of PET/CT fusion is the ability of the system to quantify radioactive activity within the desired field of interest. Moreover, the PET permits the utilization of positron-emitting radionuclides which are tagged with certain types of radiopharmaceutical agents. This facilitates a great multitude of possibilities in investigating biochemical pathways which participate in cardiac metabolism without modifying the properties of their substrates. Nevertheless, the proper design of the radiotracers and the interpretation of image quantification poses a wide array of complexity and time-consuming schemes which contributing to the major disadvantages of using cardiac PET as imaging modality of heart function (87).

1.6.2 The radiotracers commonly used in metabolic cardiac PET/CT evaluation

The radionuclides are normally coupled into elements such as oxygen (^{15}O), carbon (^{11}C), nitrogen (^{13}N), and hydroxyl group substituting fluorine (^{18}F) compound which are found ubiquitous in the body and participate biologically as substrate analogues in organic metabolism as described previously. Several radiotracers have been used to quantify myocardial oxygen consumption (VO_2) and oxidative phosphorylation during exercise such as ^{15}O-Oxygen- and ^{11}C-Acetate-based radionuclides, however the measurement steps are complex and requiring multi-tracer study. The visualization of cardiac metabolism as one of the parameters of cardiac chamber and function analysis can be performed by injecting radiotracers which participating in cardiac carbohydrate

and fatty acid turn-over such as ^{18}F-Fluorine-, ^{11}Carbon-, ^{11}C-Lactate, ^{11}C-Palmitate-, and various fatty acid analogue-incorporated radionuclides (88).

Table 2. The most commonly applied PET radiotracers to measure cardiac metabolic function (88).

Radionuclide	Half-Life	Compound	Present use
^{15}O	2.04 min	$^{15}O_2$	Oxygen consumption
^{11}C	20.4 min	Acetate	Indirect measure of oxygen consumption
		Palmitate	Fatty acid uptake, oxidation, and storage
		Glucose	Glucose uptake, glycolysis, oxidation, and glycogen turnover
		Lactate	Lactate uptake and oxidation
^{18}F	110 min	Deoxyglucose	Glucose uptake
		Fluoro-6-thia-heptadecanoid acid (FTHA)	Fatty acid uptake and oxidation
		Fluortriopride (FTP)	Fatty acid uptake and oxidation
		Fluoro-cyclopropylhexadecanoid acid (FCPHA)	Fatty acid uptake and oxidation

One of the most common radiotracers used in cardiology to measure carbohydrate cardiac uptake is 2-deoxy-2-[^{18}F]fluoro-D-glucose (^{18}F-FDG) which is a radiolabeled glucose molecule with half-life of 110 minutes. The main reason of using ^{18}F-FDG is due to the ability of cardiomyocytes to take significant amount of glucose besides fatty acid and ketone bodies as energy substrates. The ^{18}F-FDG competes with the non-tagged normal glucose molecules on the sarcolemmal GLUT (glucose transporter) transport receptor for a mediated facilitated diffusion and is metabolized subsequently through the cytosolic hexokinase-mediated phosphorylation into FDG-6-phosphate. The trapped myocardial FDG participates later in glycolytic as well as tricarboxylic acid cycle and reflects the overall myocardial both aerobic and anaerobic capacity (89). Other advantages of ^{18}F-FDG are cost effective, able to produce high spatial resolution with lower amount of radioactivity, suitable for delayed imaging protocols as well as stress imaging (90).

Administration of inhalative isoflurane as anesthesia method has been shown to augment the myocardial FDG uptake remarkably which required careful interpretation of the acquired results (91). Several anabolic and catabolic hormones such as insulin, insulin like growth factor, glucagon, and corticosteroid could affect the cardiac metabolic rate, thus altering the rate of myocardial FDG uptake (92). Although some of these limitations, using^{18}F-FDG as radiotracers both in clinical and pre-clinical research provides a robust accurate and valid information regarding the metabolic activity of the heart tissue, as well as mostly readily available in certain health care or facilities and easily to be administered. It has also a reliable elimination profile and half-life avoiding the radiotracer accumulation in the body and long side effects caused by ionization radiation (87).

1.6.3 The research application of metabolic cardiac PET/CT

The assessment of myocardial metabolic capacity using cardiac PET/CT is commonly used in the animal research discovery in the field of aging, myocardial ischemia, non-ischemic dilated cardiomyopathy, obesity, insulin resistance, diabetes mellitus, vascular inflammation, and left ventricular hypertrophy (84). In human studies the same cardiac PET/CT technique is used for evaluation of myocardial viability after infarction, differentiating between hibernating and scar tissues, diagnosis sarcoidosis and other cardiac inflammatory conditions (myocarditis, pericarditis, and endocarditis), cardiac malignancy, determination of left ventricular pump, and metabolic function (93). Small animal PET/CT imaging modality is one of the current innovative approaches which allows both two- and three-dimensional quantification of ventricular volumes and accurate non-invasive cardiac function assessment. An automated software-based application by certain commercial provider could simplify the process of endocardial segmentation, ventricle inner as well as outer surfaces contouring at different levels in all axes, and determination of volume of interest (VOI). The metabolic volume (LVMV), and the percentage of injection activity/gram cardiac tissues serve as surrogate parameters of heart muscle mass during pressure-overload left ventricle hypertrophy and glucose metabolic process in the heart which can be deducted by analysis static reconstructed images. The ECG-gated reconstructed images on the other hand can be used as a basis to perform functional systolic and diastolic cardiac analysis based on radiotracers uptake as well as created normative database and permit the automatic metrics of EDV, ESV, SV, % of ejection fraction, heart rate, CO, CI, mid-myocardial surface area, and LV volume/time kinetic curve (94-96). The ^{18}F-FDG PET-scan has been already widely used in pre-clinical animal studies to validate these described parameters on myocardial left anterior descending (LAD) coronary artery ligation for ischemia model and trans-aortic constriction model for cardiac hypertrophy induction model (96, 97). Though, the utilization of this method to evaluate cardiac hypertrophy and changes in cardiac performances after forced intensity-controlled endurance training in animal model has not been observed in recent literatures.

1.7 Aim and objectives of this study

The reviewed literatures described above have shown that chronic and regular endurance exercise training led to exercise induced cardiac remodeling (EICR) which attributed to various alteration in morphologic and hemodynamic profile (32-36). Although endurance training is frequently associated with a lower incidence and prevalence of cardiovascular-related morbidity and mortality, the training's profile to create these desirable advantages remains scientifically under scrutiny. Furthermore, both adaptive structural and functional changes are expected to envisage in training athletes after several weeks of moderately intense regular endurance training. Cardiac hypertrophy is one of the adaptive results of chronic volume and pressure overload during training (34). Nonetheless, the exact time point of observed cardiac hypertrophy, duration, frequency, training intensity, and additional scientific data regarding phenotyping and characterization of morphometric parameters are still largely under debate (35). Studies to investigate the physiological effects of endurance training on heart function are commonly performed using experimental small animal models. The endurance training with commercially available treadmill machine encompasses a forced and intensity-controlled exercise conditioning which may lead to generation of hypertrophied heart (72, 80). The realization and practicability of this method on the opposite have elucidated a great amount of controversy (74). Furthermore, more detail phenotyping and characterization of physiologic cardiac hypertrophy by combining histological staining as gold stand-

ard and cardiac imaging modalities in training heart has not yet been published in recent literatures. Previous work successfully utilized small animal PET/CT as a valid imaging modality to characterize three-dimensional quantification of left ventricular volumes and accurately delineating cardiac function assessment in myocardial ischemia and pressure overload-induced cardiac hypertrophy models (95, 96). Though, the application of this innovative method to evaluate cardiac hypertrophy and alteration of cardiac performances after forced intensity-controlled endurance training in animal model has not been previously performed. Chronic forced intensity-controlled endurance training combined with cardiac PET/CT-scan and expression analysis using RNA-Seq techniques could serve as an innovative method to investigate physiological cardiac hypertrophy in animal research.

The study presented here was intended to:

1. Analyze the changes of morphometric parameters such as body weight, heart weight, and heart weight/tibia length ration after certain points of forced and intensity-controlled endurance training in animal study.
2. Describe the occurrence of cardiac hypertrophy and possible pathological hallmarks in relation to chronic endurance training by means of histopathological analysis under the microscope as gold standard of measurement.
3. Clarify the role of small animal cardiac PET/CT as a method to evaluate cardiac function and left ventricular performance after chronic endurance training.
4. Explore the molecular signaling pathways that participate in physiological cardiac hypertrophy induced by endurance training compared to sedentary controls.

2. Materials and methods

2.1 Materials

2.1.1 Reagents and chemical substances

^{18}F-FDG	LMU Munich Hospital Pharmacy (Munich, Germany)
Acetic Acid glacial	Merck (Darmstadt, Germany)
Aqua 1000 ml	B-Braun (Melsungen, Germany)
Bovine Serum Albumin 96%	Sigma-Aldrich (Steinheim, Germany)
Chloroform anhydrous 100%	Sigma-Aldrich (Steinheim, Germany)
Direct Red 80 (Picrosirius Red)	Sigma-Aldrich (Steinheim, Germany)
Eosin G Solution 0.5%	Carl Roth (Karlsruhe, Germany)
EtOH absolute, 96%, 70%, 50%	Sigma-Aldrich (Steinheim, Germany)
Formaldehyde 4% in PBS	Sigma-Aldrich (Darmstadt, Germany)
Goat Serum	Sigma-Aldrich (Steinheim, Germany)
HCl 37%	Merck (Darmstadt, Germany)
Isopropanol 99.7%	Sigma-Aldrich (Steinheim, Germany)
Isotonic saline solution 0.9% 10 ml	Fresenius Kabi (Bad Homburg, Germany)
Meyer's Hematoxylin Solution	Carl Roth (Karlsruhe, Germany)
Picric Acid 1.3% in H_2O	Sigma-Aldrich (Steinheim, Germany)
RNAse free water	Thermo Fisher (Waltham, USA)
Saponin	Sigma-Aldrich (Steinheim, Germany)
Sucrose 30% in PBS	Sigma-Aldrich (Steinheim, Germany)
Trizol® Reagent	Life Technologies (Carlsbad, USA)
Tween® 20 0.1% in PBS	Sigma-Aldrich (Steinheim, Germany)
Xylene	Sigma-Aldrich (Steinheim, Germany)

2.1.2 Buffers and mediums

Blocking Solution:	0.5% Saponin
	1% BSA
	10% Goat Serum
Dulbecco's PBS	Biowest (Nuaillé, France)
Hanks' Balanced Salts Solution	Biowest (Nuaillé, France)
HCl 1 N:	8.28 ml 37% HCl

	100 ml Aqua
HCl 0.01% N:	2 ml 1N HCl
	198 ml Aqua
PBS Medium	LMU Munich Hospital Pharmacy (Munich, Germany)
Sirius Red 0.1%:	0.2 g Direct Red 80
	200 ml picric acid

2.1.3 Commercially used technologies and software

bcl2fastq 2.20.0.422 primary data analysis	Illumina (San Diego, USA)
CLC Genomics Workbench 21.0.4	CLC Bio Qiagen (Aarhus, Denmark)
Illumina Sequence Analysis Viewer (SAV) 2.4.7	Illumina (San Diego, USA)
NEBNext® Ultra™ II Directional RNA Library Prep technology	New England Biolabs (Ipswich, USA)
NovaSeq Control Software (NVCS) v1.6.0	Illumina (San Diego, USA)
NovaSeq® 6000 next generation sequencing system	Illumina (San Diego, USA)
Novaseq ® Real Time Analysis 3.4.4 Software	Illumina (San Diego, USA)

2.1.4 Immunohistology antibodies

SYTOX Green nucleic acid stain (1:1000 REF S7020)	Invitrogen (Eugene, USA)
Wheat germ agglutinin Alexa Fluor 647 Conjugate (1:100 REF W32466)	Invitrogen (Eugene, USA)

2.1.5 Consumables

A-PAP Pen for immunostaining	Sigma-Aldrich (Schnelldorf, Germany)
Bephantene® eye and nose cream	Bayer Pharmaceuticals (Leverkusen, Germany)
Cover slips 24 x 50 mm	R. Langenbrinck GmbH (Emmendingen, Germany)
Eppendorf tubes 1.5 ml	Eppendorf AG (Hamburg, Germany)
Falcon tubes 15 ml	Corning Science (Tamaulipas, Mexico)
Falcon Tubes 50 ml	Corning Science (Tamaulipas, Mexico)
Fine bore polythene tubing 0.28 mm ID	Smiths Medical International Ltd. (Kent, UK)
Injekt® syringe 1 ml, 5 ml, 10 ml	B-Braun (Betlehem, USA)
Isoflurane USP	Dechra Pharmaceuticals (Aulendorf, Germany)
Leica 819 microtome blades	Leica Biosystems (Nussloch, Germany)
Micro tube 2 ml	Sarstedt AG (Nümbrecht, Germany)

Microlance sterile needle 30G	BD Biosciences (Heidelberg, Germany)
Nitril BestGen ® Handgloves size M	Meditrade (London, UK)
Petri Dish 10 cm diameter	Carl-Roth (Karlsruhe, Germany)
Pipette tips 10 µl, 200 µl, 1000 µl	Sarstedt AG (Nümbrecht, Germany)
ProLong® Gold anti-fade reagent	Invitrogen (Eugene, USA)
Q-tips®	Unilever (Mannheim, Germany)
Roti® Histokitt II	Carl Roth (Karlsruhe, Germany)
Serological pipette Cellstar® 25 ml	Greiner Bio-One (Frickenhausen, Germany)
Serological pipette Costar 5 ml	Corning inc. (Corning, USA)
Sterile surgical blades	Aesculap AG (Tuttlingen, Germany)
Superfrost Plus adhesion microscopes slides	Epredia (Breda, Netherlands)
Tissue-Tek Cryomold standard 25 x 20 x 5 mm	Sakura Finetek (Alphen aan den Rijn, Netherlands)
Tissue-Tek OCT mounting medium	Sakura Finetek (Alphen aan den Rijn, Netherlands)
Type F Immersion Liquid	Leica Microsystems (Wetzlar, Germany)

2.1.6 Devices

Centrifuge 5418 R	Eppendorf AG (Hamburg, Germany)
Confocal microscope Leica TCS SP8 X	Leica Microsystems (Wetzlar, Germany)
Cryotome Leica CM3050 S	Leica Biosystems (Wetzlar, Germany)
Fridges -20°C and 4°C	Bosch (Gerlingen-Schillerhöhe, Germany)
Fridges -80°C	Thermo Scientific (Waltham, USA)
Histology slides staining jar	DWK Life Sciences (Mainz, Germany)
Humid dark chamber	Simport Scientific (Beloeil, Canada)
IKA T10 Ultra-Turrax basic Homogenizer	Janke & Kunkel KG (Staufen i. Breisgau)
IKA-Rocker 3D Basics	Janke & Kunkel KG (Staufen i. Breisgau)
Integra Pipetboy 2	Integra Biosciences (Biebertal, Germany)
Isoflurane Vapor 2000 vaporizer	Dräger Medical (Unterhaching, Germany)
Micro needle holder	Fine Science Tools (Heidelberg, Germany)
Micropipette Eppendorf 20 µl, 200 µl, 1000 µl	Eppendorf AG (Hamburg, Germany)
Nanoscan® PET/CT scanner	Mediso Medical Imaging Systems (Budapest, Hungary)
Nanodrop 2000 Spectralphotometer	Thermo Fisher (Waltham, USA)

NeoLab vortex	NeoLab Migge GmbH (Heidelberg, Germany)
Kendall Neonatal ECG electrodes 26G	Cardinal Health (Norderstedt, Germany)
Panlab® Five Lanes Treadmill for Mice	Harvard Apparatus (Holliston, Massachusetts)
Stereomicroscope Leica M205 FA	Leica Microsystems (Wetzlar, Germany)
Pioneer Ohaus analytical balance	Sigma-Aldrich (Steinheim, Germany)
Preciva® digital caliper	BellaCocool GmbH (Berlin, Germany)
Sartorius precision balance	Sartorius AG (Göttingen, Germany)
Surgical instruments set Aesculap	B-Braun (Melsungen, Germany)

2.1.7 Software

Affinity Designer v1.10.5	Serif Ltd (Nottinghamshire, UK)
BioRender	Toronto, Ontario, Canada
DESeq2 v. 1.36.0	BaseSpace Labs Illumina (San Diego, California)
EndNote X9.3.3	Thomson Reuters (NYC, USA)
Fgsea (fast GSEA) v.1.22.0	GitHub (San Francisco, USA)
GraphPad Prism 8.0.1.244	GraphPad Software Inc. (San Diego, USA)
ImageJ 2.9.0	NIH (Maryland, USA)
InterView FUSION 3.09.008.0000	Mediso Medical Imaging System (Budapest, Hungary)
Inveon Research Workplace 4.2	Siemens Medical Solutions (Malvern, PA, USA)
LAS X Life Science Microscope Software 1.4.4	Leica Microsystem (Wetzlar, Germany)
Microsoft Office Professional Plus 2016	Microsoft Corporation (Redmond, USA)
Msigdbr (molecular signature database) v.7.5.1	UC San Diego–Broad Institute (San Diego, USA)
Nucline NanoScan 3.04.018.0000	Mediso Medical Imaging System (Budapest, Hungary)
QPS and QGS® SPECT Software v4.0	Cedar-Sinai Medical Centers (Beverly Hills, CA, USA)
R/Bioconductor v.4.2.0	Bioconductor Core Team (Buffalo, USA)
RSEM (RNA-Seq by Expectation-Maximization v. 1.3.3	GitHub (San Francisco, USA)
STAR (Spliced Transcripts Alignment to a Reference) v. 2.7.10a	GitHub (San Francisco, USA)

2.2 Methods

2.2.1 Animals

A total of 89 male adult C57BL/6 mice age between 5-8 weeks old with the weight of 23.04 g ± 2.27 were purchased from Charles River (Sulzfeld, Germany) and included in the study. During the experiment period, they were kept in the Multispecies Barrier (MSB) room of Core Facility Animal Model (CAM) at Biomedical Center LMU Munich. Animal husbandry and experimental procedures were carried out according to the guideline by the European Directive 63/2010/EU and extrapolated to Animal Protection Law in the scope of the German legislation. The animals received humane care, food and water *ad libitum* and optimized clean living environments with recommended temperature, humidity, and light and dark cycles. Our study protocols complied with the guidelines published from the institute and were also approved by the governmental animal ethics committee and the local government.

2.2.2 Acclimatization and training protocols

After arriving at our institute, the animals will be rested for at least two weeks in the behavior room of MSB CAM to avoid unnecessary stress and aggressive behaviors during the application of training protocol. Wild type mice were randomly and equally assigned to chronic forced endurance training or their sedentary counterparts. Forced exercise training was performed using a treadmill machine (Panlab Harvard Apparatus, Holliston, Massachusetts). There were in total five training groups and every training regimen began with one-week acclimatization.

The acclimatization started with the speed of 10 m/min for 10 minutes on the first day. The speed and duration of training were incrementally increased each day until the fifth day namely 11 m/min, 12 m/min, 13 m/min, and 14 m/min for 20, 30, 40, 50 minutes respectively. After one-week acclimatization, the training protocol started with the speed of 15 m/min at the same time of the day, five days a week ranging from 0 until 12 weeks depending on their allocated groups. The 2- and 4-weeks groups allocated to run for 60 minutes/day. The 8- and 12-weeks groups in the other hand ran for maximum 120 minutes/day.

Ten animals ran for 2, 4, and 8 weeks each, however only 5 animals trained for 12 weeks. The same number of mice were allocated as sedentary control on each group. As baseline measurements, 10 animals were trained for only one week using acclimatization protocol, designed as 0 weeks training group, and compared with their respective sedentary control (**figure 7)**.

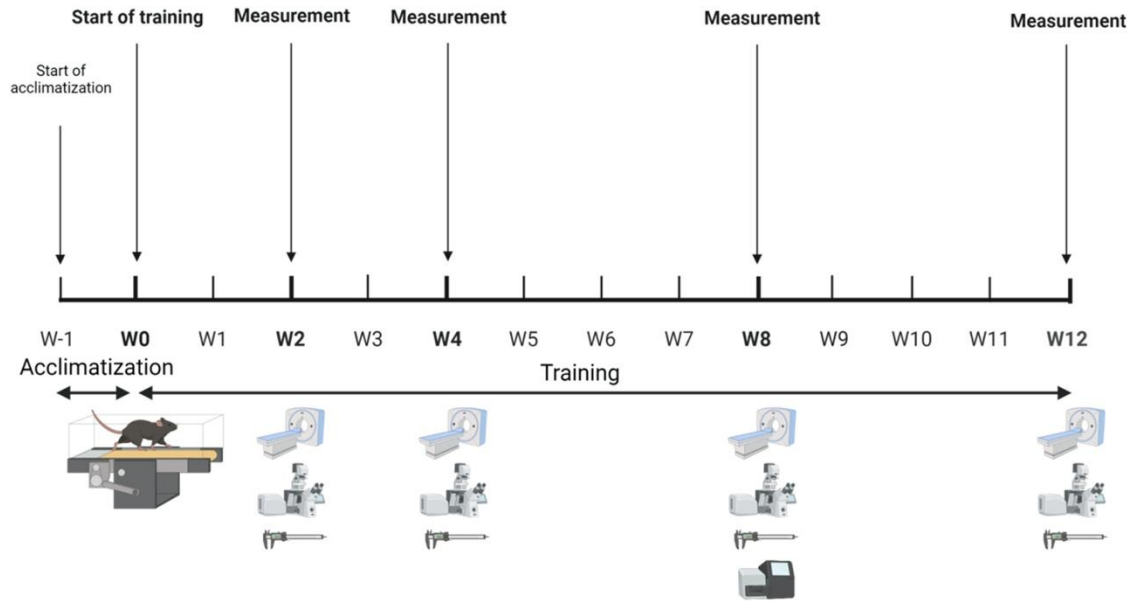

Figure 7. The training protocol used in this study. The training started after one week of acclimatization period. The morphometric measurements, cardiac PET-Scan, and histology were made after each selected timepoints (weeks 0, 2, 4, 8, and 12). Only ten heart samples on week 8 (five training mice and five controls) were taken for expression analysis using RNA-Seq. Image was created using BioRender (Toronto, Ontario, Canada).

Before each training frames, mice were adapted to the treadmill environment for 15 minutes. They were allowed to rest every 15 minutes for 2 minutes during each training session. The animals were rewarded with food pellets and stimulated with air puff to motivate them running. The air puff was triggered only when the animals touched the metal grid behind each running lane. The training was stopped if exhaustion occurred or when the animals stayed for more than five consecutive seconds on the metal grid without any attempt to return to run on the treadmill. The running distance, total time, and the duration when the animals were on the metal grid were recorded accordingly per lane. The animals will be excluded from the final data analysis if the total running duration was less than 15 minutes/day for more than 3 days/week. The treadmill was cleaned thoroughly after each training session before other animals from another group were loaded onto the lane.

2.2.3 *In vivo* cardiac PET/CT image acquisition

After each training duration, the animals were transferred to the department of nuclear medicine in the LMU University Hospital for PET/CT scanning purpose. The induction and maintenance of anesthesia were performed using 2.5% and 1.5% Isoflurane respectively. The oxygen flow was maintained at a rate of 1.0-1.4 L/min throughout the scan duration and delivered using a closed tubing system with a face mask. The administration of Isoflurane as anesthetic agent enhances the myocardial uptake of ^{18}F-FDG, thus any particular premedication was not necessary to be administrated to reach this desirable effect.

^{18}F-FDG was administrated intravenously using a catheter in a volume of 200 µl, which gave approximately 20 MBq radioactivity, through one of the lateral superficial tail veins. After each administration, the catheter was flushed using isotonic saline solution 0.9% (Fresenius Kabi, Bad Homburg, Germany) in a volume of 500 µl. A 30-minutes delay time from injection until the start

of scanning was crucial to allow enough radiotracer distribution into the myocardium. Then ECG-gated micro-PET image acquisitions using a Nanoscan® dedicated small animal PET scanner (Mediso Medical Imaging Systems, Budapest, Hungary) were accomplished on 0, 2, 4, 8, 12 weeks groups on each animal, both training and sedentary control. A heating pad and a rectal thermometer for tight temperature monitoring were placed under and in the prone-positioned animals respectively to regulate normal core body temperature. The animals were remained anesthetized, and the ECG activity was carefully recorded real-time throughout the entire 30 minutes scan duration using Kendall neonatal ECG electrodes (Cardinal Health, Norderstedt, Germany), which were placed on animal's both forepaws and left hind paw. The animals' eyes were protected using Bephantene® cream to avoid dryness during the anesthesia. After a successful image acquisition, the animals were observed closely by a veterinarian until fully recovered from anesthesia effect. The recorded data were further reconstructed, analyzed, and quantified using Nucline NanoScan 3.04.018.0000 (Mediso Medical Imaging System, Budapest, Hungary), Inveon Research Workplace 4.2 (Siemens Medical Solutions, Malvern, PA, USA) and QPS-QGS® SPECT Software (Cedar-Sinai Medical Centers, Beverly Hills, CA, USA) respectively.

2.2.4 Morphometric phenotyping of the animals

The morphometric analysis was performed after each successful scan at the desired age on the end of training period. After a minimum 6-hours of post-scan latency to allow ^{18}F-FDG to be discharged from the animals' body to a safe level, the animals were anesthetized using induction dose of Isoflurane (2.0-2.4%) and euthanized by cervical dislocation. The method to sacrifice the animals was approved by the animal's ethic committee of our institute and the authorities from the Government of Upper Bavaria. The animals were weighed, disinfected, and dissected followed by organ perfusion using cold PBS to remove unwanted blood in the tissues. The heart, lungs, femoral quadriceps, and gastrocnemius muscles were then removed, washed in cold PBS, and carefully weighed using Pioneer Ohaus analytical balance (Sigma-Aldrich, Steinheim, Germany). The hearts and skeletal muscles were then directly put into 4% Formaldehyde solution (Sigma-Aldrich, Darmstadt, Germany) for histological processing. The right tibia was disconnected and cleaned from the surrounding muscles using a sterile surgical blade (Aesculap AG, Tuttlingen, Germany) and the tibial length (mm) was measured using Preciva® digital caliper BellaCocool GmbH (Berlin, Germany).

2.2.5 Tissue preparation for histology and frozen section

The harvested hearts and skeletal muscles were fixated in 4% Formaldehyde solution for 4-24 hours under agitation, followed by incubation in 30% sucrose solution (Sigma-Aldrich, Steinheim, Germany) overnight for dehydration. The hearts were cut transversally at the height of left ventricular papillary muscle and embedded in Tissue-Tek OCT mounting medium (Sakura Finetek, Alphen aan den Rijn, Netherlands) inside the Tissue-Tek Cryomold standard size of 25 x 20 x 5 mm (Sakura Finetek, Alphen aan den Rijn, Netherlands). In the other hands, the skeletal muscles were uniformly cut in the middle of muscle's belly and likewise embedded in the Cryomold and OCT mounting medium. The specimens were then stored in -20^{o}C fridge overnight or in -80^{o}C for long term storage.

The frozen hearts and skeletal muscles were further cut using cryotome Leica CM3050 S (Leica Biosystems, Wetzlar, Germany) with a thickness of 8 µm and 12 µm respectively. The chamber and knife temperature were maintained at -25^{o}C and -20^{o}C respectively. The tissue sections were

attached onto the Superfrost Plus® adhesion microscopes slides (Epredia, Breda, Netherlands) and stored in -20°C for the next processing steps.

2.2.6 Wheat germ agglutinin (WGA) immunofluorescence staining

The slides with the heart and skeletal muscle tissue sections were warmed up in room temperature for 10 minutes followed by refixation in 4% Formaldehyde solution for 10 minutes. The fixated sections were washed three times for 5 minutes each with PBS-Tween 20® 0.1% (Sigma-Aldrich, Steinheim, Germany). The specimens' glasses were made dry in room temperature for 10-15 minutes and the desired staining area were encircled using A-PAP Pen for immunostaining (Sigma-Aldrich, Schnelldorf, Germany). The application of 50µl blocking solution (PBS with 0.5% saponin, 1% BSA and 10% goat serum (Sigma-Aldrich, Steinheim, Germany)) onto each specimens' circle were done to prevent unspecific bindings with other proteins.

After one hour of incubation time, the blocking solution were washed off three times using Hanks' Balanced Salts Solution/HBSS (Biowest, Nuaillé, France). Wheat germ agglutinin (WGA) conjugated with Alexa Fluor® 647 (Invitrogen, Eugene, USA, cat. W32466) staining solution was diluted 1: 100 in HBSS and poured onto the specimens for 1.5 hours incubation at room temperature inside a dark, humid incubation chamber (Simport Scientific, Beloeil, Canada). The incubation followed by two times washing with HBSS. After the washing steps, SYTOX® green dye (Invitrogen, Eugene, USA, cat. S7020) diluted 1: 1000 in HBSS was applied to the specimens followed by 10 minutes incubation inside the dark and humid chamber at room temperature. The specimens were again soaked with HBSS for three times and kept dry for 10-15 minutes in room temperature. Subsequently, the sections were covered with ProLong® Gold anti-fade reagent (Invitrogen, Eugene, USA) as mounting media, sealed with cover slips size 24 x 50 mm (R. Langenbrinck GmbH, Emmendingen, Germany), and dried at room temperature for 24 hours in the dark before analysis on the microscope. The stained sections could be stored at 4°C in the dark until usage not exceeding one week.

2.2.7 Hematoxylin-Eosin staining

The specimens' glasses were made warm in the room temperature for 10 minutes and initially washed in Aqua (B-Braun, Melsungen, Germany) and PBS for 10 and 5 minutes respectively to remove the OTC mounting media. The washed specimens were then put into Meyer's Hematoxylin Solution (Carl Roth, Karlsruhe, Germany) for 3-5 minutes followed by washing steps under the flowing tap water for 15 minutes. The specimens were then reconditioned in Aqua solution for 2 minutes and dipped into Eosin G Solution 0.5% (Carl Roth, Karlsruhe, Germany) mixed with one drop of Acetic Acid glacial (Merck, Darmstadt, Germany) as buffer and preservatives for 3 minutes. The stained specimens were washed one time using distilled water for 2 seconds followed by dehydration steps into sequence of incrementally concentrated alcohol solution 70%, 96%, and 100% (Sigma-Aldrich, Steinheim, Germany) for 5 minutes each. As the last step, the specimens were put into Xylene I and II solution (Sigma-Aldrich, Steinheim, Germany) for 5 minutes each, dried in room temperature, mounted in Roti® Histokitt II (Carl Roth, Karlsruhe, Germany), and covered with cover slips size 24 x 50 mm before analysis under the microscope.

2.2.8 Picrosirius red staining

After warming up for 10 minutes in room temperature, the heart and skeletal muscle specimens were washed in PBS for 5 minutes followed by staining in Direct Red 80 (Sirius Red) 0.1% solution

(Sigma-Aldrich, Steinheim, Germany) for 1 hour. The stained samples were then washed in 0.01N Hydrochloric acid (Merck, Darmstadt, Germany) for 2 minutes followed by serial dipping into sequence of concentrated alcohol solution of 50%, 70%, 96%, and 100% for dehydration purpose. Finally, the dehydrated stained specimens were immersed in Xylene I and II solution for 2 minutes each, dried in room temperature, mounted in Roti® Histokitt II, and covered with cover slips size 24 x 50 mm before analysis under the microscope. The samples could be stored in room temperature for further use.

2.2.9 Microscopical image acquisition and analysis

A confocal microscope Leica TCS SP8 X (Leica Microsystems, Wetzlar, Germany) was used in collaboration with Core Facility of Bioimaging in Biomedical Center (BMC) LMU Munich to image the cross-sectional area of transversally cut both heart and skeletal muscle fibers at 40x and 20x magnification respectively. The Type-F Immersion Liquid (Leica Microsystems, Wetzlar, Germany) was applied on each image acquisition for a better object visualization. The images were taken utilizing two laser lines: 488 nm to detect SYTOX® green and 633 nm to visualize WGA respectively. The heart samples were analyzed at the height of papillary muscles on the left ventricle and the skeletal muscles images were taken in the middle of the muscle's belly. The images were made in triplicate and the surface area analysis was performed blindly using Image J2 (NIH, Maryland, USA). The quantification of both heart and skeletal muscles surface area was performed manually in one-to-one section basis (n > 200 cells per section, 600-800 cells per heart samples and n >100 per section, 300-400 cells per skeletal muscle specimen) and the triplicate results were averaged. Different from cardiomyocytes, the skeletal muscles were cut right in the middle of muscle belly and embedded perpendicularly in O.T.C. medium against the cryotome cutting surface. This allows the muscle fibers to be uniformly cut cross-sectionally across different samples for further quantification. The same confocal microscope laser settings were used to record the skeletal myocytes surface area, but this time with 20x objective to expand the visualization field, while skeletal muscle fibers are normally larger than cardiomyocytes. Four to five images per section comprising of approximately 300-400 skeletal myocytes were captured in triplicates and cell surface area were blindly quantified using ImageJ2 (NIH, Maryland, USA) application. As like the cardiomyocytes, the percentage of cell numbers in gradually increasing surface area size categories were also done in skeletal muscle tissue samples.

A stereo microscope Leica M205 FA (Leica Microsystems, Wetzlar, Germany) was utilized for visualizing stained specimens with Hematoxylin-Eosin and Picrosirius Red. Overview images with corresponding magnification for heart and skeletal muscle specimens were taken in triplicates with Leica DFC7000 T camera and analyzed using Image J2 software to detect inflammatory cells infiltration and fibrosis.

2.2.10 PET image analysis

The acquired images were then reconstructed as static and ECG-gated sequences using Nucline NanoScan 3.04.018.0000 (Mediso Medical Imaging System, Budapest, Hungary). Both static and ECG-gated image reconstruction was performed using built-in Tera-Tomo 3D reconstruction algorithm with normal regularization, application of median filter, spike filter, edge artifact reduction, 8 iterations, 0.50 voxels size, and subsets number of 6. Moreover, the gated images using 16 bin frames was also normalized, corrected for randoms, dead-, decay time, attenuation, and scatter. The reconstructed images were then exported utilizing InterView FUSION 3.09.008.0000 (Mediso

Medical Imaging System, Budapest, Hungary) for further processing. These exported PET images were then analyzed by employing the Inveon Research Workplace 4.2 (Siemens Medical Solutions, Malvern, PA, USA) to assess the percentage of the injected dose, myocardial injected activity per gram (cardiac %IA/g) and left ventricular metabolic volume (LVMV) as a surrogate parameter to measure myocardial mass using static reconstructed images.

LVMV was measured by creating a cubic volume of interest (VOI) around the desired left ventricular area in axial, sagittal, and coronal projections. A subtraction of a threshold value of 30% least hot voxels was then performed to measure volume in mm^3 and mean activity in Bq/ml. The percentage of total injected dose was calculated by multiplying total body volume area (mm^3) and mean activity of the radiotracer on the whole body (Bq/ml) and divided by default of 10^9. In the other hand, the cardiac %IA/g values were calculated by dividing mean LVMV activity to % injected dose and 10^4 by default.

The heart rate records during the scan were extracted from the automatically saved log data and used to verify the accuracy of ECG-triggering signal. This verification process is very important to be used as a baseline to analyze three-dimensional ECG-gated images. Both the static and gated images were then cropped to bring focus on the left ventricle and rescaled by augmenting the values to the factor of 10 using the R Program for Statistical Computing (Lucent Technologies, Murray Hill, NJ, USA) for further analysis. Only the gated images were smoothen using Gaussian σ 0.75 algorithm in x, y, and z axis.

The static images were further scrutinized using QPS® (Cedars-Sinai, Los Angeles, CA, USA) based on the created normative database to calculate myocardial viability by dividing the left ventricular surface area and automatically generated volume measurements. Moreover, the three-dimensional left ventricular function parameters (EDV, ESV, SV, and EF) were quantified utilizing QGS® (Cedars-Sinai, Los Angeles, CA, USA) on the ECG-gated reconstruction images. Subsequently, the cardiac output (µl/min) was calculated by multiplying the quantified SV with the recorded average heart rate/minute.

2.2.11 RNA isolation and bulk RNA-Seq analysis

The specimens used for RNA isolation were taken from the mice's whole heart consisting of both atriums (Including the left and right atrial appendages) and ventricles. The animal's hearts were soaked directly after extraction into Trizol® reagent (Life Technologies, Carlsbad, USA) (1 ml Trizol® reagent was used pro 100 mg heart tissue) and homogenized using IKA T10 Ultra-Turrax basic Homogenizer (Janke & Kunkel KG, Staufen i. Breisgau). The chloroform solution (Sigma-Aldrich, Steinheim, Germany) was added onto the homogenized tissues with an amount of 0.2 ml pro milliliter Trizol. The mixture was agitated top to bottom for 15 seconds followed by an incubation in room temperature for 2-3 minutes. The samples were afterwards centrifuged 13000 rpm in 4°C for 15 minutes to separate the upper aqueous-, lower emulsion- and middle interphase. The upper aqueous phase contains the desired RNA was carefully transferred into new clean tubes. The isolated RNA was washed by agitation for 15 seconds with 500 µl Isopropanol 99.7% (Sigma-Aldrich, Steinheim, Germany) each 1 ml sample followed by 10 minutes incubation in the room temperature. Subsequently, the samples were recentrifuged with the same settings as previously described. The pellets contain the precipitated RNA were afterwards cleansed with 1 ml 75% Ethanol followed by centrifugation 10000 rpm in 4°C for 8 minutes. The supernatant was discharged and the isolated pellet containing the desired RNA was dried in the room temperature before adding 30 µl RNA free water for dilution. A Nanodrop 2000 Spectralphotometer (Thermo

Fisher, Waltham, USA) was used to determine to quantity and quality of the isolated RNA. High-quality total RNA samples have an A260/280 ratio ≥ 1.9 indicating the absence of contaminating substances such as protein and other organic materials. The samples could be storage in -80°C fridge for further use.

A total of 10 samples of five 8 weeks-training and five sedentary mice at the same age were delivered to IMGM Laboratories for bulk RNA-Sequencing analysis. The RNA sequencing libraries were generated with NEBNext® Ultra™ II Directional RNA Library Prep technology (New England Biolabs, Ipswich, USA) according to the manufacturer's instructions and internal laboratory quality control. The library generation uses fragmentation, a poly-T oligo and sequencing adapter ligation. One RNA sequencing library pool was prepared from the 10 generated RNA-Seq libraries. The template amplification and clustering were performed using the Illumina NovaSeq® 6000 next generation sequencing system applying the exclusion amplification chemistry (Illumina, San Diego, USA) and its high output mode was made with 1 x 100 bp single-read chemistry. The cluster generation and RNA sequencing were operated under the control of the NovaSeq Control Software (NVCS) v1.6.0 (Illumina, San Diego, USA). The processing of primary images was performed on the NovaSeq instrument using Real Time Analysis (RTA) 3.4.4 software (Illumina, San Diego, USA). The evaluation of the imaging and sequencing running performance utilized the Illumina Sequence Analysis Viewer (SAV) v2.4.7 (Illumina, San Diego, USA). The CLC Genomic Workbench 21.0.4 (CLC bio, Qiagen, Aarhus, Denmark) was used for read-mapping and generation of transcript lists.

Sequencing reads were aligned to the mouse reference genome (version GRCm39.107) with STAR (version 2.7.10a). Expression values (TPM) were calculated with RSEM (version 1.3.3). Post-processing was performed in R (version 4.2.0) using default parameters if not indicated otherwise. Differential gene expression analysis was performed with 'Deseq2' (version 1.36.0). An adjusted p-value (FDR) of less than 0.1 was used to classify significantly changed expression.

Gene set enrichment analyses were conducted with package 'fgsea' (version 1.22.0) using the GO gene sets (biological process only) of 'msigdbr' (version 7.5.1). Genes were ranked based on the Deseq2 test statistic. The Analysis was limited to gene sets with a size range from 15 to 500 basepairs.

2.2.12 Statistical analysis

The whole statistical analysis on this work were performed using GraphPad Prism 8 software. All results were demonstrated as means with standard deviation. One-way and two-way ANOVA analysis inclusive multiple comparison, paired, and unpaired Student's t-test were performed where applicable for normally distributed sets of data. For not normally distributed groups, the Wilcoxon sign-rank, Kruskall-Wallis, or Mann-Whitney U-test was used. The Pearson's coefficient using linear regression method was used to determine correlation between two variables. The differences between two groups were considered statistically significant if the p-value ≤ 0.05.

3. Results

3.1 Morphometric parameter changes after endurance training

3.1.1 Endurance training induced body weight loss in exercising mice

The mice body weight was first measured using precision scale once they arrived at our animal facility and every first day of the week during the training period until the final day of organ removal. The training and sedentary animals were at the same age, kept in the same living conditions, and exposed to the same amount of food, water, temperature, humidity, as well as light dark cycle. Starting on the second week, the body weight has been observed lower in the training group compared to the sedentary control. The body weight discrepancy reached a significant level after four weeks of training. The mean average body weight of 4-week training group was 24.65 g ± 2.71 compared to 28.55 g ± 2.47 in their sedentary counterpart (**figure 8. A**, $p < 0.001$). The same observations were also seen after 8- and 12-weeks training. The mean average body weight on 8-weeks training 25.96 g ± 1.63 in comparison to 28.59 g ± 1.53 in sedentary group ($p < 0.001$) as well as 27.84 g ± 1.80 on the 12-weeks training group as opposed to 30.50 g ± 1.58 on the 12-weeks sedentary groups ($p < 0.05$). The divergence of the body weight's average among the groups was seen as early as 2 weeks and shown on **figure 8. B**, which portrayed that the endurance training induced weight loss in exercising mice. ($p < 0.001$).

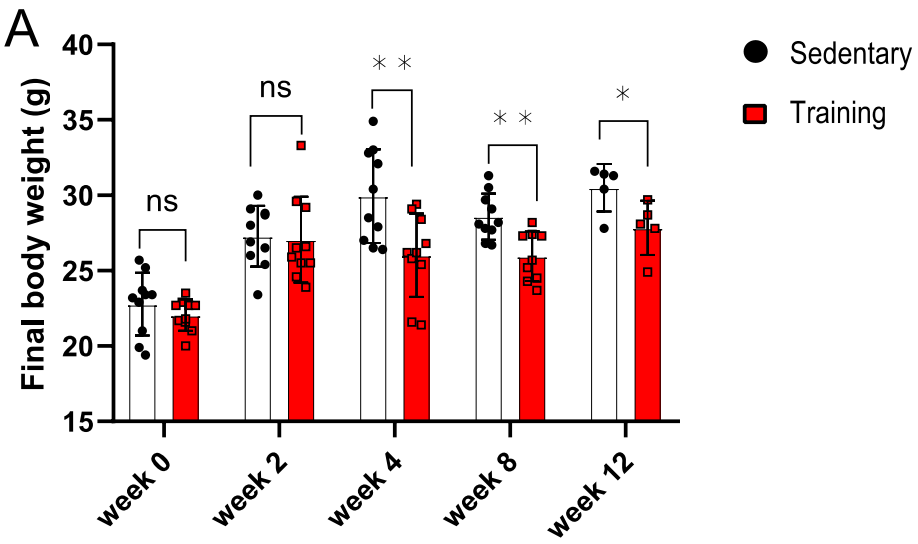

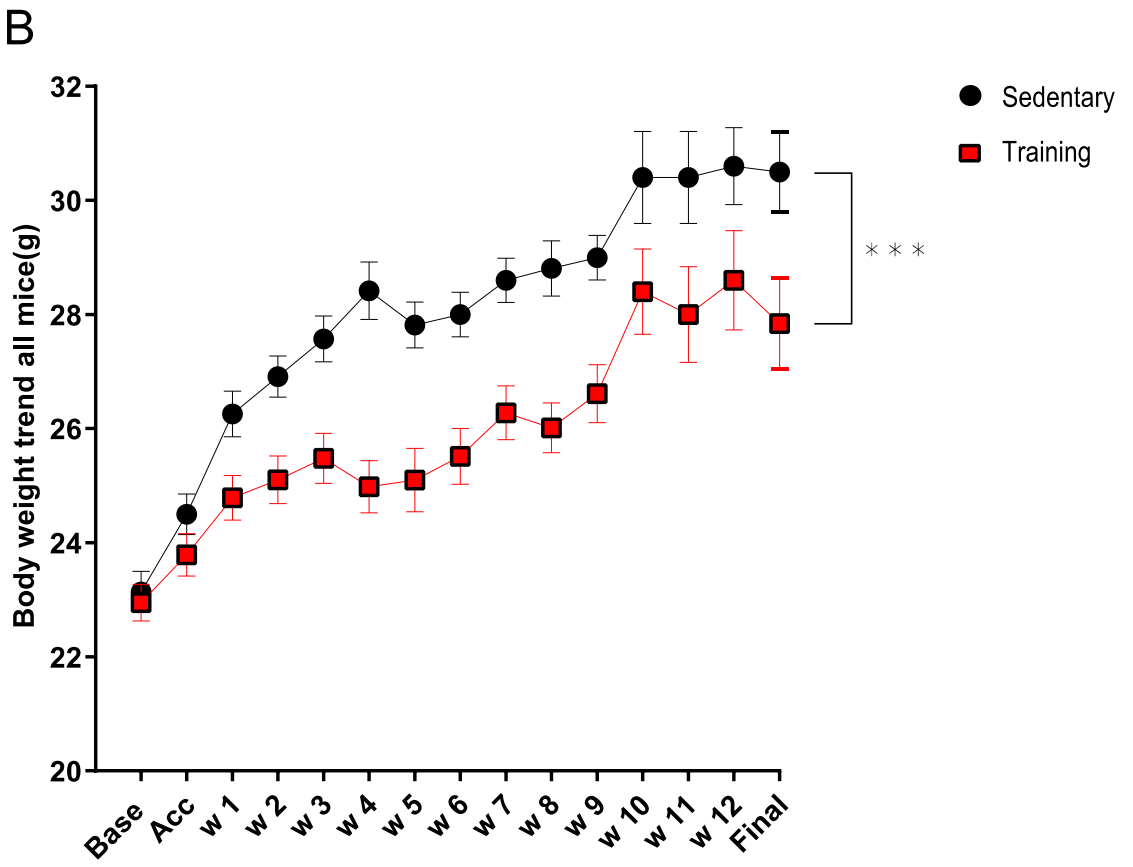

Figure 8. (A) The mice body weight recorded on the corresponding weeks (0, 2, 4, 8, and 12 weeks) at the end of the training period. The sedentary mice served as control group. The averages of each group were shown (n = 5 mice per group), ± SD from two representative experiments (except for 12 weeks group which was done without replication) *p < 0.05, **p < 0.001, ***p < 0.0001, unpaired two-tailed Student's t-test was used within each group (B) Body weight trend changes for all mice at different time-point (n =45 for sedentary group and n= 44 for training group). The group means were represented (n = 5 mice per group), ± SD from two independent representative experiments (except for 12 weeks group which was done without replication), black represents sedentary, training animals were shown in red, ns = not significant, *p < 0.05, **p < 0.001, ***p < 0.0001, two-way ANOVA with Turkey's multiple comparison test was used in statistical analysis between each group.

3.1.2 Heart weight was significantly increased after 8 weeks of training

To determine the effect of endurance training on gross heart morphology, inspection of the heart after organ removal was performed and their weights were carefully measured. After 8 weeks, we observed a larger heart mass in training mice as opposed to their matched sedentary controls. The representative image of mice's heart gross morphology on 8-weeks training was presented on **figure 9**.

Figure 9. Representative gross heart anatomy in 8-weeks training group (right-hand side) and their matched sedentary control (left-hand side). n = 5 mice per group from two independent experiments.

Figure 10 depicted the results of heart weight measurement between two groups on different training time-points. As a baseline measurement, we have also evaluated the heart weight on 0-week training time point after acclimatization showing that both training and sedentary groups showed no difference (p = 0.12). The 8-weeks training group showed an increased cardiac mass compared to their matched control (0.18 g ± 0.01 vs. 0.17 g ± 0.01 respectively, p = 0.04). The similar trend was also observed on the 12-weeks training group (training 0.19 ± 0.02 vs. control 0.17 g ± 0.02, p = 0.08). Furthermore, the endurance training effects on the cardiac mass gain had not yet been perceived after 2- and 4-weeks of training.

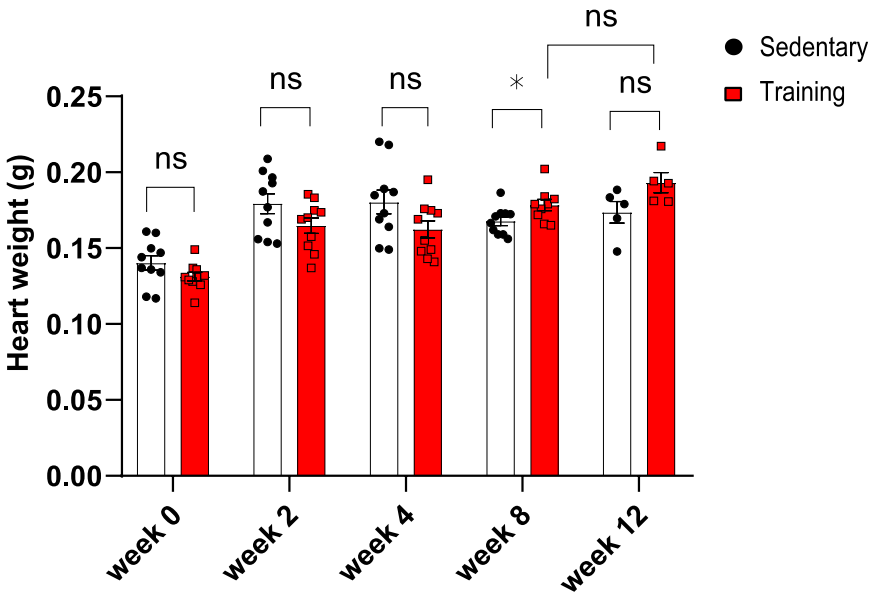

Figure 10. The overall recorded heart weight on 0-, 2-, 4-, 8-, and 12-weeks training timepoints compared exercising animals with their matched sedentary control. The means of each group were shown (n = 5 mice per group), ± SD from two representative experiments (except for 12 weeks group which was done without replication), black represented sedentary mice, training animals were shown red. ns = not significant, *p < 0.05, unpaired two-tailed Student's t test was used within each group and two-way ANOVA Turkey's multiple comparison test was used between groups in statistical analysis.

To further investigate this observation in detail, we continued to measure the tibia length to create the ratio between the heart weight and tibia length. The results were shown in **figure 11**. We concluded that the tibias were getting longer with mean ranging of 16.31 mm ± 0.55 to 18.61 mm ± 0.34 across different time-points. However, these changes were never reached a significant difference between training and sedentary animals. This confirmed that the tibia length could be used reliably as an objective denominator on the characterization of phenotypic changes in morphometry.

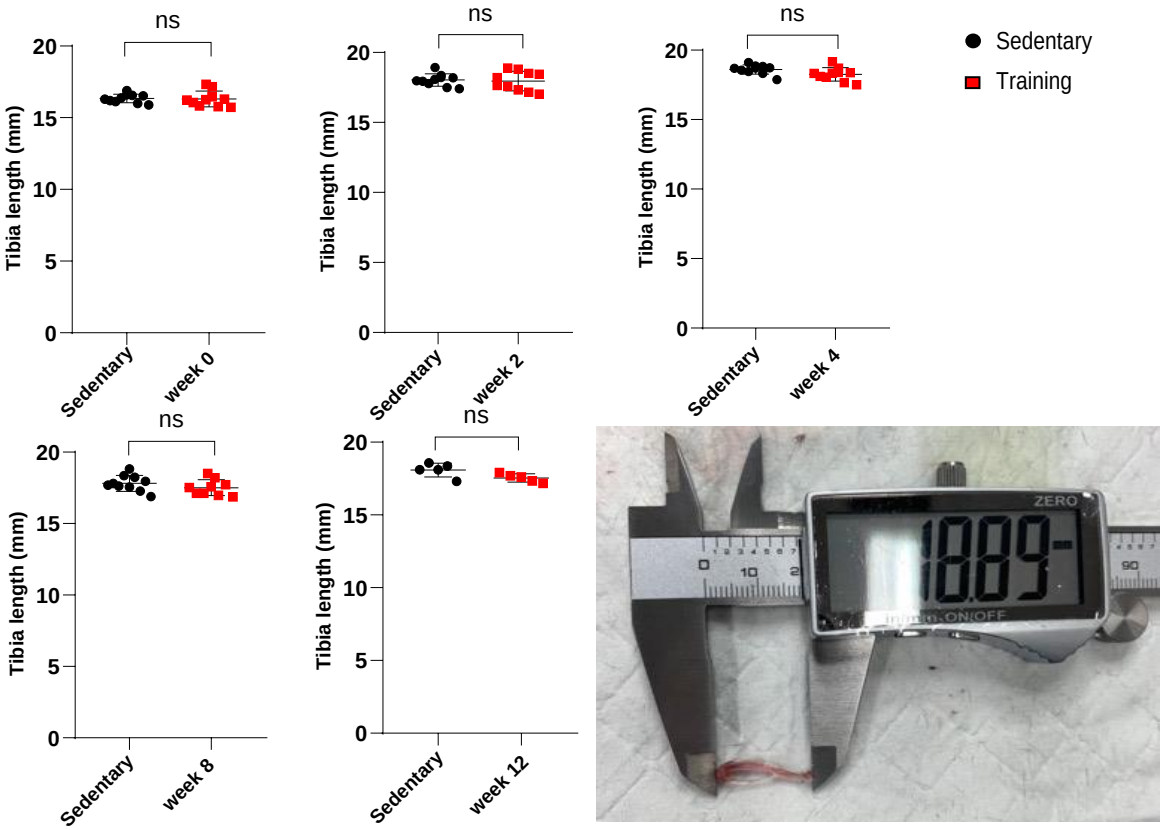

Figure 11. Tibia length measured using precision line scale. The graphs presented the right-sided tibia length measured in mm from each training group (0, 2, 4, 8, 12 weeks) compared to their matched sedentary control. The means of each group were shown (n = 5 mice per group), ± SD from two representative experiments (except for 12 weeks group which was done without replication), black showed sedentary control, red represented training group, ns = not significant, unpaired two-tailed Student's t test was used within each group.

The corresponding heart weight was subsequently divided with tibia length generating a ratio of heart weight/tibia length (mg/mm) as an indicator of cardiac hypertrophy (**figure 12**).

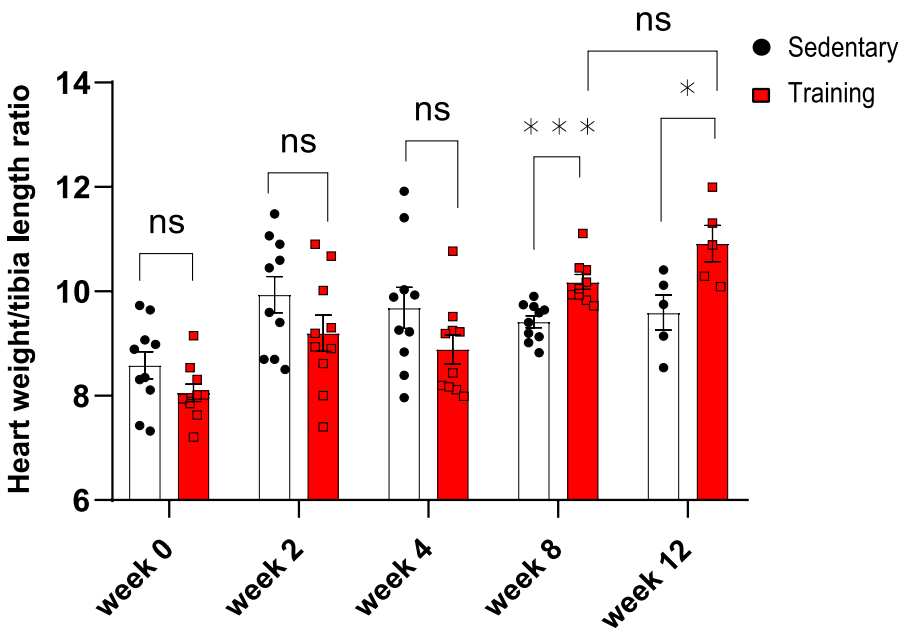

Figure 12. Heart weight/tibia length ratio (mg/mm) across different training time-points (0, 2, 4, 8, 12 weeks). The means of each group were shown (n = 5 mice per group), ± SD from two representative experiments (except for 12 weeks group which was done without replication), black represented sedentary, training animals were pictured red, *p < 0.05, ***p < 0.0001, ns = not significant, unpaired two-tailed Student's t test was used within each group and two-way ANOVA Turkey's multiple comparison test was used between groups in statistical analysis.

These findings underlined the difference of heart weight/tibia length between 8-weeks training mice and their control with counted mean average of 10.2 mg/mm ± 0.4 and 9.7 mg/mm ± 1.3 respectively ($p < 0.0001$). We saw that the heart weight/tibia length ratio was significantly higher in 12-weeks training animals compared to their sedentary control (mean average 10.9 mg/mm ± 0.8 vs. 9.6 g/mm ± 0.8, $p < 0.05$). This finding also further confirmed our hypothesis that continuous increase in cardiac mass was observed starting on 8 weeks of training as a critical time-point.

3.1.3 Skeletal muscle weight trends increased starting from 8 weeks of endurance training

Next, we investigated the effects of forced endurance training on the skeletal muscle weight gain. We isolated the mice skeletal muscles from the *quadriceps femoris* and the *gastrocnemius* muscles. **Figure 13** illustrates the skeletal muscle weight changes among training and sedentary animals.

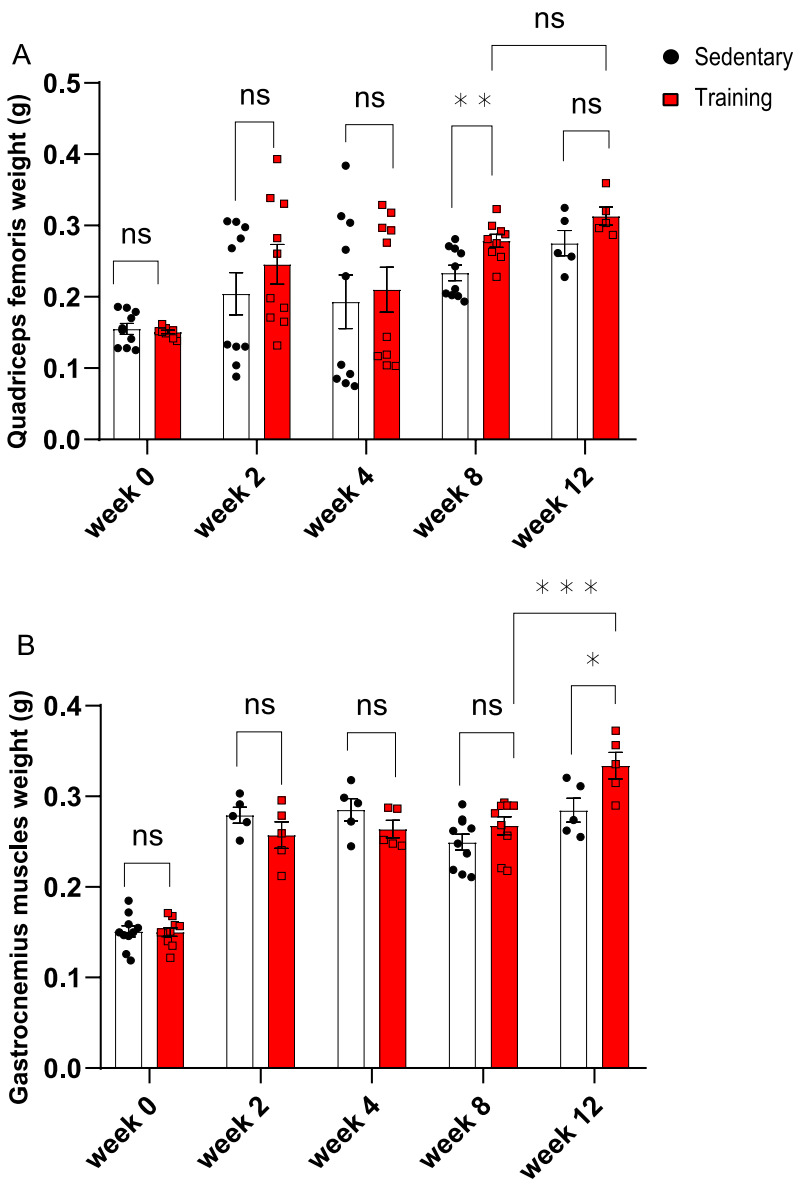

Figure 13. (A) The *quadriceps femoris* weight among groups in three different time-points (0, 2, 4, 8, 12 weeks) (B) The *gastrocnemius* muscles weight measured on 0, 2-, 4-, 8-, and 12-weeks training compared to their matched sedentary control. The means of each group were shown (n = 5 mice per group), ± SD from two representative experiments (except for 12 weeks group which was done without replication), black represented sedentary, training animals were colored red, ns = not significant, *p < 0.05, **p < 0.001, ***p < 0.0001, unpaired two-tailed Student's t test was used within each group and two-way ANOVA Turkey's multiple comparison test was used between groups in statistical analysis.

Here both of *quadriceps femoris* and *gastrocnemius* muscles weight failed to show significant differences between training and sedentary groups on 2 and 4 weeks (p = 0.32 and p = 0.74 for *quadriceps femoris*, p = 0.23 and p = 0.21 for *gastrocnemius* muscle respectively). The *quadriceps femoris* muscle weight was significantly increased in 8-weeks training group compared to sedentary control (mean weight average of 0.28 g ± 0.03 in training compared to 0.23 g ± 0.03 in sedentary control, p < 0.001). This increase was though not observed significant in the 12-weeks training group (p = 0.12). Similarly, the gastrocnemius muscle also showed significant weight gain

in 12 weeks of training (mean average weight of 0.33 g ± 0.03 in training vs. 0.29 g ± 0.03 in sedentary groups, $p < 0.05$). This result confirmed that not only cardiac but also skeletal muscles mass was increased starting at training week 8 in response to forced chronic endurance exercise.

The following tables (**table 3 and 4**) described the morphometric analysis between training and sedentary groups. The data presented by mean average ± standard deviation of morphometric parameters in each group on different time-points (total n = 89 mice, 45 mice in sedentary controls, 44 mice in training groups).

Table 3. Morphometric measurements of sedentary groups (n = 45)

Sedentary mice	Final body weight (g)	Heart weight (g)	Tibia length (mm)	Heart weight/Tibia length (mg/mm)	Gastrocnemius length (g)	Quadriceps femoris weight (g)
0 week	22.78 ± 2.08	0.14 ± 0.02	16.34 ± 0.31	8.60 ± 0.83	0.15 ± 0.02	0.16 ± 0.02
2 weeks	27.46 ± 1.27	0.18 ± 0.02	18.03 ± 0.44	9.9 ± 1.1	0.28 ± 0.02	0.20 ± 0.09
4 weeks	28.55 ± 2.47	0.18 ± 0.03	18.61 ± 0.34	9.7 ± 1.3	0.29 ± 0.03	0.19 ± 0.12
8 weeks	28.59 ± 1.53	0.17 ± 0.01	17.82 ± 0.56	9.4 ± 0.4	0.25 ± 0.03	0.23 ± 0.03
12 weeks	30.50 ± 1.58	0.17 ± 0.02	18.09 ± 0.48	9.6 ± 0.8	0.29 ± 0.03	0.28 ± 0.04

Table 4. Morphometric measurements of training groups (n = 44)

Training mice	Final body weight (g)	Heart weight (g)	Tibia length (mm)	Heart weight/Tibia length (mg/mm)	Gastrocnemius length (g)	Quadriceps femoris weight (g)
0 week	22.06 ± 1.04	0.13 ± 0.01	16.31 ± 0.55	8.1 ± 0.5	0.15 ± 0.02	0.15 ± 0.01
2 weeks	26.57 ± 1.92	0.17 ± 0.02	17.96 ± 0.70	9.2 ± 1.1	0.26 ± 0.03	0.25 ± 0.09
4 weeks	24.65 ± 2.71	0.16 ± 0.02	18.26 ± 0.48	8.9 ± 0.9	0.26 ± 0.02	0.21 ± 0.01
8 weeks	25.96 ± 1.63	0.18 ± 0.01	17.52 ± 0.56	10.2 ± 0.4	0.27 ± 0.03	0.28 ± 0.03
12 weeks	27.84 ± 1.78	0.19 ± 0.02	17.54 ± 0.29	10.9 ± 0.8	0.33 ± 0.03	0.31 ± 0.03

3.2 Cardiomyocytes and skeletal myocytes surface area in endurance training

Based on our previous findings that the heart and skeletal muscle weight/tibia length ratio increased after exposed to 8 weeks of forced exercise training on the treadmill, we examined the hearts by histology. We stained the tissue with antibodies which bond particularly to cardiomyocytes or skeletal muscle fiber cell membrane and their nuclei.

3.2.1 Cardiomyocytes cross-sectional surface area was increased throughout endurance training period but plateaued in 12 weeks measurement.

Figure 14 showed the representative microscopic images taken to compare cross-sectional area of cardiomyocytes in the middle cardiac section at the height of papillary muscles to visualize both left and right ventricles wall as well as their chambers. The cardiomyocytes were then counted based on the corresponding numbers of SYTOX-green stained nuclei and the circumferential WGA-stained cell membrane were calculated manually using image processing application ImageJ2 (NIH, Maryland, USA) for quantification of cross-sectional areas in mm^3. Four to five images using 40x confocal objective were captured in one heart section covering approximately 600-800 cardiomyocytes and the counting was done blindly in triplicates to allow a valid and highly reliable surface area measurement. The cells which touched the image borders and without stained nuclei were excluded from the counting. The measured surface areas were then tabulated and compared between training and sedentary control groups. Furthermore, the percentage of cell numbers in corresponding categories of surface area size were also completed to represent a better information regarding the cell size proportion across the examined samples.

The baseline measurement was made using the comparison of 0-week training and their matched 0-week sedentary controls which showed a roughly similar delineation of cardiomyocytes surface area (**figure 14 A** and **B**). The 2- and 4-week training groups and their control were pictured on **figure 14 C** and **D** as well as **E** and **F**, respectively. As shown in **figure 14 G** and **H,** the cardiomyocytes in 8-weeks training group were apparently larger compared to their sedentary control which matched consistently with the previously obtained morphometric measurements. The same trends were observed in the 12-weeks timepoint (**figure 14 I** and **J**)

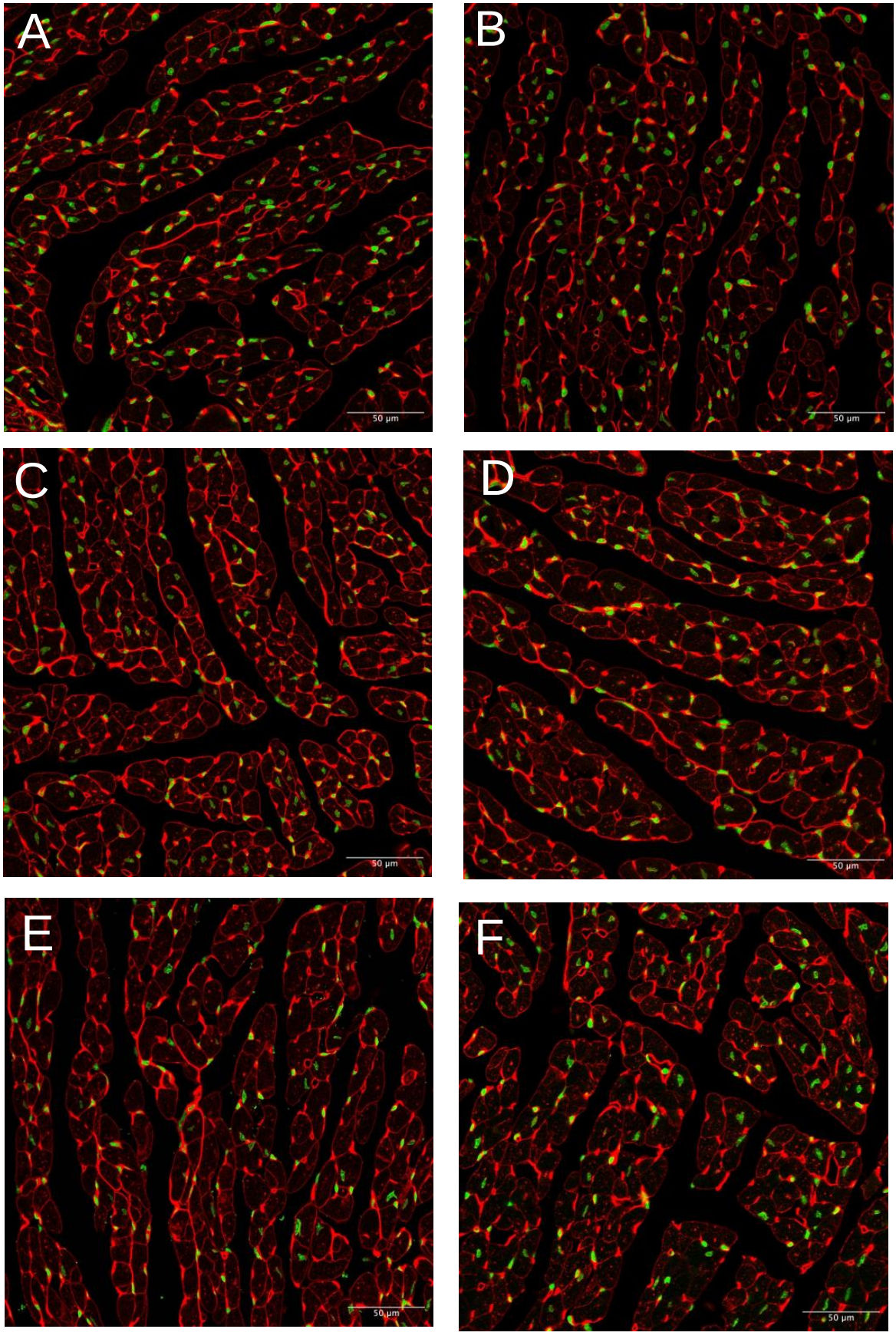
A
50 µm
B
50 µm
C
50 µm
D
50 µm
E
50 µm
F
50 µm

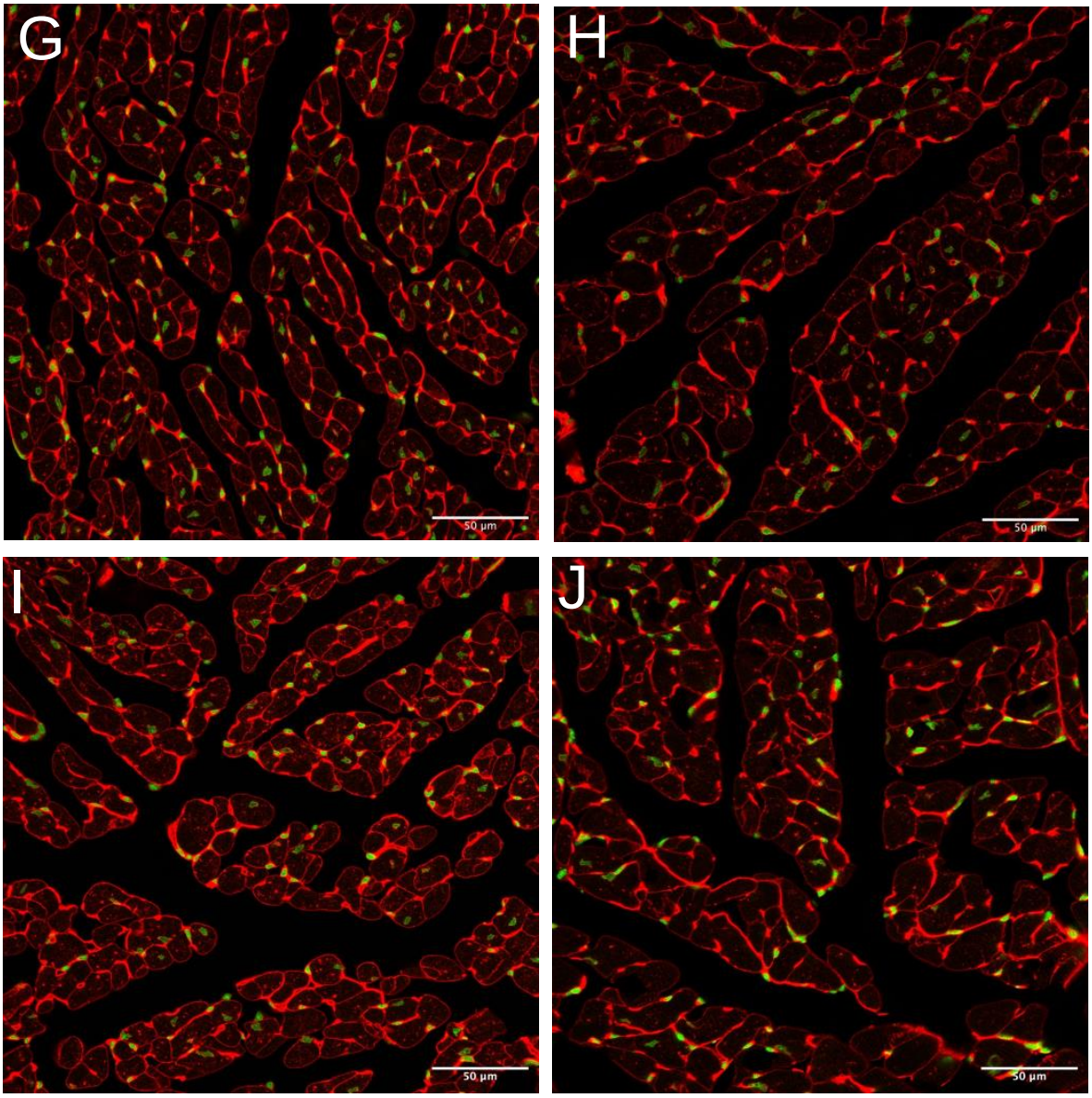

Figure 14. The representative microscopic images of cross-sectionally cut cardiomyocytes of left ventricles after staining the sarcolemma with WGA-Alexa Fluor® 647 (1:100 dilutions, showed in red) and the nuclei with SYTOX green® (1:1000 dilution, showed in green). (A) The cardiomyocytes of matched 0-week sedentary mice compared to (B) their 0-week training counterpart as baseline measurement. (C) The 2-weeks sedentary and (D) their training counterpart. The 4-weeks control and training were pictured in (E and F, respectively). (G) The 8-weeks sedentary control cardiomyocytes in comparison with (H) the 8-weeks training heart showed an enlargement of cardiomyocytes in endurance training group. This trend could be also observed in 12-weeks-duration (I, sedentary and J, training) (n = 5 mice per group, two independent experiments, bar length represents 50 µm).

The differential average cell size in mm^2 quantification and the proportional shifts on cardiomyocytes cross-sectional area among training and sedentary groups were pictured in **figure 15**. The evaluation of cardiomyocytes cross-sectional area rearrangement was done by manually categorizing the percentage of cell number into their corresponding gradually increased sizes.

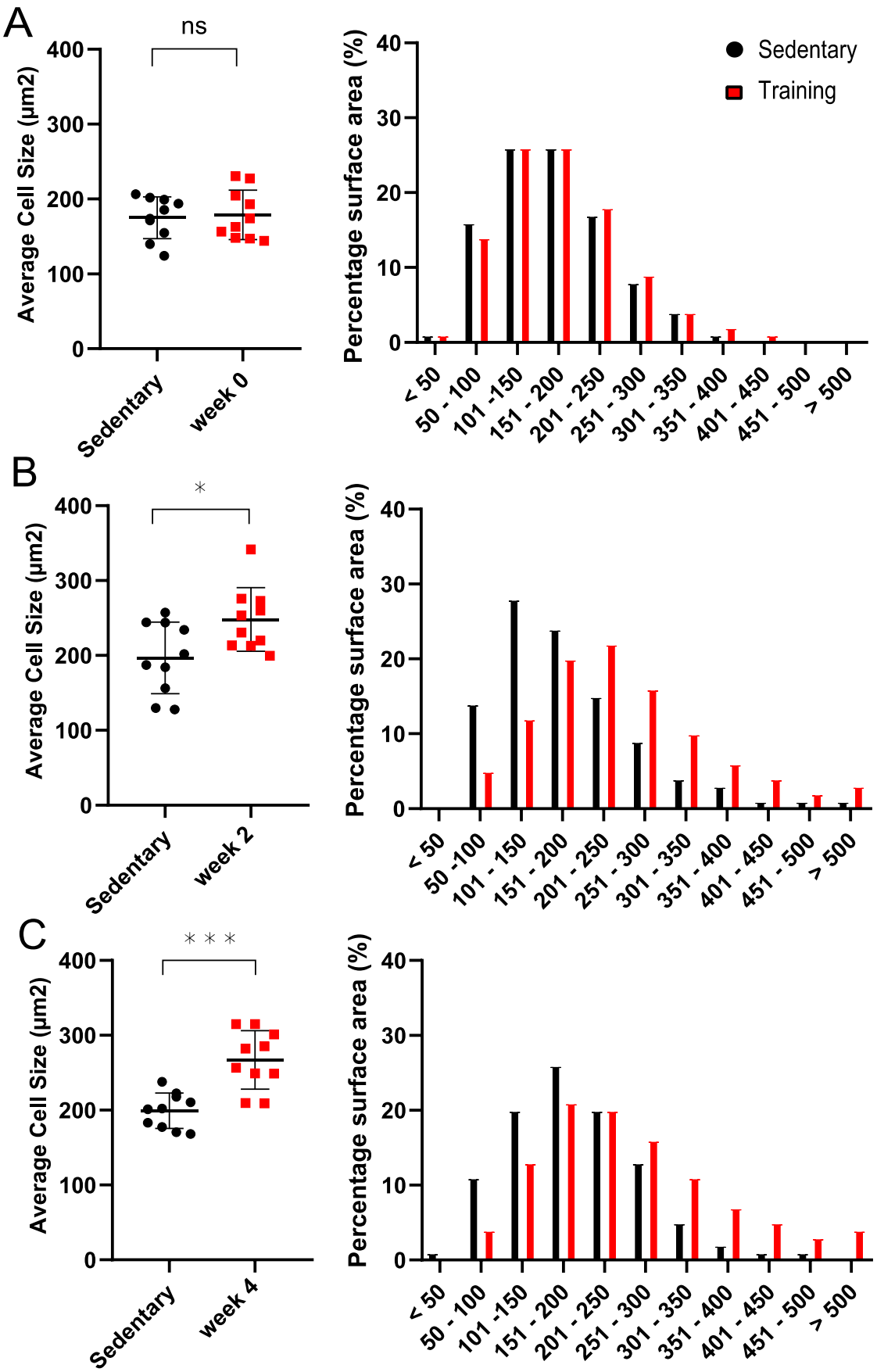
A
ns
Average Cell Size (µm2)
400
300
200
100
0
Sedentary
week 0
Percentage surface area (%)
40
30
20
10
0
Sedentary
Training
< 50
50 - 100
101 -150
151 - 200
201 - 250
251 - 300
301 - 350
351 - 400
401 - 450
451 - 500
> 500
B
*
Average Cell Size (µm2)
Sedentary
week 2
Percentage surface area (%)
C
* * *
Average Cell Size (µm2)
Sedentary
week 4
Percentage surface area (%)

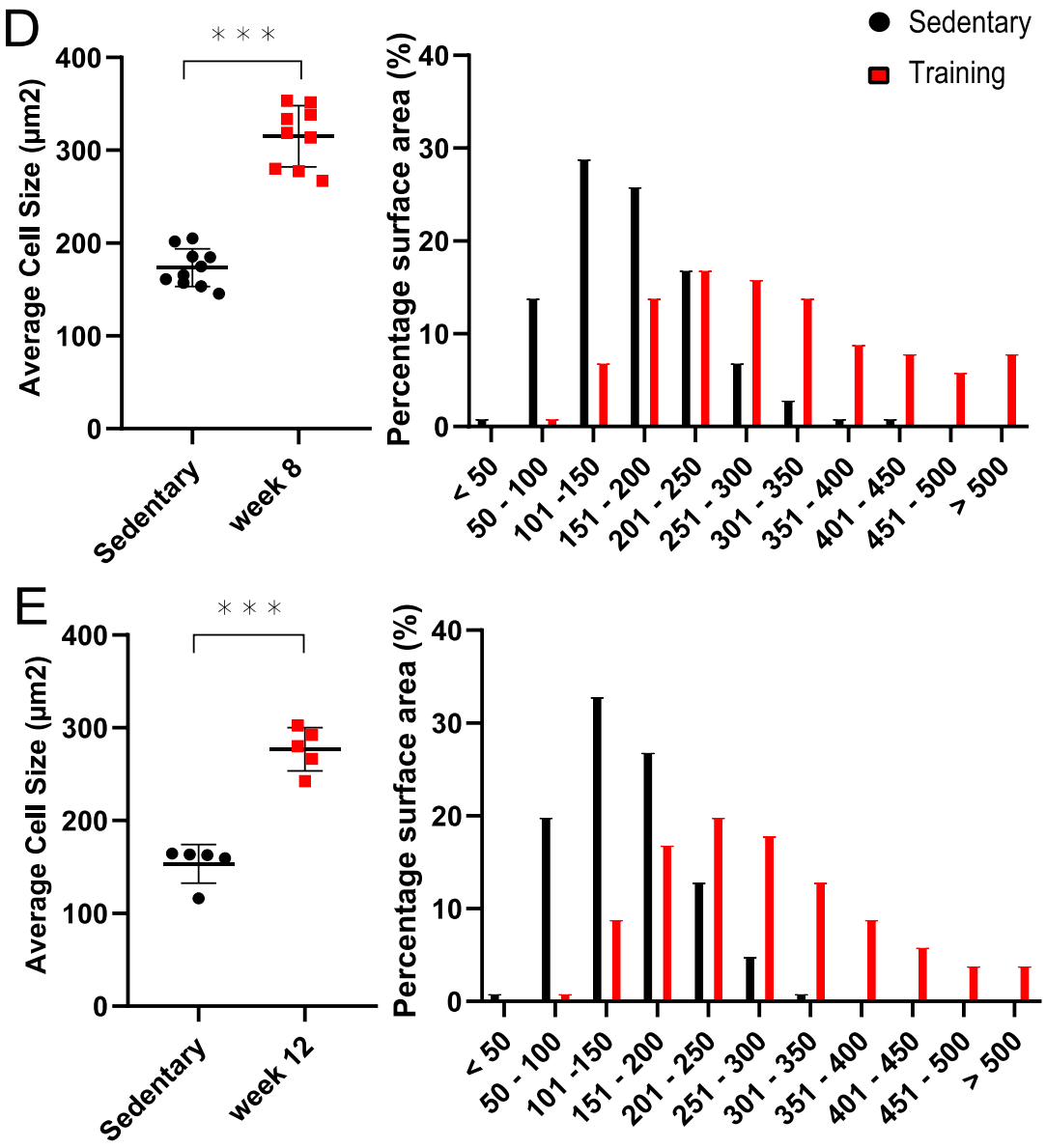

Figure 15. The average cross-sectional size of cardiomyocytes and their percentage of cell number in the categorical size were depicted for (A) Baseline 0-week, (B) 2-weeks, (C) 4-weeks, (D) 8-weeks, and (E) 12-weeks training groups, each compared with their corresponding sedentary controls. The means of each group were shown (n = 5 mice per group), ± SD from two representative experiments, black represents sedentary, training animals were shown in red, ns = not significant, *p < 0.05, ***p < 0.0001, an unpaired two-tailed Student's t test was used within each group.

There was no significance difference appreciated on mean average cell size between 0-week training compared to their sedentary control (178.90 mm^2 ± 33.08 vs 175.10 mm^2 ± 27.86, p = 0.79) as well as in cardiomyocytes number-size proportion (**figure 15 A)**.

We found a statistically significant difference in mean average cardiomyocytes surface area quantification between 8-weeks training and control groups (315.10 mm^2 ± 32.94 and 173.50 mm^2 ± 20.41 respectively, p < 0.0001). Furthermore, the shifting of cardiomyocytes number percentage

to the right was also appreciated in 8-weeks training group (**figure 15 D**) indicating a higher proportion of cells which possessed larger surface area (201-300 mm^2 in training compared to 101-200 mm^2 in sedentary group).

Figure 15 E showed the larger mean cardiomyocytes surface area of 12-weeks training compared to the sedentary group (276.80 mm^2 ± 23.37 vs. 153.30 mm^2 ± 20.90, $p < 0.0001$). The shift of cardiomyocytes size to the right corresponding to an increase proportion towards the larger surface area (201-300 mm^2) was also confirmed in these groups.

Due to different batches of animals from at least two independent experiments used in this study, the data from training mice was averaged and normalized against the mean of their corresponding sedentary counterparts. From **figure 16**, we concluded that cardiac hypertrophy in exercising animals was first became apparent starting from 8 weeks of training duration and plateaued afterwards, while we have not observed any significant difference of cardiomyocytes surface area recorded between 8-weeks and 12-weeks training group. The maximum fold-change of cardiomyocytes surface area was recorded in 8-weeks as well as 12-weeks training group which showed approximately 1.8-times enlargement compared to the sedentary controls. Meanwhile the 2- and 4-weeks training group showed only 1.26 and 1.34-times cardiomyocytes enlargement in opposed to their sedentary controls, respectively.

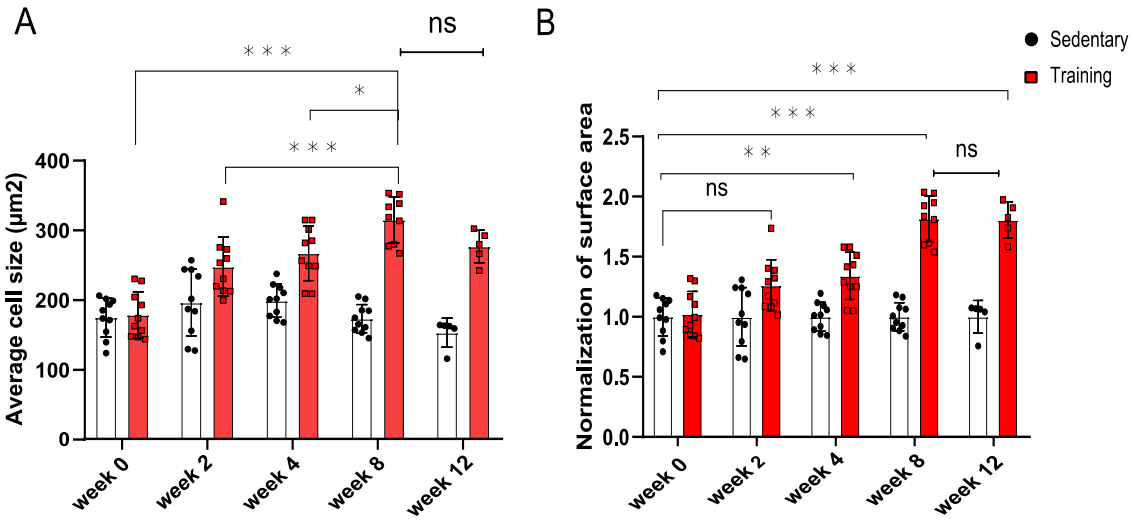

Figure 16. The tabulation of average cardiomyocytes surface area among 0, 2-, 4-, 8-, and 12-weeks training groups without (A) and with (B) normalization against the mean of corresponding sedentary controls. The minimum and maximum normalization method was used in this study. The means of each group were shown (n = 5 mice per group), ± SD from two representative experiments (except for 12 weeks group which was done without replication), black represents sedentary, training animals was shown red, ns = not significant, *p < 0.05, **p < 0.001, ***p < 0.0001, unpaired two-tailed Student's t test was used within each group and two-way ANOVA Turkey's multiple comparison test was used between groups in statistical analysis.

3.2.2 Skeletal myocytes fibers surface area increase was observed in training animals

After analyzing the cardiomyocytes histological surface area, we also investigated the skeletal muscle's histological changes using the same methods. **Figure 17** showed the representative

microscopic images taken to compare cross-sectional area of skeletal myocytes cut evenly at the center of muscle belly.

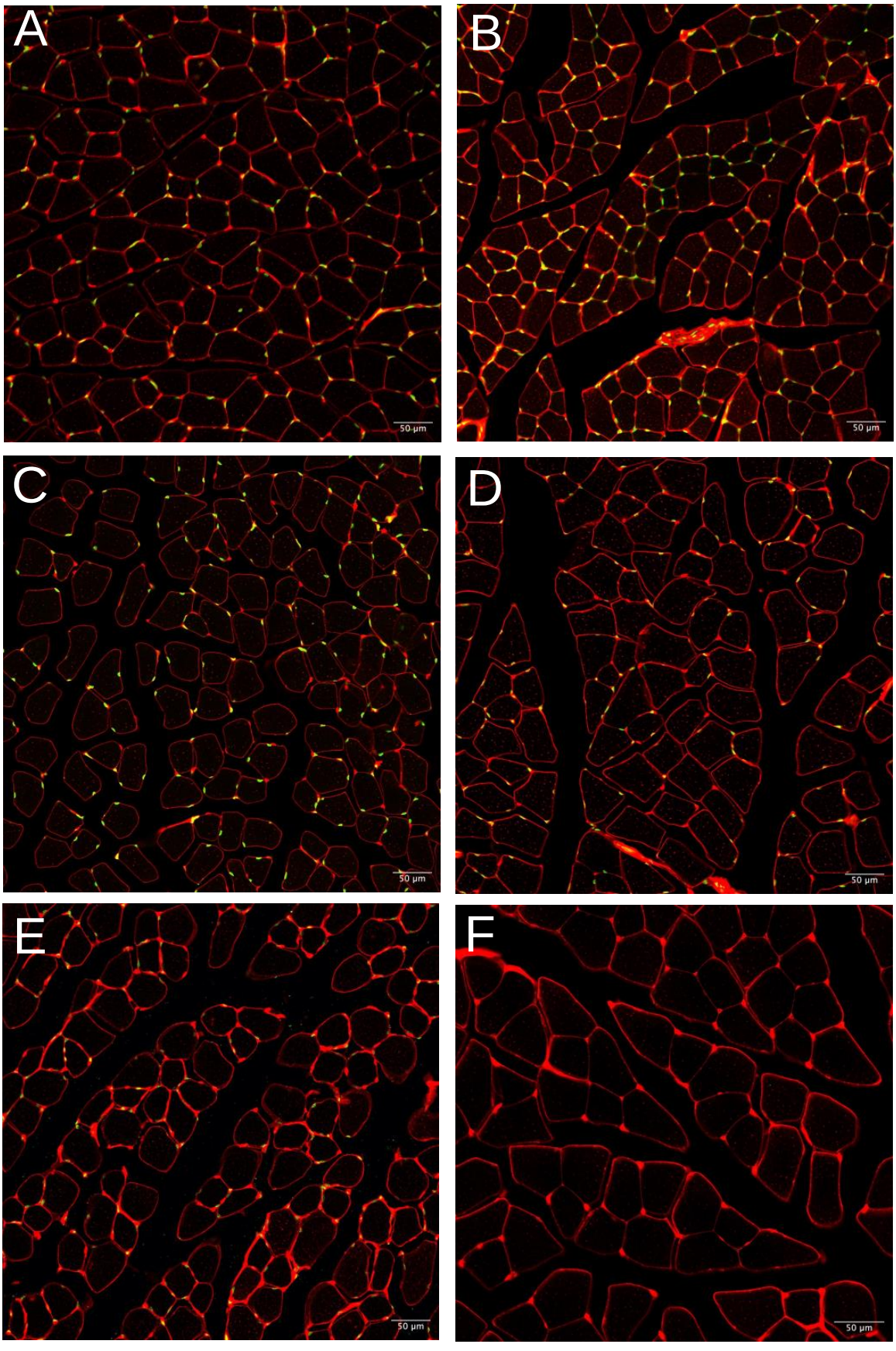

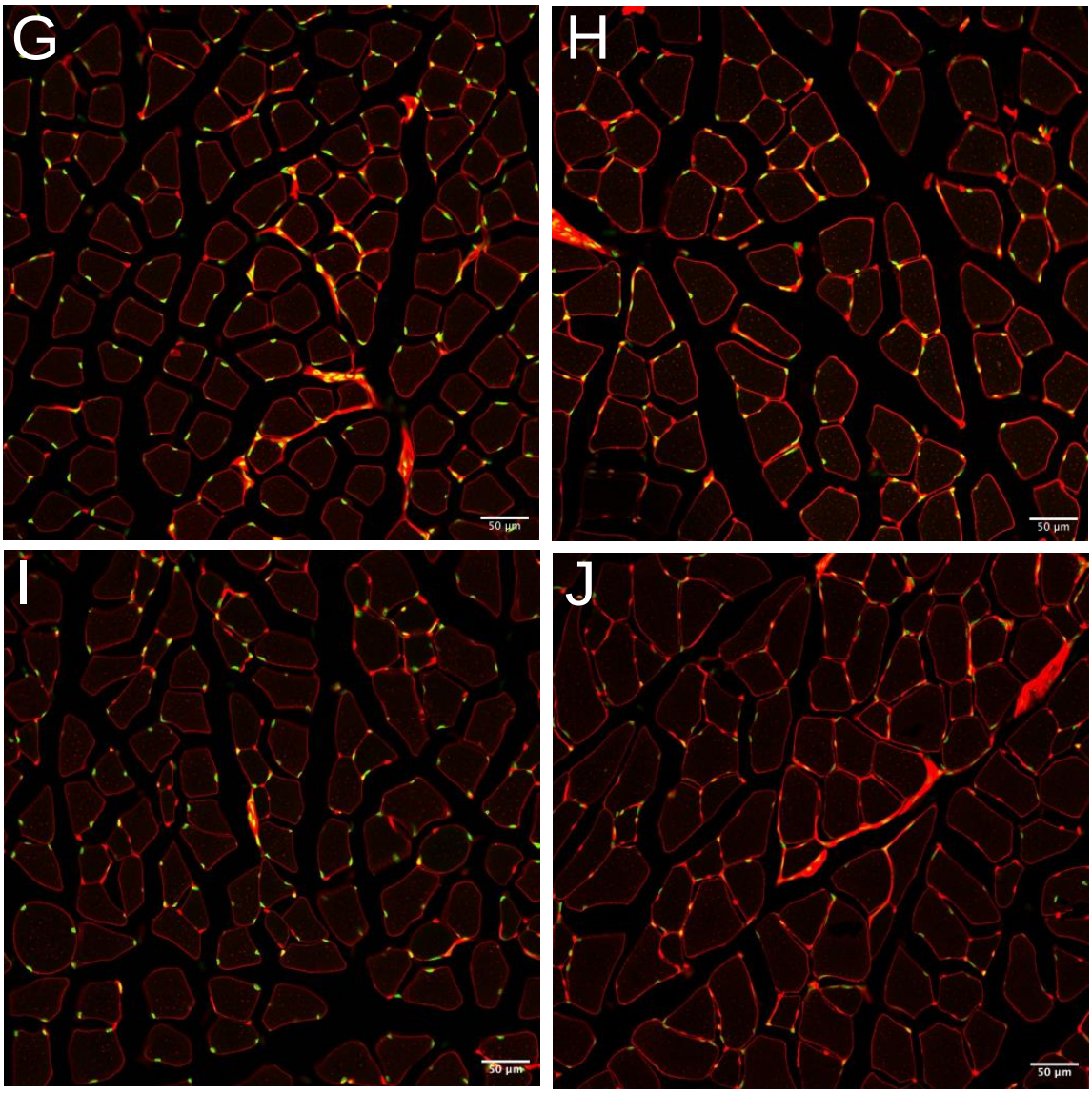

Figure 17. The representative images of skeletal myocytes in cross-section stained with WGA-Alexa Fluor® 647 (1:100 dilution, shown in red) and SYTOX green® (1:1000 dilution, shown in green). (A) The skeletal muscle fibers of matched 0-week sedentary mice compared to (B) their 0-week training counterpart as baseline measurement. (C) Sedentary and (D) 2-weeks training. The 4 weeks sedentary and training were depicted on (E) and (F). (G) The 8-weeks sedentary control skeletal myocytes in comparison with (H) the 8-weeks training animals showed a relative myocytes enlargement in endurance training group. These changes could be also observed in the 12-weeks' time point (I, sedentary and J, training).

Figure 18 showed the baseline images of 0-week training and sedentary groups which did not differ (mean average myocytes surface area size of 1420 $mm^2 \pm 233.90$ in training vs. 1546 $mm^2 \pm 226.60$ in sedentary animals, $p = 0.24$). In the 8-weeks training group however, a slightly larger cross-sectional area was observed in comparison to the sedentary counterparts (mean average myocytes surface area size of 1743 $mm^2 \pm 160.20$ in training and 1490 $mm^2 \pm 252.70$ in sedentary group, $p < 0.05$). The percentage of skeletal myocytes were also largely located in the 1001-2000 mm^2 area measured in the baseline groups and shifted to the right towards 1501-2500 mm^2 region in 8-weeks training group in relative to their control. A large proportion of skeletal myocytes in 8-

weeks sedentary control however fell into 1001-2000 mm^2 which mirrored the quantification results in baseline 0-week group. These results verified that the endurance training increases the myocytes caliber not only in heart tissue but also in skeletal muscle fibers starting from 8 weeks of training.

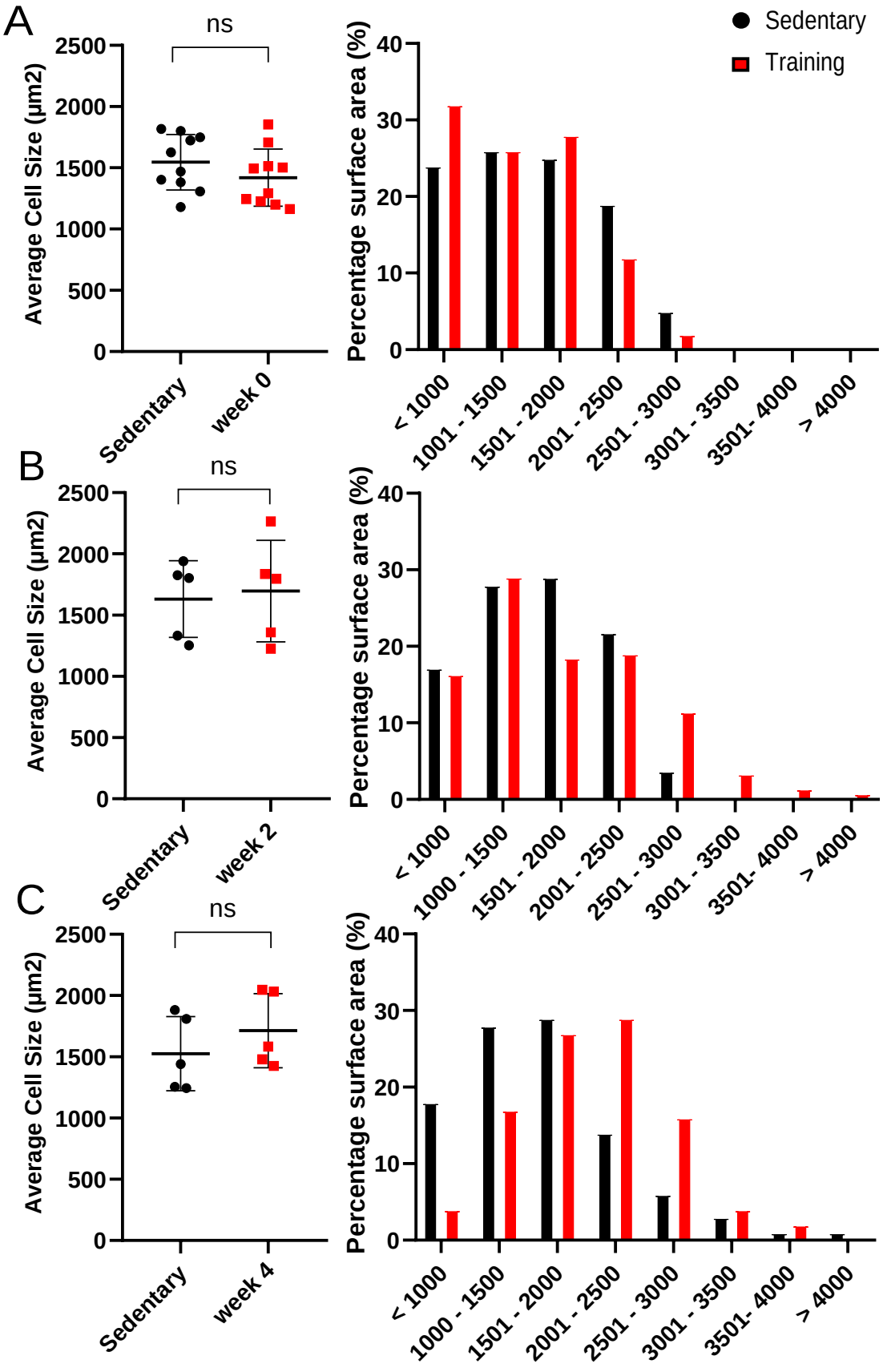

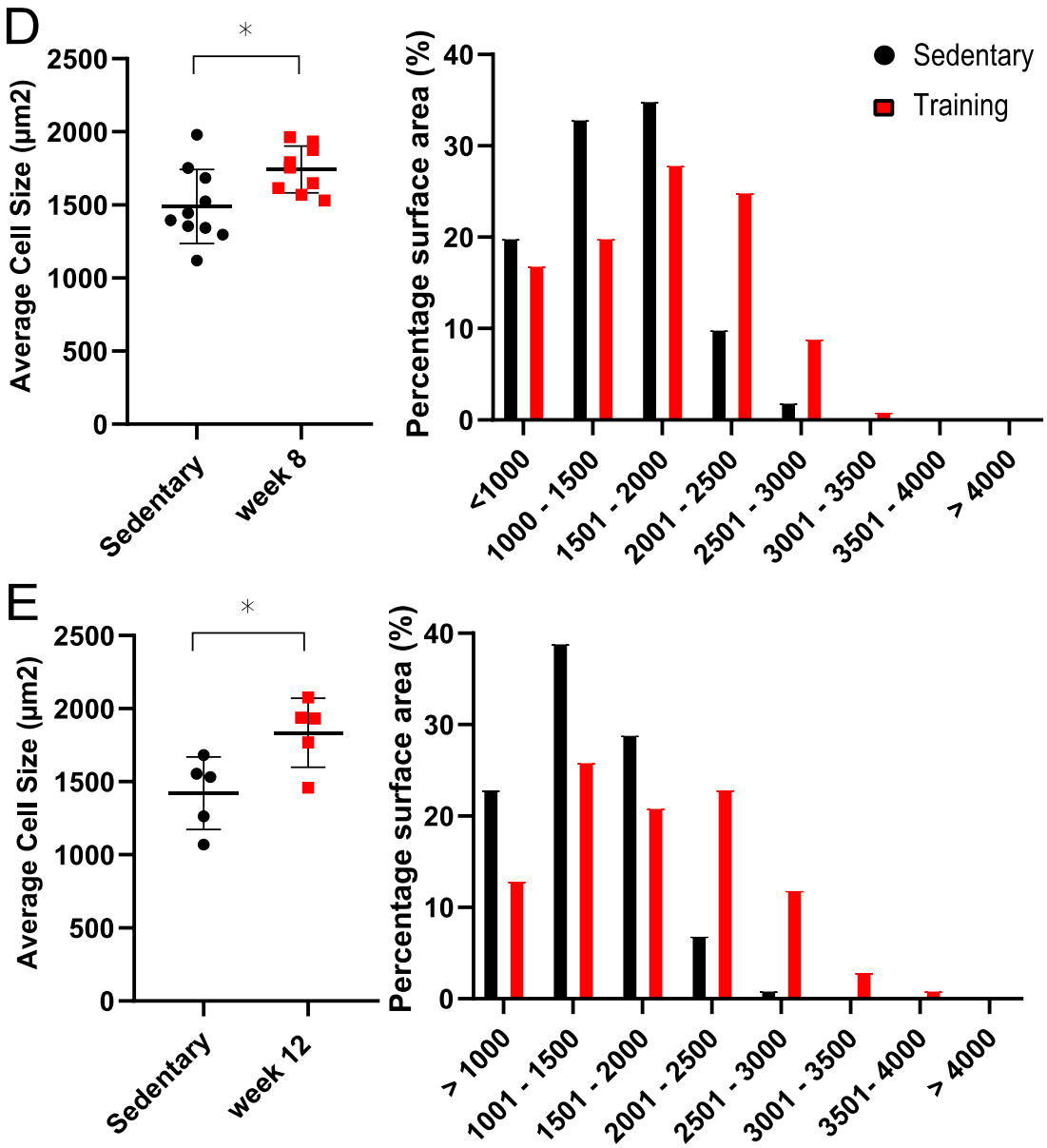

Figure 18. The average cross-sectional size of skeletal myocytes and their percentage of cell number in the categorical size were depicted for (A) Baseline 0-week, (B) 2-weeks, (C) 4-weeks, (D) 8-weeks, and I 12-weeks training groups, each compared with their corresponding sedentary controls. The means of each group were shown (n = 5 mice per group), ± SD from two representative experiments, black represented sedentary, training animals were shown in red, ns = not significant, *p < 0.05, an unpaired two-tailed Student's t test was used within each group.

The outcomes in 12-weeks again replicated the 8-week training group with mean average skeletal myocytes surface area of 1835 $mm^2 \pm 236.30$ in training and 1421 $mm^2 \pm 248.20$ in control group ($p < 0.05$). The shift of myocytes percentage which having larger surface area to the right towards 1501-2500 mm^2 also occurred in this treatment group validating the presence of skeletal muscle hypertrophy on the 12 weeks of endurance training.

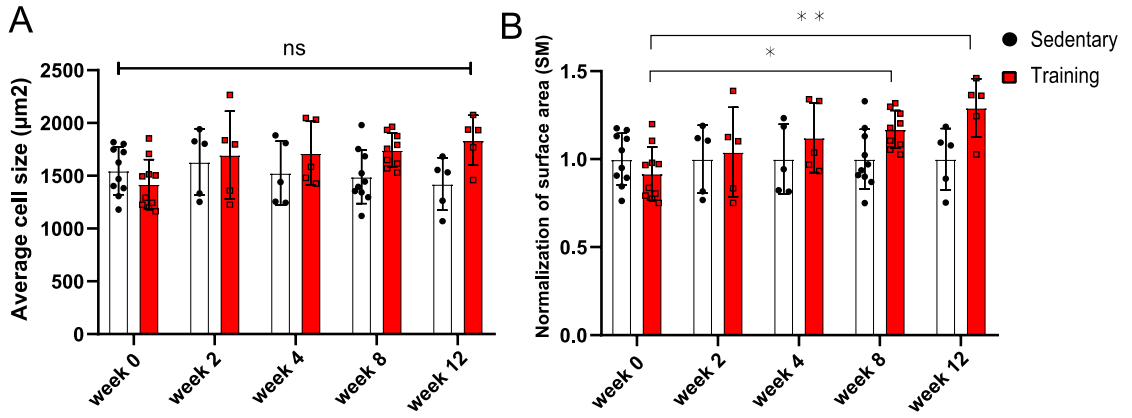

Figure 19. The documented average skeletal myocytes surface area among 0, 2-, 4-, 8-, and 12-weeks training groups without (A) and with (B) normalization against the mean of corresponding sedentary controls. The means of each group were presented, n = 5 mice per group, ± SD from one representative experiment, black represented sedentary, training group showed in red, ns = not significant, *p < 0.05, **p < 0.001, an unpaired two-tailed Student's t test was used within the group, and two-way ANOVA Turkey's multiple comparison test was used between groups in statistical analysis, bar length represents 100 µm).

Figure 19 A and B represented the normalized data on muscle fibers size fold-change which showed 1.17- and 1.29-times enlargement in 8-weeks and 12-weeks training groups respectively in comparison with 0-week baseline reflecting the skeletal muscle hypertrophy.

3.3 The hypertrophied cardiac and skeletal muscles in trained animals showed neither inflammation nor fibrosis

The quantification of cardiomyocytes and skeletal myocytes cross-sectional area showed the development of hypertrophy in trained animal started on 8 weeks and 12 weeks. Therefore, we evaluated that physiological hypertrophy on these time-points was not associated with pathological inflammation and fibrosis. We stained the frozen sections of both heart and skeletal muscle with hematoxylin-eosin to visualize inflammatory cells infiltration as well as picrosirius red to envisage fibrotic area. The representative results are presented on **figure 20**.

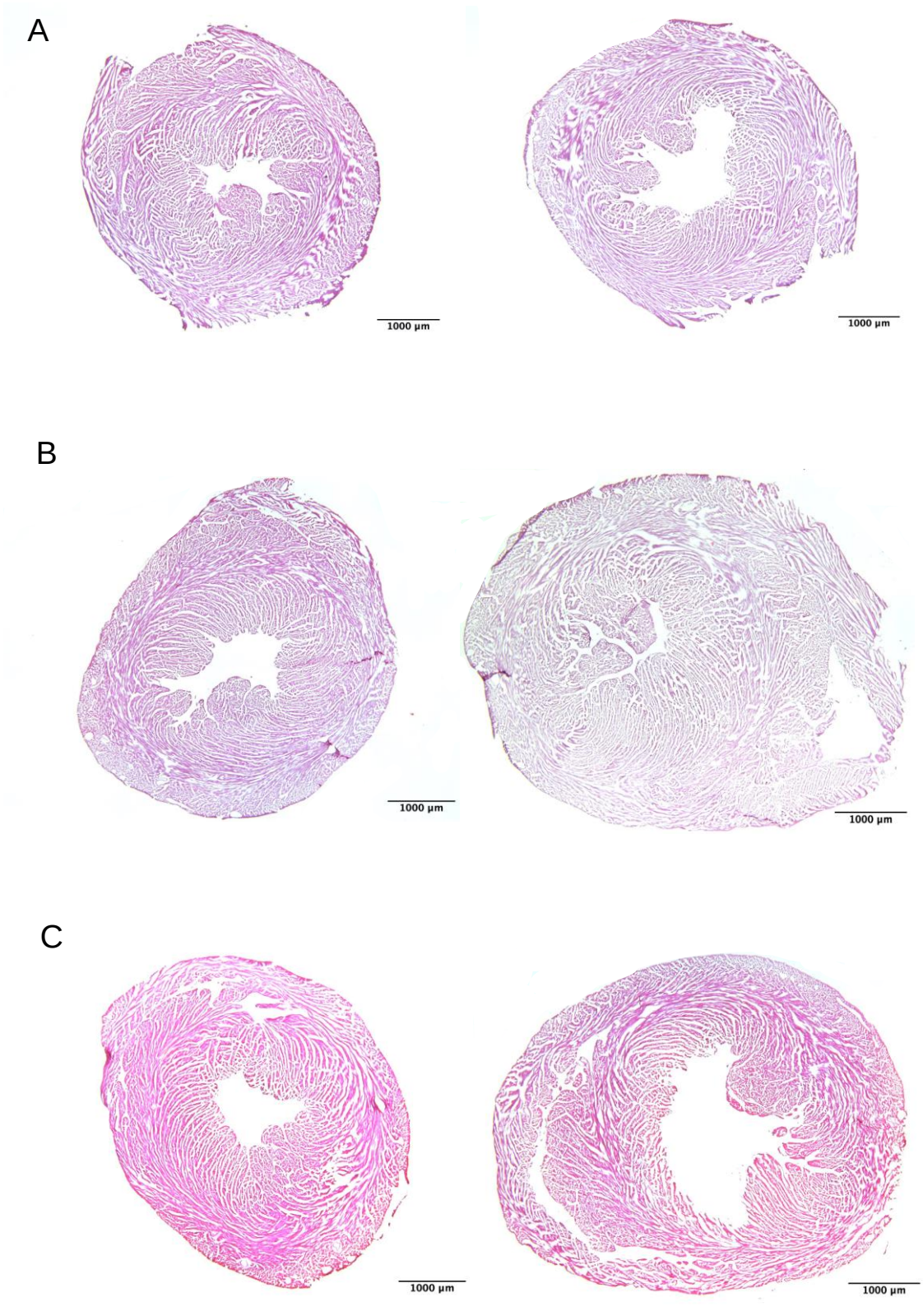
A
1000 µm
1000 µm
B
1000 µm
1000 µm
C
1000 µm
1000 µm

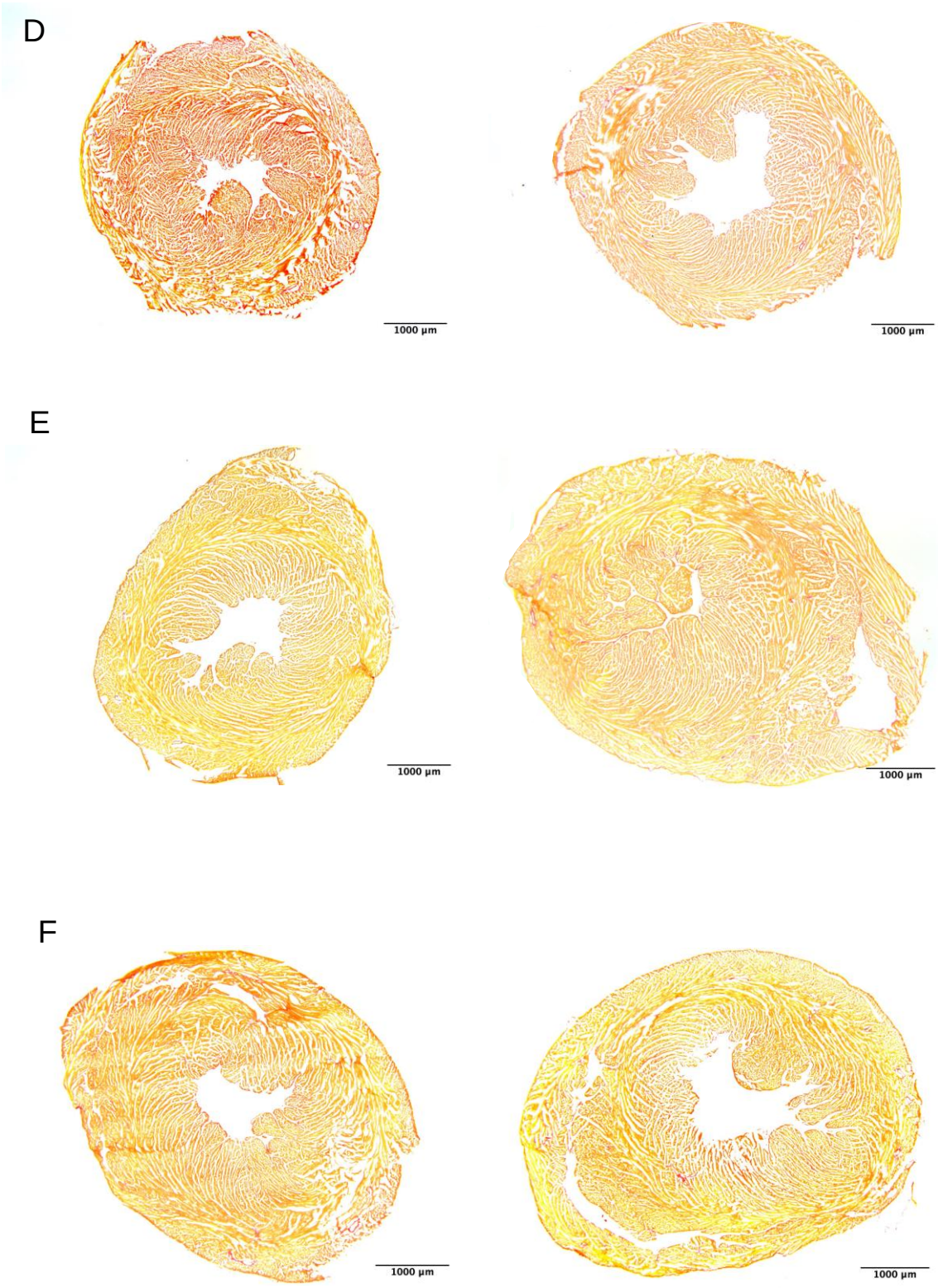

Figure 20. The representative heart images stained with hematoxylin-eosin (HE) and picrosirius red to show inflammation and fibrosis. On each staining section, the sedentary controls were always pictured on the left and their training counterparts on the right (A) Baseline 0-week HE, (B) 8-weeks HE, (C) 12-weeks HE, (D) 0-weeks picrosirius red, I 8-weeks picrosirius red, (F) 12-weeks picrosirius red. (n = 5 mice per group, two independent experiments, bar length represented 1000 µm).

The same methods were implemented to study the inflammatory cells infiltration causing fibrosis in skeletal muscle samples of training animals. The results are shown in **figure 21**. After an overview appraisal of the heart and skeletal muscles specimens, the inflammatory cells and fibrosis on training hearts were not observed after 8- and 12-weeks training.

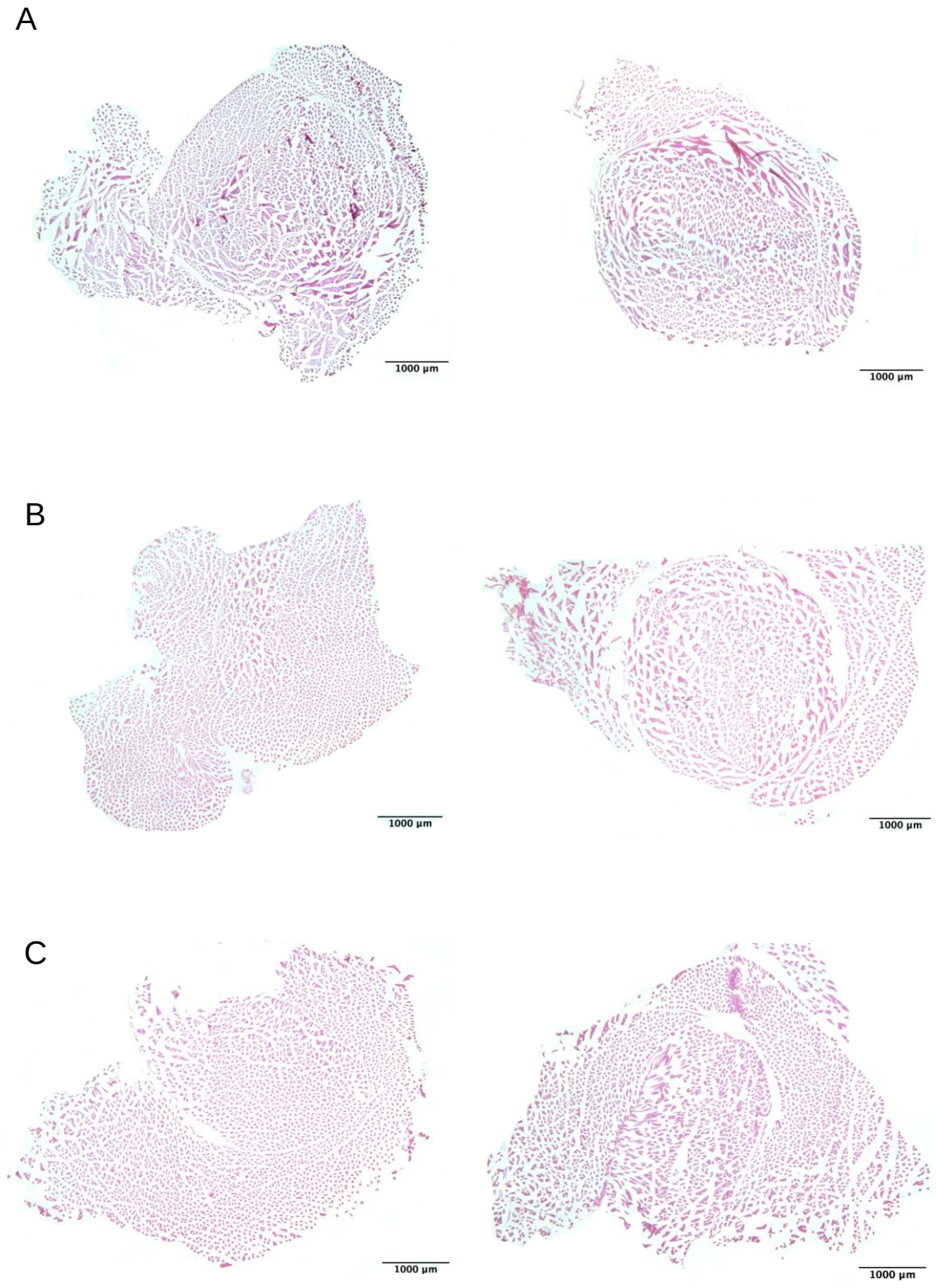

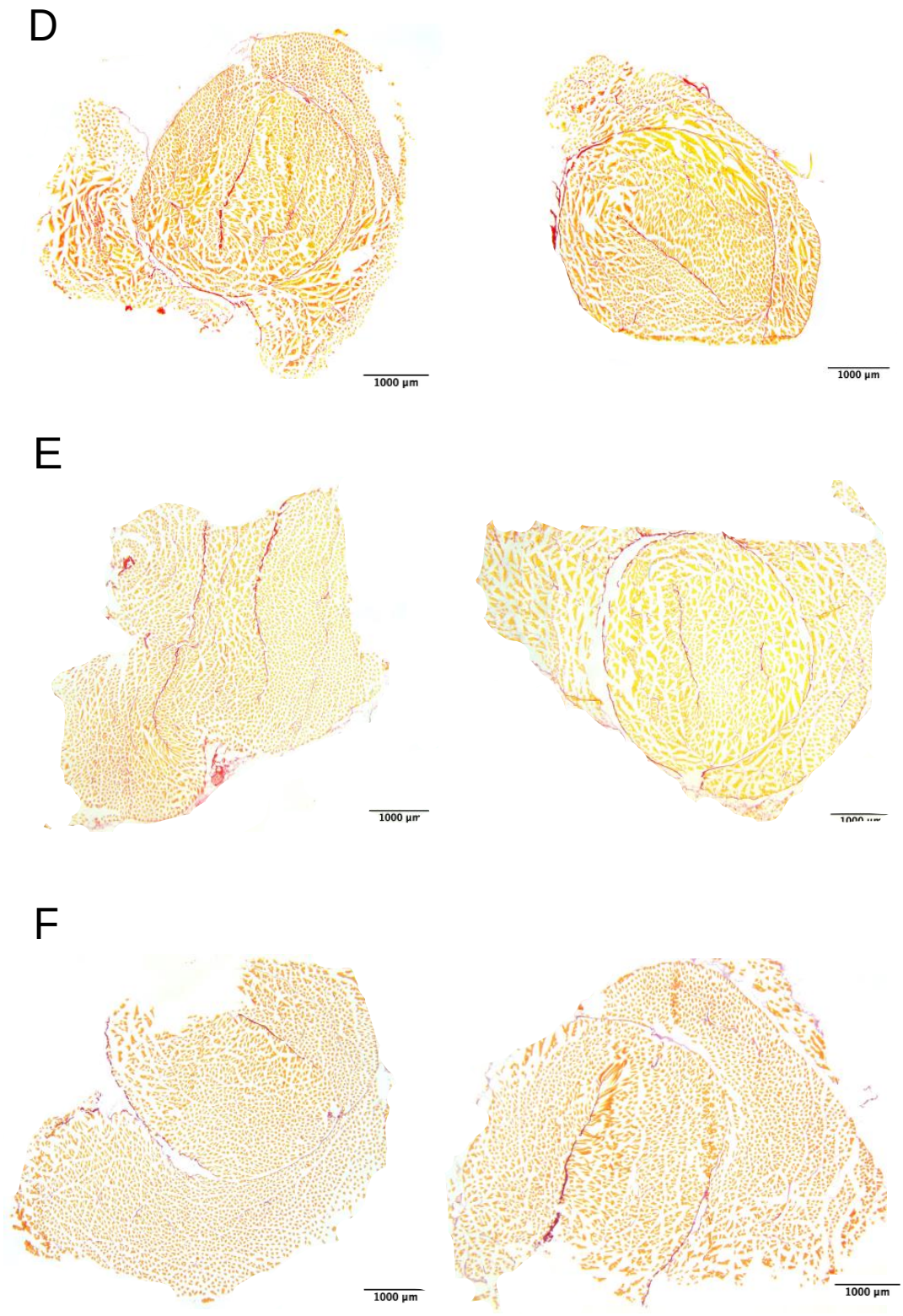

Figure 21. The HE and picrosirius red staining on trained skeletal muscles. The sedentary controls pictured on the left and training groups on the right on each staining section. (A) Baseline 0-week HE, (B) 8-weeks HE, (C) 12-weeks HE, (D) 0-week picrosirius red, (E) 8-weeks picrosirius red, (F) 12-weeks picrosirius red. (n = 5 mice per group, two independent experiments, bar length represents 1000 µm).

3.4 Cardiac function analysis derived from small animal PET/CT data

3.4.1 Training hearts showed a trend of increased LVMV and cardiac %IA/g

Based on the phenotypic and histological analysis, the endurance training starting from 8 weeks promoted cardiac hypertrophy. Based on this information, we investigated further whether forced chronic endurance training influenced the cardiac metabolic, volumetric, and functional state using multimodal approached. We performed a small animal dedicated PET/CT image acquisition to assess cardiac metabolic and volumetric function.

The recorded data was subsequently reconstructed and analyzed by using corresponding software which has been described in the materials and methods section. The LVMV and cardiac %IA/g were created using the static image acquisition to determine cardiac left ventricular mass (**figure 22 A**). The LVMV and cardiac %IA/g results across the experimental groups were presented in **figure 22 B** and **C**.

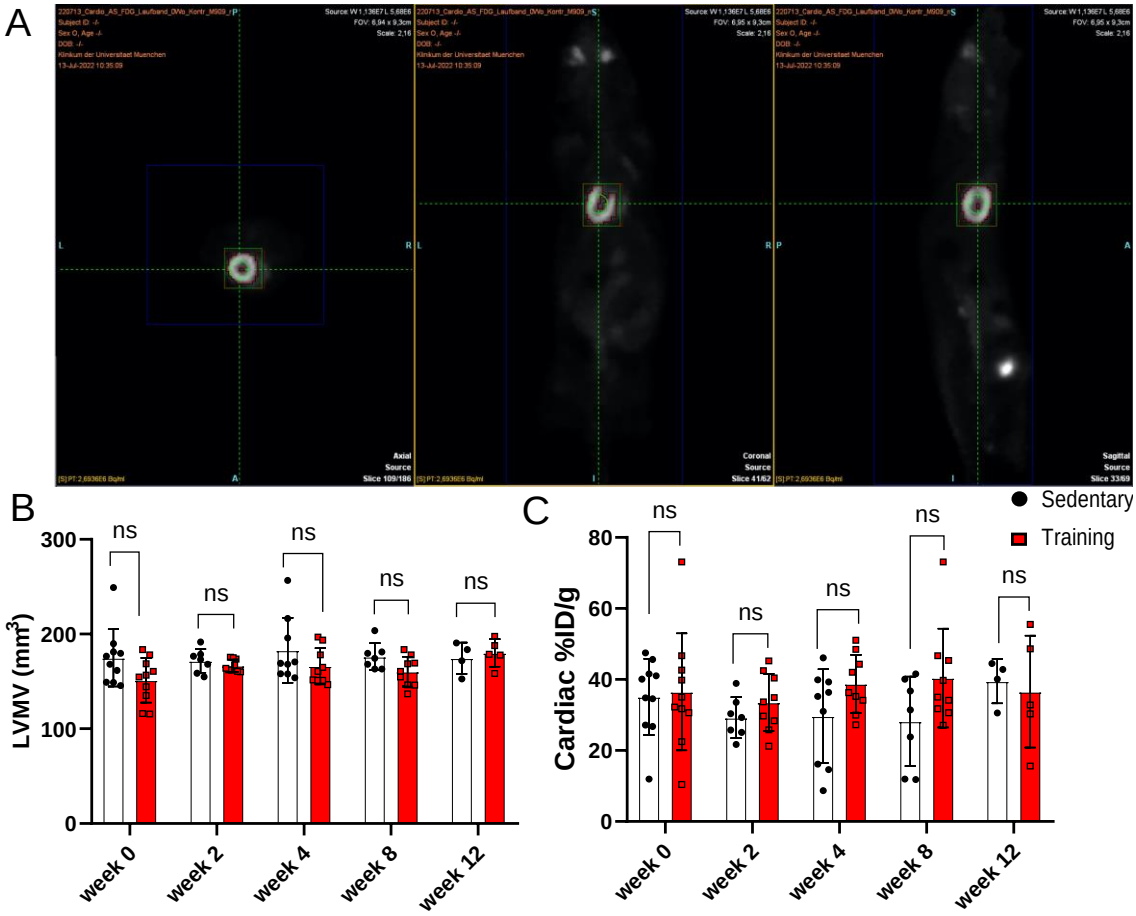

Figure 22. (A) The processes involved in image analysis to determine the LVMV and cardiac IA%/g. (B) The recorded changes of LVMV and (C) cardiac IA%/g across training and sedentary groups at different time points. The means of each group were shown (n = 10 mice per group), ± SD from two representative experiments (except for 12 weeks group which was done without replication), black represented sedentary, training animals showed in red, Three QPS data from

2 weeks sedentary, one from 2 weeks training, one from 4 weeks each sedentary as well as training, two from 8 weeks sedentary, and one from 12 weeks sedentary groups were also excluded in the data analysis due to abnormality in the QGS left ventricular volume filling curve pertaining to invalidity. ns = not significant, unpaired two-tailed Student's t test was used within each group and two-way ANOVA Turkey's multiple comparison test was used between groups in statistical analysis.

The LVMV served as a surrogate parameter of left ventricular muscle mass. The observed LVMV trend was found to be lower in the 0-, 2-, 4-, and 8-weeks training compared to their corresponding sedentary groups. Reversely, the LVMV trend was recorded higher in 12-weeks training group compared to controls. The cardiac IA%/g appeared to be higher in 2-, 4-, and 8-weeks training groups in comparison to the matched sedentary controls. Nevertheless, this trend was not observed in both 0-, and 12-weeks groups. The detailed measurement results are presented in **table 5** and **6**.

3.4.2 The volumetric and functional assessment after training

Beside assessment of LVMV and cardiac IA%/g, the PET images could be reconstructed three-dimensionally using acquired ECG-gated images as the reference. This three-dimensional volumetric evaluation served as the basis of cardiac function analysis by measuring the changes of volume on each cardiac cycle over time. Several volumetric parameters have been described such as EDV, ESV, and SV. The ejection fraction (EF) could be derived by dividing SV to EDV and expressed as percentage of ejected blood from left ventricle during each systole. We presented here the alterations of these parameters during 0, 2, 4, 8, as well as 12 weeks of endurance training compared to the matched sedentary counterparts (**figure 23 and 24**).

Functional cardiac analysis at 8 weeks showed only slight alteration after training. The sedentary EDV was higher than the training mice (mean EDV of 33.57 µl ± 3.55 in sedentary and 29.56 µl ± 4.39 in training group and, p = 0.07). The ESV and SV showed trend of higher values in sedentary as the training group (8-weeks sedentary vs. 8-weeks training, mean ESV of 4.57 µl ± 2.44 vs. 4.56 µl ± 2.88, p = 0.99, mean SV of 28.71 µl ± 4.65 vs. 25.33 µl ± 4.42, p = 0.16). On the other hand, The EF on 8-weeks training group remained stable when compared to the sedentary group (mean EF of 85.00% ± 9.64 in training and 85.57% ± 7.61 in sedentary, p = 0.90). Similar trend of relationships was observed both in the 2- as well as 4-weeks groups. The exact numbers were explained in more detail on **table 5** and **6**.

On the other hand, the EDV slightly increased in 12-weeks training group (mean of 36.60 µl ± 5.60 in training vs. 29.25 µl ± 10.31 in control, p = 0.21). The SV trend was also higher in the training hearts (mean of 30.20 µl ± 4.21 in training vs. 23.00 µl ± 10.71 in sedentary**,** p = 0.21). Thus, the ESV was recorded higher in training mice (mean of 6.20 µl ± 3.03 in training vs. 6.00 µl ± 4.69 in sedentary, p = 0.94), resulting in higher trend of the left ventricular EF calculation in exercising hearts (83.20% ± 7.60 in training vs. 77.00% ± 21.31 in sedentary**,** p = 0,56). However, none of these observed parameter differences reached statistical significance.

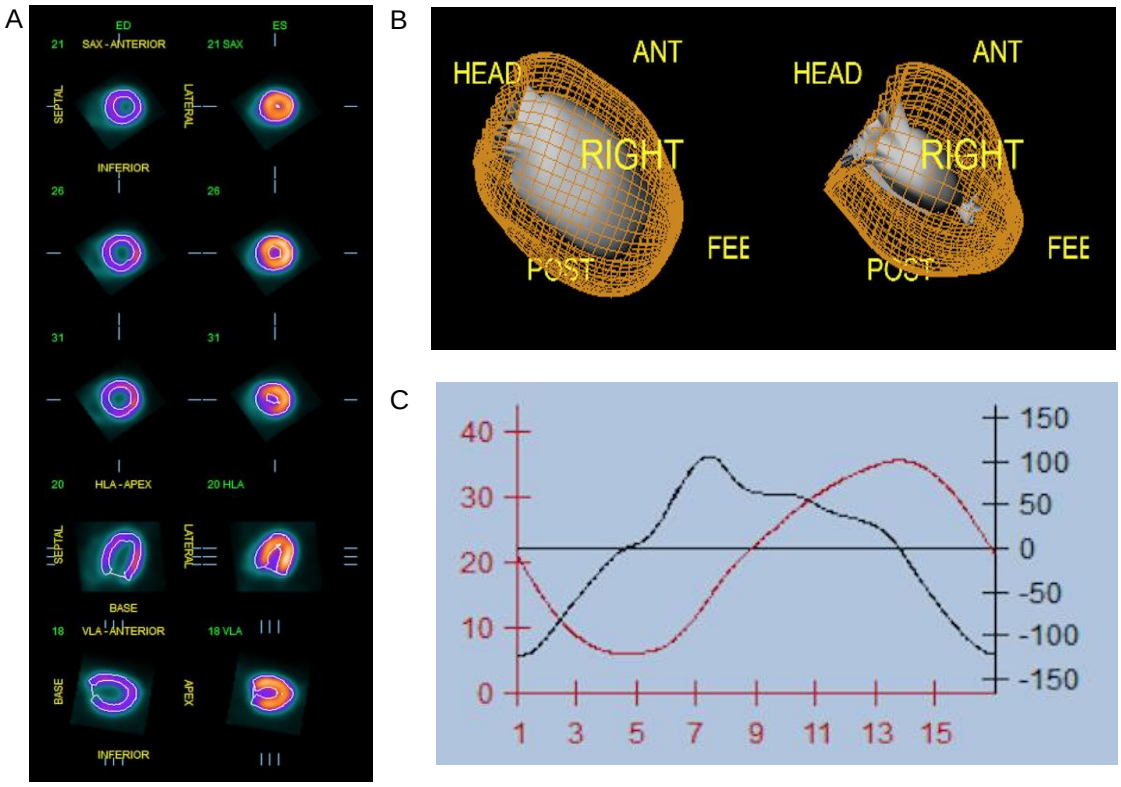

Figure 23. The three-dimensional PET images assessment of volumetric and cardiac function analysis. (A) Representatives of different slices of left ventricular PET images in different axes and levels during end-diastole (left) and end-systole (right). (B) Three-dimensional reconstruction of gated PET images showing the left ventricle. (C) The corresponding left ventricular volume (µl) and filling curve (µl/s).

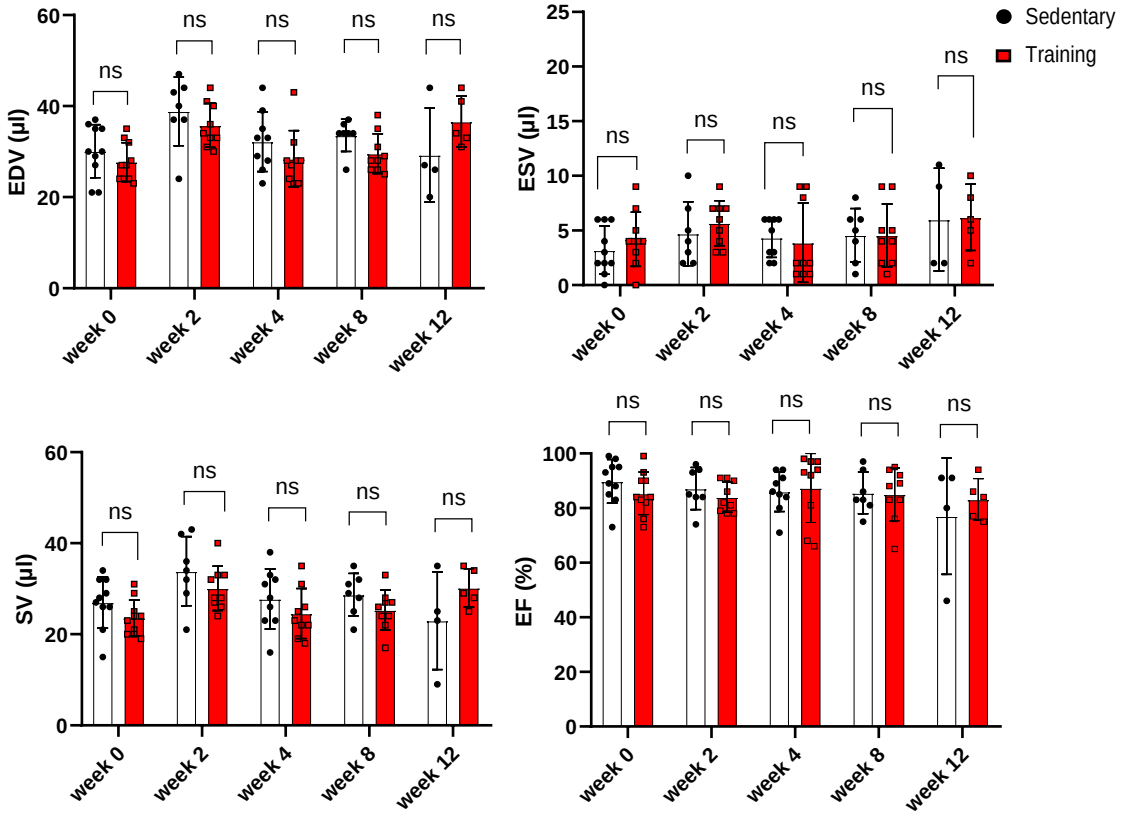

Figure 24. The comparison of different PET volumetric parameter of left ventricular function (EDV, ESV, SV, and EF) between training and sedentary groups at different time points. The means of each group were shown (n approximately 10 mice per group), black represented sedentary controls, training mice were shown in red, ± SD from two representative experiments (except for 12 weeks group which was performed without replication). Three QGS data from 2 weeks sedentary, one from 2 weeks training, one from 4 weeks each sedentary as well as training, two from 8 weeks sedentary, and one from 12 weeks sedentary groups were also excluded in the data analysis due to abnormality in left ventricular volume filling curve pertaining to invalidity. ns = not significant, unpaired two-tailed Student's t test was used within each group and two-way ANOVA Turkey's multiple comparison test was used between groups in statistical analysis.

Table 5. Multiparametric longitudinal PET evaluations in sedentary mice (n = 38)

Sedentary mice	LVMV (mm^3)	EDV (µl)	ESV (µl)	SV (µl)	EF (%)	%IA/g	Final weight (g)
0 week	174.90 ± 30.23	30.10 ± 5.84	3.20 ± 2.20	27.00 ± 5.64	89.80 ± 7.97	35.11 ± 10.71	22.78 ± 2.08
2 weeks	171.60 ± 12.50	38.86 ± 7.52	4.71 ± 2.93	33.86 ± 7.60	87.14 ± 7.71	29.24 ± 5.77	27.46 ± 1.27
4 weeks	182.90 ± 34.24	32.22 ± 6.57	4.33 ± 1.80	27.78 ± 6.59	86.00 ± 7.31	29.71 ± 13.19	28.55 ± 2.47
8 weeks	176.10 ± 14.12	33.57 ± 3.55	4.57 ± 2.44	28.71 ± 4.65	85.57 ± 7.61	28.22 ± 12.60	28.59 ± 1.53
12 weeks	174.60 ± 16.62	29.25 ± 10.31	6.00 ± 4.69	23.00 ± 10.71	77.00 ± 21.31	39.52 ± 6.23	30.50 ± 1.58

Table 6. Multiparametric longitudinal PET evaluations in training mice (n = 42)

Training mice	LVMV (mm^3)	EDV (µl)	ESV (µl)	SV (µl)	EF (%)	%IA/g	Final weight (g)
0 week	151.30 ± 23.55	27.70 ± 4.27	4.20 ± 2.49	23.60 ± 3.95	85.40 ± 7.81	36.49 ± 16.48	22.06 ± 1.04
2 weeks	166.60 ± 6.46	35.78 ± 4.84	5.67 ± 2.06	30.11 ± 4.86	84.00 ± 5.57	33.55 ± 8.05	26.57 ± 1.92
4 weeks	166.00 ± 19.09	28.44 ± 6.19	3.89 ± 3.62	24.56 ± 5.50	87.33 ± 12.59	38.76 ± 8.20	24.65 ± 2.71
8 weeks	160.40 ± 15.75	29.56 ± 4.39	4.56 ± 2.88	25.33 ± 4.42	85.00 ± 9.64	40.40 ± 13.91	25.96 ± 1.63
12 weeks	180.10 ± 14.54	36.60 ± 5.60	6.20 ± 3.03	30.20 ± 4.21	83.20 ± 7.60	36.58 ± 15.77	27.84 ± 1.80

3.4.3 Heart rate and cardiac output after training

As we completed the three-dimensional volumetric data assessment on the previous section, we analyzed the average heart rate/minute among experimental groups during the PET scan. The acquired heart rate/minute means were then multiplied with the corresponding SV to produce cardiac output (CO) which was expressed in µl/minute. **Figure 25** showed the tabulated data on the means heart rate/minute and CO.

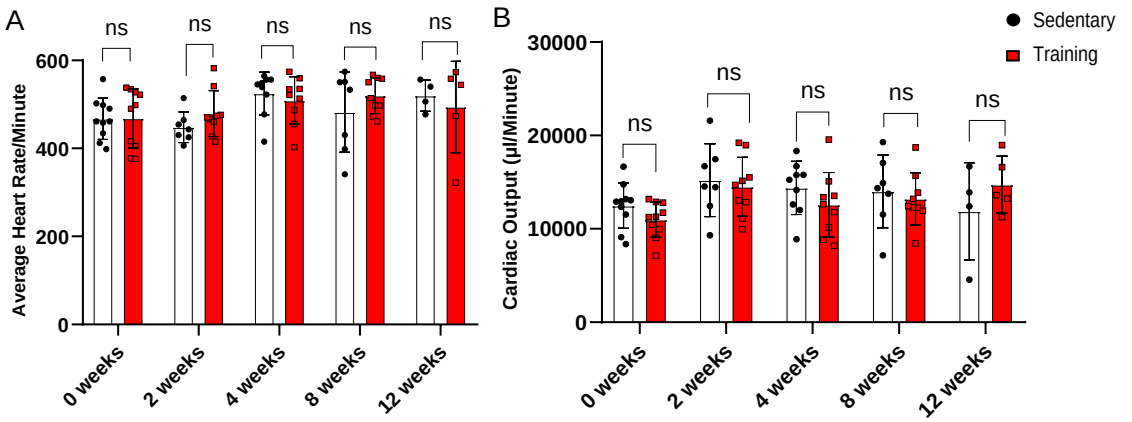

Figure 25. (A) The heart rate/minute means of training and control animals. (B) Cardiac output derived from SV and heart rate/minute. The means of each group were shown (n approximately 10 mice per group), black represented sedentary controls, training mice were shown in red, ± SD from two representative experiments (except for 12 weeks group which was done without replication). Three QGS data from 2 weeks sedentary, one from 2 weeks training, one from 4 weeks each sedentary as well as training, two from 8 weeks sedentary, and one from 12 weeks sedentary groups were also excluded in the data analysis due to abnormality in left ventricular volume filling curve pertaining to invalidity. ns = not significant, unpaired two-tailed Student's t test was used within each group and two-way ANOVA Turkey's multiple comparison test was used between groups in statistical analysis.

The 0-weeks groups showed similar heart rates between sedentary and training groups (467 ± 47 and 468 ± 67 respectively, p = 0.96). The mean heart rate/minute was observed higher in training groups at 8 weeks (520 ± 40 vs. 482 ± 91 in sedentary controls, p = 0.29). At 12-weeks groups, the heart rates trend was lower in the training hearts (mean heart rate/minute of 494 ± 104 in training vs. 520 ± 35 in control group, p = 0.65). The difference of heart rate/minute means was also found not statistically significant in both 2- and 4-weeks groups (p = 0.20 and 0.53, respectively). The cardiac output measurement showed no difference in 12-weeks training group (14741 µl/min ± 3042) in relative to their matched sedentary controls (11892 µl/min ± 5203, p = 0.33). The lowest CO was recorded in baseline 0-week groups (12488 µl/min ± 2429 in sedentary and 10979 µl/min ± 1898 in training group, p = 0.14). The mean CO at 8 weeks was found to be lower in training group compared to the sedentary control (13205 µl/min ± 2816 vs. 14010 µl/min ± 3896, p = 0.64). A statistical significance in the CO difference was also not observed in both 2- and 4-weeks groups (p = 0.69 and 0.24 respectively).

3.4.4 The heart rate correlated positively with LVMV in training hearts

The heart rate played a significant role in cardiac metabolism during training. The changes in cardiac metabolism during exercise could alter the uptake of myocardial ^{18}F-FDG.

Based on **figure 26**, the average heart rate/minute does not statistically significant correlate with %IA/g (r = 0.24, p = 0.13 in training and r = 0.26, p = 0.13 in sedentary groups). Furthermore, the average heart rate/minute and LVMV (mm^3) showed no correlation in sedentary group (r = 0.06, p = 0.73). Meanwhile, the positive correlation between the average heart rate/minute and LVMV (mm^3) reached statistical significance in training hearts (r = 0.34, p < 0.05).

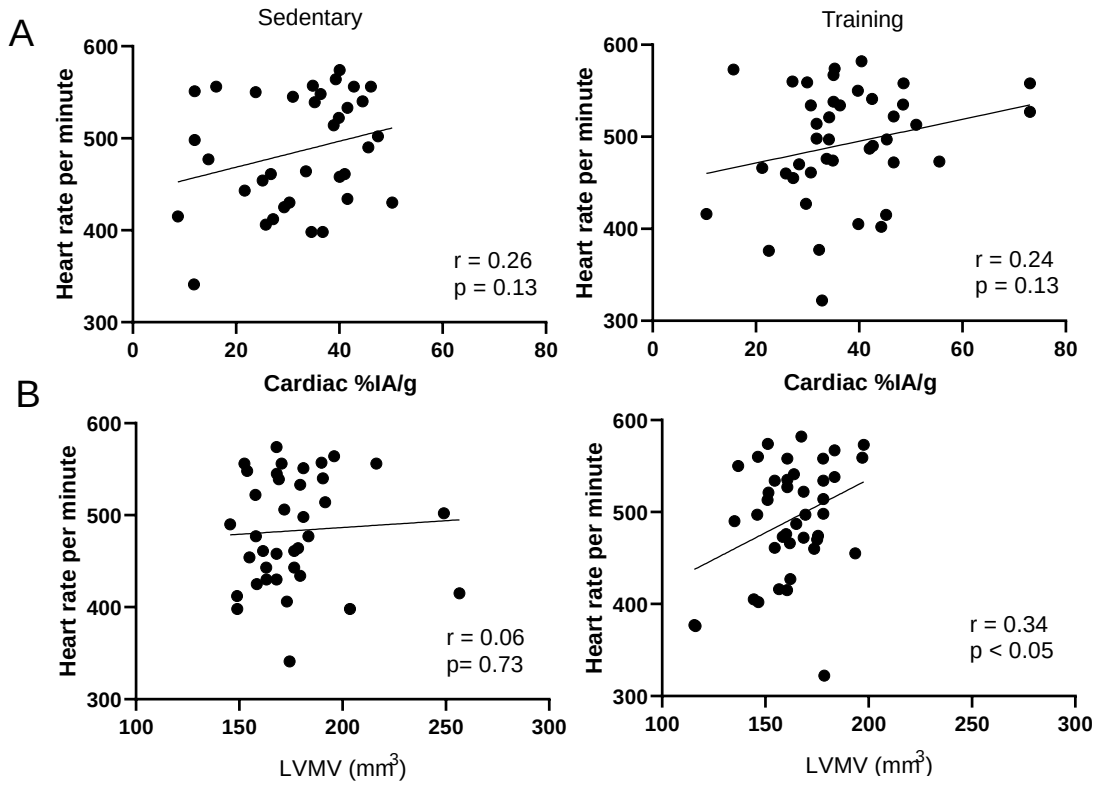

Figure 26. The linear regression analysis using Pearson's correlation coefficient to determine the relation between two parameters. (A) The correlation between the average heart rate/minute and cardiac %IA/g in sedentary (left) and training group (right). (B) The average heart rate/minute was correlated with LVMV (mm^3) only in training group (right), but not in sedentary group (left). Total number of mice are 80 (n = 42 in training and n = 38 in sedentary control), correlation coefficient was expressed as r, statistical significance was expressed when $p < 0.05$.

3.4.5 The LVMV positively correlated with EDV, but showed no relation with LVEF in training animals

Figure 27 showed these relations between left ventricular mass, cardiac volume during diastole, and ejection fraction both in training animals and their sedentary control.

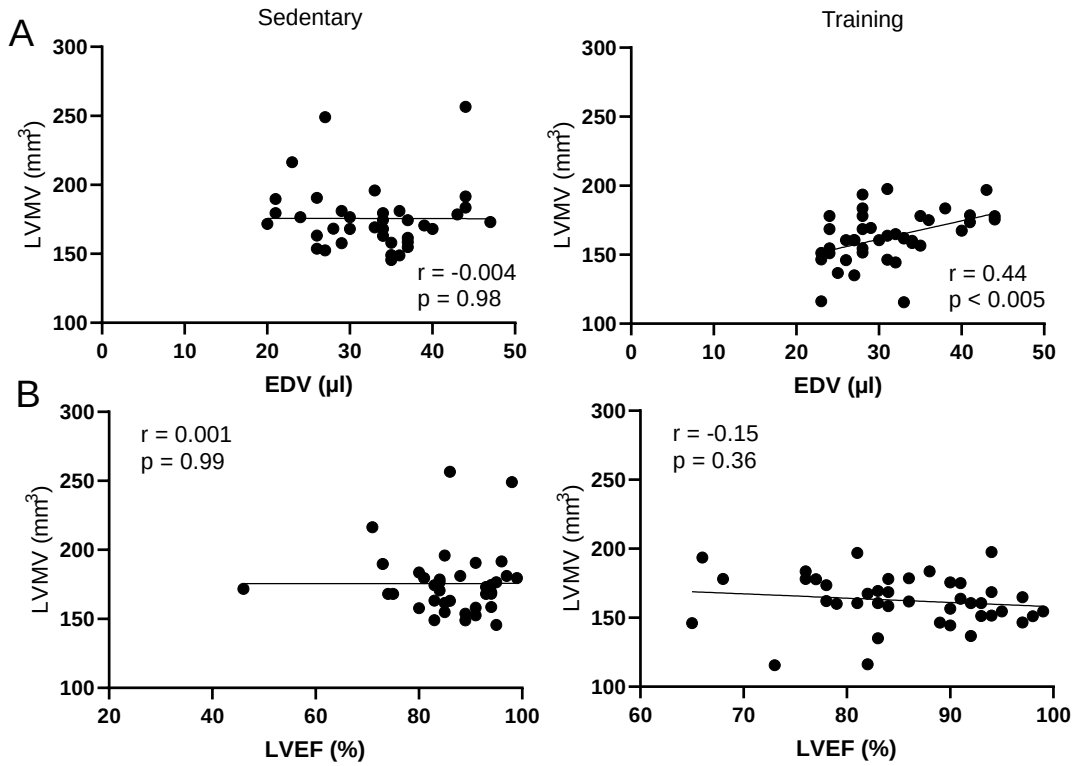

Figure 27. (A) The correlation of LVMV (mm^3) and EDV (µl) in sedentary (left) and training group (right). (B) Both in sedentary (left) and training group (right) the LVMV (mm^3) was not correlated with left ventricular EF (%). The Pearson's correlation coefficient (r) using linear regression analysis was used in total of 80 training and sedentary control animals (sedentary animals n = 38, training n = 42). $p < 0.005$ indicates statistical significance.

The LVMV (mm^3) found to be positively correlated with EDV (µl), but only significantly in training group ($r = 0.44$, $p < 0.005$ in training group). On the contrary, the LVEF as an indicator of cardiac pump function has been shown to be not correlated with the measured LVMV ($r = 0.001$, $p = 0.99$ in sedentary and $r = - 0.15$, $p = 0.36$ in training group).

3.5 Overview of RNA-seq analysis: The signaling cascades other than classical pathways contributed to cardiac hypertrophy in endurance training

While we started to observe the signs of cardiac hypertrophy at 8 weeks of training, we investigated the signature molecular pathways of physiological cardiac hypertrophy by performing bulk-RNA sequencing analysis on the whole heart samples. Total five training and five sedentary whole hearts were extracted after 120 minutes/day of 8 training weeks and their RNA was isolated according to protocol described in the materials and methods section. First, we generated a heat map table confirming the most 20 differentially expressed genes between training and control groups. Subsequently, the evaluation continued by creating volcano as well as MA plot to achieve further information such as average expression levels, extent of comparison, and *p*-value. The cutoff *p*-values used in the statistical analysis was 0.05 and the log fold-changes threshold above 1 was considered statistically significant. **Figure 28** and **table 7** depicted the heat map, volcano,

MA plots, GSEA and a table explained the gene predicted function taken from NCBI website (https://www.ncbi.nlm.nih.gov/gene).

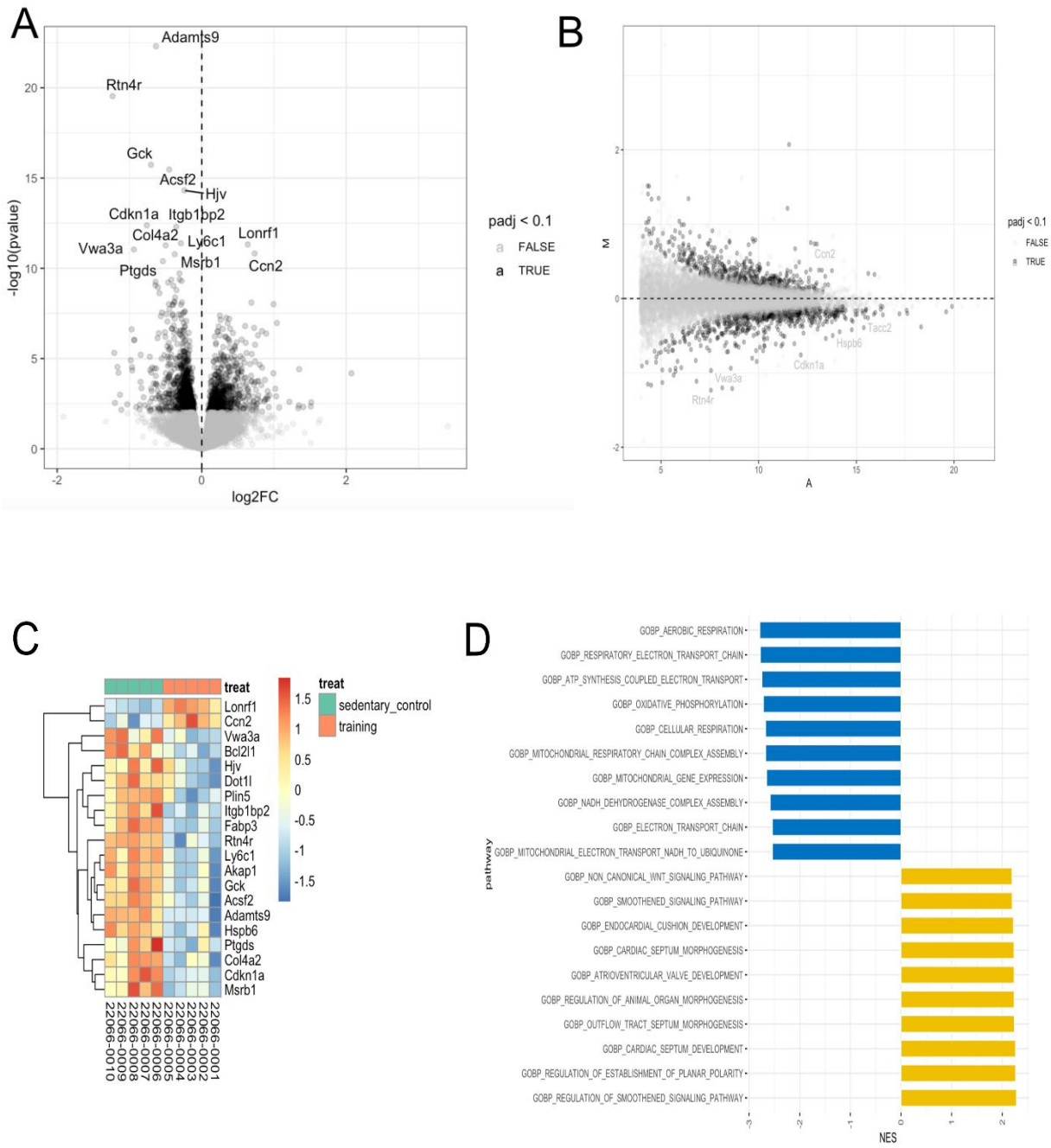

Figure 28. (A) Volcano, (B) MA plots, (C) Heat maps table showing the top 20 most differentially regulated genes between 8-weeks training group and their matched sedentary control. (D) Gene Set Enrichment Analysis (GSEA) of gene ontology sets which showed only most relevant biological processes. Total mice number used was 10 (five training and five sedentary animals).

Table 7. The 20 most differentially regulated genes between training and control groups (predicted functions are derived from NCBI)

Abbreviation	Gene Name	Up/Downregulated in training groups	Predicted function
Lonrf1	LON Peptidase N-Terminal Domain and Ring Finger 1	Upregulated	Metal Ion Binding activity, involved in Class I MHC APC expression
Ccn2	Cellular Communication Network family member 2	Upregulated	Involved in cellular proliferation and differentiation, cell adhesion, fibroblast growth factor induced DNA synthesis
Vwa3a	Von Willebrand Factor A domain containing 3a	Downregulated	Precursor of the multimeric von Willebrand factor which is involved in blood coagulation
Bcl2l1	BCL2-like 1	Downregulated	Apoptosis regulator, regulator of G2 checkpoint and progression to cytokinesis during mitosis
Hjv	Hemojuvelin BMP Co-receptor	Downregulated	Iron homeostasis by interaction with hepcidin
Dot1l	DOT1-like histone H3 methyltransferase	Downregulated	Posttranslational histone modification, negative gene expression, regulator of cell cycle progression and development
Plin5	Perilipin 5	Downregulated	Negative regulation of PPAR, positive regulation of sequestering triglycerides, regulation of lipid metabolic process
Itgb1bp2	Integrin subunit beta 1 binding protein 2	Downregulated	Interacts with integrin beta 1, acts as chaperone, calcium binding, associated with dilated CM and cardiac hypertrophy related to stress
Fabp3	Fatty acid binding protein	Downregulated	Lipid homeostasis, positive regulation of lipid transport and import to cell
Rtn4r	Reticulon 4 receptor	Downregulated	Negative regulation of neuronal projection, neuronal development, and signal transduction
Ly6c1	Lymphocyte Antigen 6 complex, Locus C1	Downregulated	Involved in ACTH receptor signaling pathway in response to stress
Akap1	A kinase anchor protein 1	Downregulated	Involved in apoptosis, located in mitochondrial membrane
Gck	Glucokinase	Downregulated	Involved in glucose metabolism, calcium ion import, positive regulation of insulin secretion
Acsf2	Acyl-CoA Synthetase family member 2	Downregulated	Fatty acid metabolic process, CoA ligase activity, located in mitochondrial membrane
Adamts9	Disintegrin-like and metallopeptidase (reprolysin type) with thrombospondin type 1 motif, 9	Downregulated	Endopeptidase activity, circulatory system development, negative regulation of endothelial migration and sprouting angiogenesis
Hspb6	Heat Schock Protein, alpha-crystallin-related B6	Downregulated	Chaperone mediated protein folding, negative regulation of cardiomyocytes apoptosis, positive regulation of angiogenesis
Ptgds	Prostaglandin D2 Synthetase	Downregulated	Prostaglandin synthesis, regulation of circadian rhythm
col4a2	Collagen Type IV, alpha2	Downregulated	Regulation of collagen IV synthesis, basement membrane integrity, inhibit angiogenesis
cdkn1a	Cycline dependent kinase inhibitor 1A	Downregulated	Regulator cell cycle progression at G1 (p53 mediated G1 arrest), inhibition cdk2 and 4, involved in tissue regeneration
msrb1	Methionine sulfoxid reductase B1	Downregulated	Repair Enzyme, protect protein from oxidative stress

The volcano and MA plots on **figure 28** showed upregulated genes beyond the selected threshold in the right and upper segments respectively. The *x*-axis of volcano plot indicated the log^2 fold change, a positive value implied upregulated gene expression in the treatment group as compared to control and a negative value indicated the opposite. The *y-axis* in the other hand explained $-log^{10}$ p value which indicated the significance level of the assigned genes, the higher the

position of the gene on the y-axis indicated a greater significance level that they were not considered as a false positive result. Certain threshold levels in the pre-analytics were applied by Dr. Tobias Straub from the bioinformatics core unit biomedical center LMU Munich to consider on which genes were differentially and significantly expressed in the treatment as compared to the control group. The similar explanation applied to the MA plot but only with the opposite axis position (log^2 fold change on the *y-axis* and $-log^{10}$ p value on the *x-axis*).

Because of the magnitude and diversity of the RNA expression analysis, not all gene will be discussed in detail in this study. The genes which are relevant to cardiac hypertrophy will be selected and their role in the biological and physiological processes will be described briefly in this section. Among these differentially expressed genes, the majority of at least five genes were normally involved in regulating progression of cell cycle and apoptosis. The *ccn2* gene was upregulated significantly in 8-weeks training heart and its protein product participates in cellular proliferation and FGF-induced DNA synthesis in the s phase of cell cycle. A strong apoptosis and G2 check point regulator from *Bcl2* family was also downregulated in the same hearts. One of the heat shock protein gene family *hspb6* which acted as a negative regulator in cardiomyocytes apoptosis was found to be downregulated by endurance training. Moreover, *cdkn1a*, an important inhibitor of cyclin dependent kinase 2 and 4 which allowing the cells cycle proceeds beyond G1 checkpoint, was expressed lower in the treated animals. The *Dot1l* gene translated to protein involves in epigenetic posttranslational histone modifications which negatively regulated gene expression of cell cycle progression. Another kinase anchoring mitochondrial membrane-bound protein involved in apoptosis was a product of *akap1* gene which was also found to be downregulated in endurance training.

Not only genes that were involved in apoptosis and cell cycles were differentially expressed between both groups, but also some genes which were participated in immune response regulation such as *lonrf1*, *Ly6c1, and Hjv, as well as gene* involved in glucose metabolism and fatty acid homeostasis such as *plin5, fabp3, gck*, and *acsf2*. Lastly, genes that participate in collagen biosynthesis process and negative regulation of angiogenesis namely *col4a2* and *adamst9* were downregulated in training hearts.

Figure 28 D shows the gene set enrichment analysis (GSEA) of gene ontology gene sets which showed only the most relevant biological processes between treatment and control groups. The enrichment score (ES) pertained to the degree on which gene sets were presented at the top or bottom of a ranked list of genes. The ES was statistically corrected for the discrepancies between multiple expressed gene sets due to the differences in their expressional size which resulting in a more reliable as well as interpretable normalized enrichment score (NES). The NES was normalized to mean enrichment of random samples of the same size. A significantly positive NES value indicated that the member genes in the GO set tend to appear at the top of the ranked transcriptomics data and the negative NES implied the opposite.

Based on our GSEA analysis, most of the upregulated genes in the training hearts were involved in regulation of cardiac morphogenesis, development as well as smoothened signaling pathways. This pathway was an important set of transmembrane proteins which were key part of hedgehog signaling cascades. This cell-to-cell communication relayed a crucial signal for embryonic differentiation and adult tissues homeostasis. Furthermore, genes involved in non-canonical *wnt* signaling pathways were also significantly upregulated in 8-week training group. Two of these complex pathways have been currently researched in oncology namely the planar cell polarity and

wnt-calcium pathway. Surprisingly, the genes involved in aerobic respiration, oxidative phosphorylation, and electron transport chain were downregulated in exercising mice compared to their sedentary control.

We investigated further the hypertrophy gene hallmarks in our training animals by selecting differentially expressed genes in several important biological processes such as cardiac hypertrophy, organ growth, cellular response to growth factor stimulus, and the regulation of IGF transport as well as uptake by the IGF binding proteins. **Figure 29** explained the heat maps generated to allow such observation.

Here, the wide arrays of differentially expressed genes which might contribute on the growth process related in response to endurance training. Surprisingly, the set of genes which normally participated in classical molecular pathways of cardiac hypertrophy such as IGF-1/PI3K/AKT/PKB/mTOR and calcineurin-calmodulin-NFAT circuits were not observed. However, some important genes involved in cardiomyocytes β-myosin heavy chain and protein synthesis such as *Myh7, Foxp1*, and *Gata6* were upregulated in training hearts. Moreover, *Akap13*, a gene which was involved in G protein-coupled signaling cascades related to downstream p38 MAP and Rho kinases activation was upregulated in the training hearts. A part of these signaling cascades linked the cAMP, EGFR, BRAF, and PKA pathways leading to downstream phosphorylation of MAPK1 or MAPK3 and HDAC5 activation by PRKD1 which promoted sarcomere formation in cardiac hypertrophy. These proteins normally played a major role for a normal adaptive cardiac hypertrophy in response to pressure overload and β-adrenergic receptor activation.

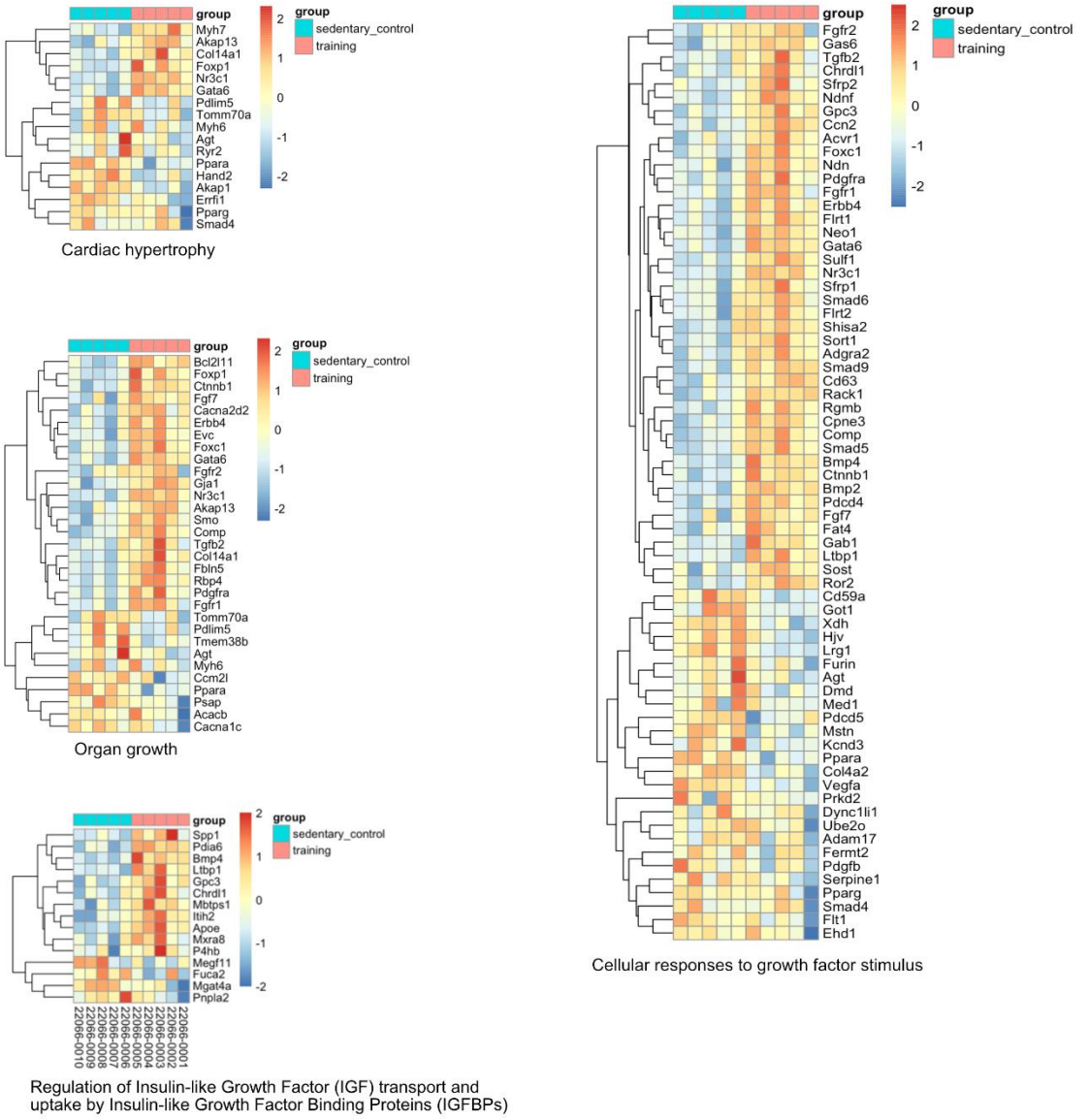

Figure 29. Heat maps showing differentially expressed genes based on clustered genes annotated in several selected biological process pertaining to cardiac hypertrophy. Four heat maps related to organ growth, cellular responses to growth factor stimulus and the regulation of IGF uptake and transport were shown. Only the genes with False Discovery Rate (FDR) < 10% according to Benjamini & Hochberg test were considered significantly differentially expressed and included in the analysis.

The *Col14a1* gene which produces fibrillary protein which was important in extracellular matrix (ECM) formation during organ remodeling in response to stress or injury was upregulated in training animals. Other upregulated genes of several biological processes might also contribute to hypertrophic response after exercise. Several genes which were involved in cholesterol metabolism, lipid homeostasis, and transport were also found to be upregulated in the training animals. The *mbtps1* gene was crucial to produce proteins which regulated the intracellular trafficking of cholesterol and fatty acids. The *apoe* in the other hand, was well-known to be involved in the catabolism of triglyceride rich lipoproteins such as Chylomicrons as well as VLDL (very low-density lipoprotein).

On our RNA sequence analysis, not only the upregulated genes might have important biological meanings. Several crucial genes were found to be downregulated in training hearts in comparison to sedentary animals. The *mgat4a* gene produces protein which involved in glucose transport and uptake was less expressed in the training hearts. The *Ppara* gene encoded the transcription factor peroxisome proliferator-activated receptor α which regulated lipoprotein metabolism were also downregulated by training.

In the other hand, the gene sets participated in additional pathways of cellular growth such as FGF, PDGF, TGF-β/BMP/SMAD, fibroblast, and collagen synthesis were more observable in our study. Two of the observables differentially expressed genes which are part of TGF-β/SMAD signaling were *bmp4* and *ltbp1*. The *bmp4* protein could be responsible for activation of non-canonical BMP pathways such as ERK/MAP kinase, PI3K/Akt, and VEGFR2 signaling thus regulated the heart development, angiogenesis, and adipogenesis. The *ltbp1* gene, on the other hand, synthesized key regulator proteins that control TGF-β activation. Interestingly, some genes for stabilization of sarcomere troponin, cytoskeletal actin, myosin, and collagen such as *tnni1*, *parva, pdlim2, myh7,* and *col14a1* were also upregulated in training hearts. The protein products of these genes participate in cellular adhesion onto collagenous extracellular matrix in response to stretch, pressure challenges, and secretion of survival signals.

Physiological cardiac hypertrophy in response to pressure and volume load stimuli was a highly regulated process on the molecular level. Although the downstream function of these genes was mostly still largely unknown and seemed to be differentially expressed between training and sedentary animals. The main molecular biological pathways of translated protein products pointed towards physiological, biochemical, and metabolically alterations which were hypothesized to be involved in cardiac hypertrophy. We found that meanwhile the genes involved in classical pathways of cardiac hypertrophy were not clearly observed in our study, the other genes responsible for variety of cellular processes found to be differentially expressed between two groups.

4. Discussion

4.1 Review of results

Our results highlighted that chronic intensity controlled forced endurance training in mice influenced several morphometric phenotyping measurements towards development of cardiac hypertrophy starting from 8 weeks (**Figure 30)**. The training animals had lower body weights, increased heart, skeletal muscle weights, as well as heart weight/tibia length ratio. Tibia length was used as denominator in our study due to minimum exercise-induced confounding alterations compared to body weight which was variously changed over time depending on the body composition. Furthermore, we have observed cardiac and skeletal muscle hypertrophies on macroscopic and microscopic level. Using high-sensitive immunofluorescence staining, we were able to show that more cardiomyocytes and skeletal myocytes proportionally shifted towards larger cross-sectional surface area sizes in 8- as well as 12-weeks training groups.

To validate these results, we subsequently investigated the metabolic cardiac function and volumetric changes during training by using small animal-dedicated PET/CT scan. Here, we saw the trend of increasing FDG-derived cardiac metabolic volume as well as %IA/g in 12- and 8-weeks training group respectively. The LVMV was found also to be positively correlated with average heart rate/minute as well as EDV in training animals. The heart volume, heart rate, and left ventricular EF as parameter of cardiac pump performance were found to be not altered across different groups at various measurement points, indicating that cardiac function and volumetric were preserved during endurance training. Furthermore, the cardiac morphological alterations in response to training was highly regulated in molecular levels. This involves several biological processes pertaining to organ growth and development in response to mechanical load. The bulk RNA sequencing analysis in 8 weeks training animals led to a discovery which presented the 20 most differentially expressed genes between training and sedentary animals. These genes were mainly involved in regulating cell cycle and apoptosis indicating that tissue transformation might play a crucial role in the development of hypertrophy. Several genes related to increase sarcomere β-myosin heavy chain, troponins, and other regulatory MAPK pathway anchoring proteins synthesis as well as glucose and lipid homeostasis were also upregulated in training animals. Surprisingly, the signaling pathways which normally involved in organ remodeling such as FGF, PDGF, TGF-β/BMP/SMAD, as well as genes involved in DNA replication, protein synthesis, cardiac morphogenesis and development were found to be upregulated as a response to training stimulus. Surprisingly, many biological processes involved in aerobic respiration, oxidative phosphorylation, and electron transport chain were found to be diminished in our GSEA results after training.

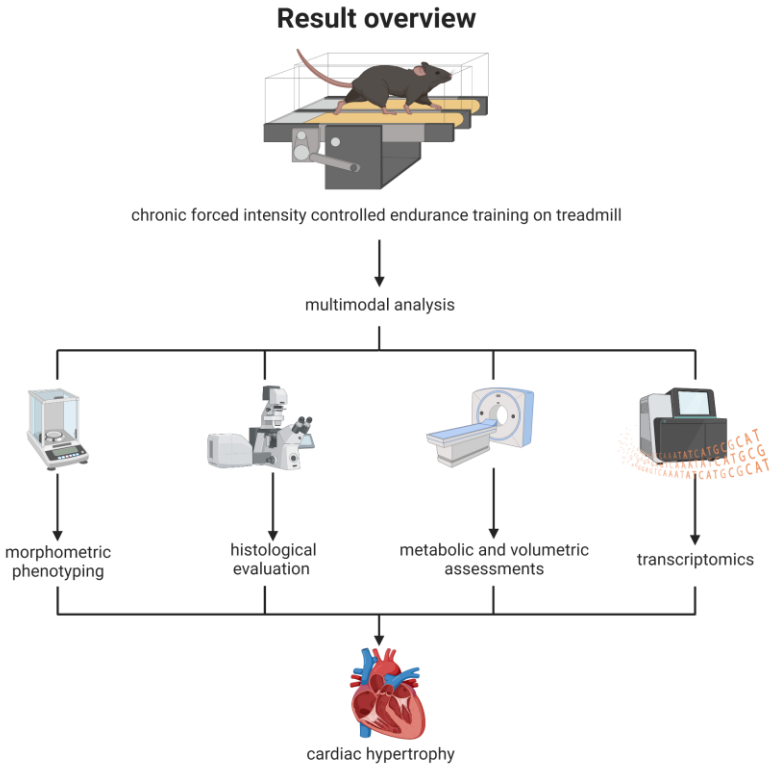

Figure 30. Overview of the multimodal analysis performed in our study. The cardiac response of chronic forced intensity-controlled endurance training using treadmill machine examined by using morphometric phenotyping, histology, metabolic, and volumetric assessments, as well as transcriptomic data. The image was created using BioRender (Toronto, Ontario, Canada)

4.2 The morphometric phenotyping as well as training protocol variations and their role in interpreting cardiac and skeletal muscle hypertrophy in endurance training

Our results showed that chronic endurance training induced body weight loss in exercising animals and was noticeable as early as 2 weeks after acclimatization. The difference of final body weight on the 12 weeks was recorded 2.66 g lesser in training group compared to sitting controls ($p < 0.0001$). The results were expected and consistent with previous studies which showed that moderate- as well as high-intensity endurance training were effective in reducing total body weight by body fat loss presumably reflecting a better glycemic metabolic control as well as fatty acid metabolism as suggested by previous publications (102, 103). A trend of skeletal muscle mass gain could also be observed in training individuals as response to mechanical loads. However, we should also point out the facts that the skeletal muscle hypertrophy would have been expectedly more pronounced in resistance training than endurance training due to the differences in mechanical load stimuli (105, 106). This was also reflected in our study, showing that both *quadriceps femoris* and *gastrocnemius* weight tend to be increased in 8- as well as 12 weeks training groups. These observations consistent with several precedented studies which proclaimed that skeletal muscle hypertrophy was observed after 12-26 weeks of high-intensity resistance training in rats (107, 108). The body weight loss in the training animals might be caused by more pro-

nounced adipose tissue loss compared to skeletal muscle mass gain during this time span. However, we have not measured the body fats composition as well as the lean body mass due to technical ground which served as a limiting factor in our study.

Our results suggested that larger cardiac mass could be observed morphometrically starting from 8 weeks of two hours per day intensity-controlled forced endurance training with the speed of 15m/min. This result contradicted an experiment using 129 SvJ/C57BL6 with shorter training protocol (40 minutes/day) and higher speed (24 m/min) which failed to detect change in heart weight/body weight ratio after 8 weeks duration (109). This previous work used body weight as the heart weight ratio denominator for cardiac hypertrophy indicator. As mentioned before, body weight was subjected to change in running animals mostly due to body fat composition alteration or reduction, thus acted as major confounding factor. We argued that the use of tibia length as denominator of heart weight to indicate cardiac mass gain was more objective when compared to body weight for the same purpose.

Furthermore, it seemed that the daily training duration, number of weeks, as well as exercise intensity played an essential role in generating whether physiological or pathological cardiac hypertrophy in experimental animals. An appropriate intensity of endurance training was preferred to elicit the desired cardiac responses without creating deleterious health effects. Several studies in the past showed that forced middle-intensity endurance training by swimming 3 hours/day in rats was able to increase the absolute heart weight by 30% after total 180 hours of training. Ninety minutes of swimming with 2% total body weight load, three times/day for 7 weeks also showed cardiac hypertrophy generation without sign of scar tissue formation (110, 111). The other study protocol concluded that higher intensity endurance training on treadmill in rats using the speed of 30 m/min, 30 minutes/day, 5 days/week for 8 weeks has also successfully induced cardiac hypertrophy characterized by the increased of the measured heart weight in training groups compared to sedentary control (112).

The higher-intensity continuous treadmill exercise in rats with speed of 26.8 m/min, 10^{o} inclination, 60 minutes duration, 5 days/week for 8 weeks was associated with cardiomyocytes injury, increased cardiac troponin I, fibrosis, and expressions of genes involved in development of pathological hypertrophy (113). However, these potential negative effects could be reversed when the high-intensity endurance training was not performed continuously. Recent studies showed that intermittent high-intensity as well as continuous but with moderate-low intensity of endurance training both in animal and human studies could potentially evoke positive effects in glucose metabolism, lipolysis, and aerobic capacity. Furthermore, they could also promote cardiorespiratory fitness augmentation pertaining to exercise-induced cardiac remodeling, reduce sarcopenia, and prevent neurocognitive deterioration in ageing individuals (114-117).

One metanalysis showed that treadmill training protocols in mice of total 5-8 weeks duration irrespective of training intensity had optimally achieved the desired outcomes compared to shorter (<4 weeks) or longer (>8 weeks) total exercise duration. The failure of training adaptation was expected in shorter exercise duration. On the opposite side, a longer training duration may contribute to overtraining situation which characterized by diminishing training capacity and performance as well as other negative physiological consequences. This might occur due to habituation towards training protocol, stress reaction against running stimuli as well as development of muscle fatigue. A training duration less than 60 minutes/day was also expected to create maximum effect in biochemical alterations induced by exercise (118). One study even indicated that the rats subjected to progressive endurance exercise for 6 weeks developed bronchial ciliated cells loss, apoptosis, increase infiltration of $CD45^{+}$ leucocytes, as well as accumulation of inflammatory cells

in respiratory lumen, showing probable deleterious effects elicited by high intensity training (119). Our study indicated that heart weight/tibia length ratio as well as microscopic cardiomyocyte surface area evaluation as indicators for cardiac hypertrophy were optimally quantified in 8-weeks training group which ran for 120 minutes/day, five days weekly. The similar effect was also found in the 12-weeks training group, although the cardiomyocytes cross-sectional surface area reached stagnancy.

Furthermore, the experimental endurance training using treadmill machine might generally induce stress in the animals due to the use of stimuli. The training was normally conducted during their inactive state during the day which may impact their natural circadian rhythm and behavior, thus resulting in stress responses multiplication. However, the recent methods to measure stress response such as blood cortisol level and behavioral assessment might pose a great challenge due to certain technical difficulties as well as limitation of valid evaluation tools in animal studies (120). A free-access voluntary running wheel experiment could potentially serve as an alternative to forced treadmill training protocols in evaluating physiological cardiac hypertrophy without exposing additional stress stimuli in training animals (74). However, the expected outcomes were varied depending on the individual motivation of the training animals. Some studies also concluded that voluntary wheel training in mice failed to alter cardiomyocytes numbers as well as cardiac volume even after longer training period (121, 122).

Although we used the genetically same animals on the same age purchased from the same source, different morphometric measurement could ensue due to batches variation in growth as well as development pattern. A continuous monitoring of morphometric changes in the same individual at multiple training duration measurement points was practically impossible. These might create an issue of the final calculation, which posed limitation of morphometric assessment in our study. Based on these discussions, although some inevitable limitations, we concluded that forced continuous medium-intensity treadmill endurance training in mice was a valid, reliable, and reproducible method to generate visible cardiac hypertrophy after 8 weeks.

4.3 Cardiac hypertrophy under the microscope

The wheat germ agglutinin (WGA) immunofluorescence staining has been used in the past years as a reliable method to stain components of cell membrane and extracellular matrix (123). Furthermore, WGA staining provided reliable visualization of fibrosis after myocardial infarction in both paraffin embedded as well as frozen sections. This enables a more sensitive quantification of scar tissues compared to its predecessor (20). The WGA staining to assess cardiac and skeletal myofiber cross-sectional area was used previously in several studies of mice swimming model (124, 125), as well as the forced treadmill running protocols (126, 127), which confirmed the validity of this approach to conveniently evaluate cardiac and skeletal muscles hypertrophy.

Cellular nuclearism and *ploidy* are crucial in differentiating normal and pathological appearance of histological specimens. While majority of normal cardiomyocytes are mononuclear, skeletal myocytes might appear multinucleated throughout life. Moreover, cells polyploidy could indicate abnormality in cell growth, maturation, and regeneration due to response against stress or pathological stimuli (128). In our study, we used SYTOX green to mark the nucleus by staining the nucleic acid of permeabilized cells. By creating the boundaries between normal and abnormal cells and avoiding area of cells which was sliced tangentially, we were able to select only the cross-sectionally cut mononuclear cells to guarantee a valid surface area quantification. With histological specimens analysis, the differentiation between normal physiological and abnormal

pathological responses was performed. The pathological cardiac hypertrophy responses differs by disorganization of cardiac structure, inflammatory cells infiltration, as well as fibrotic changes (129). Hence, in addition to WGA-staining, we also performed hematoxylin-eosin and picrosirius red staining to detect the presence of possible pathological hallmarks of cardiac hypertrophy. We found neither sign of inflammation nor fibrosis in training hearts irrespective of training duration. These results were in line with previous studies which showed that chronic moderate intensity endurance training in rats (duration varied from 28 days until 35 months) reduced inflammatory cytokines and fibrosis markers in blood, tissues, as well as their molecular expression level in chemotherapy-damaged and ageing hearts (130, 131). Nevertheless, to fully rule out the possibility of patchy inflammation and fibrosis, the whole organ histological sample should be examined further thoroughly in addition to tissue specific protein expression analysis. This outcome further affirmed our hypothesis that cardiac remodeling induced by endurance training exhibited no signs of pathologic histology hallmarks.

4.4 The interpretation of FDG-derived cardiac volumetric and function analysis in training hearts using small-animal dedicated PET/CT scan.

Previous publications have shown that LVMV was increased in hypertrophic myocardium due to afterload pressure augmentation by ligating ascending aorta in mice (96). As previously described, the enlarged cardiomyocytes in this pathological hypertrophy model have apparently taken up more glucose as primary energy substrates. The higher proportion of myocardial ^{18}F-FDG in hypertrophied cardiomyocytes was visualized as elevated ^{18}F-FDG derived metabolic volume as well as %IA/g. As opposed to this, the radiotracers uptake in myocardial infarction model was substantially diminished due to cardiomyocytes loss, fibrotic tissue formation, and pathological cardiac chamber dilatation (95). The mice which had undergone both permanent as well as transient left coronary anterior descending artery ligation were observed to have lower LVMV and higher cardiac %IA/g values in acute phase compared to their sham control, contributed to ischemic-related cardiomyocytes death and inflammatory reaction (132).

The automated measurements of LVMV as well as cardiac %IA/g have not been used before to validate the cardiac morphological, functional, and ^{18}F-FDG derived metabolic alterations in response to physiological endurance training. So far, only the studies of heart morphological and functional assessments using two-dimensional echocardiography as well as cardiac MRI have been published with limited information and high variability due to measurement bias (133). Thus, we aimed in this study to better characterize these volumetric, functional, and 18F-FDG uptake occurred in animals which performed chronic forced endurance training using small animal dedicated PET/CT scan.

Acute training shifts indeed cardiac metabolism towards glucose utilization instead of ketone bodies from fatty acid β-oxidation. During endurance training, glucose is readily available from glycolysis, glycogenolysis, as well as external uptake using glucose transporters and metabolized aerobically in heart tissue quickly to produce ATP for sarcomere contraction. Several physiological adaptations occurred in response to acute increase of body metabolic demands such as heart rate and cardiac output as well as oxygen uptake augmentation. These alterations would further increase the myocardial glucose demand (134-136).

Moreover, recent studies have reported that myocardial ^{18}F-FDG uptake was enhanced by using inhalative agent (isoflurane) in contrast to injectable anesthesia (ketamine/xylazine) both in normal and inflamed hearts. Thus, the LVMV and cardiac %IA/g were expected to raise when the ^{18}F-FDG PET/CT scan was directly performed under anesthesia in acute training phase (91, 137, 138). However, all the mice participated in our study were rested for several days before scan to allow reconditioning and avoid the influence of stress and adrenergic/sympathetic nerve activation in cardiac function evaluation directly after training. During the reconditioning phase, we assumed that cardiac homeostasis was again reached equilibrium towards fatty acid utilization as normal major myocardial energy substrates, thus no significance in LVMV and cardiac %IA/g differences were observed in our training mice in comparison to their matched sedentary controls. In the previous study, the LVMV has been reported raising in mice from the age 8-18 weeks parallel to their growth (94). Although the training hearts after 8 weeks duration was shown in our study to be enlarged in both gross and histological appearances, the LVMV as marker of cardiac mass and cardiac %IA/g as marker of tracer uptake did not show any significant alterations, thus indicating that other factor might have more influence in LVMV independent of training status.

Theoretically, physiological cardiac hypertrophy after endurance training maintained their normal metabolism pathways independent of glucose as ATP substrate, thus the LVMV and cardiac %IA/g kinetics were practically recorded similar to the untreated controls due to unchanged uptake of ^{18}F-FDG. Furthermore, the increase demand for glucose could indicate various of pathological processes such as increase in metabolic activity in hypoxic-injured myocardium, inflammation, immune cell infiltration, or in hypertrophic cardiomyopathy which did not occur in physiological hypertrophy state (139, 140). Several physiological stress hormones such as insulin, glucagon, cortisol, and IGF-1 have been reported to alter myocardial ^{18}F-FDG uptake, which was not evaluated further in our study (141). Sex and hormones were considered as influencing factors in myocardial ^{18}F-FDG uptake (142). In this study, we examined only the PET/CT images of training male mice which posed a limitation in scrutinizing the detailed results on the different sexes.

The most common used technique to study left ventricular mass and cardiac volume both in healthy and disease states is cardiac magnetic resonance imaging (MRI) and PET/CT scan (143). Nevertheless, the PET/CT modality is utilized for the same purpose with additional information regarding cardiac functionality in terms of tracer uptake. The ECG-gated reconstructed PET/CT image acquisitions were processed to derive the information of chamber volumes on each cardiac cycle which is comparable to cardiac MRI (144). The left ventricular EF and CO as indicators of cardiac performance can be subsequently derived by evaluating the dynamic alterations in EDV, ESV, SV, and heart rate/minute.

Eccentric cardiac hypertrophy which systematically reviewed after 2 years of chronic training in athletes who perform triathlon was characterized by mild pronounced increase in EDV and SV with relatively higher maintained ESV as well as LVEF (145). Physiological hypertrophy could also compensate the lower baseline heart rate with an increase in SV to maintain the equation of relatively normal CO indicating a prevailing overall cardiac function in humans (147). Our study did not show significant difference of heart volumetric parameter across different timepoints other than EDV in 8-weeks training animals. The training mice had similar SV, LVEF, and relatively stable ESV referring to a persisted cardiac performance. However, we have only used one replicate experiment of total 10 mice in this group, which may contribute to a weaker statistical power on the analysis. The use of different batches of mice across groups in different training duration might also provide source of measurement bias due to inter-individual variability among the experimental animals leading to the inconsistent results.

Complementing the previous results, we managed to show that the heart rate was positively correlated with LVMV in training groups. This highlighted back the basic cardiovascular physiology, in which larger hearts principally eject more blood to meet the body´s oxygen demand compared to smaller one, thus only require a lower baseline heart rate to maintain the CO (2, 24). The use of light-to-moderate inhalative anesthesia isoflurane to sedate the animals during the image acquisition depresses indeed the myocardial contractility, thus increases slightly the heart rate to maintain the CO (91). This also contributed as a confounding factor and limitation in our study.

Furthermore, the correlation between LVMV and heart volumetric indicators could prompt a new approach in three-dimension evaluation of cardiac function. The increasing heart volumes (EDV in this case) was well correlated with LVMV of training animals. The LVMV was observed to be not correlated with cardiac pump performance (LVEF) both in training and sedentary animals. This underlines the consensus that endurance training indeed promotes an increase in the left ventricular cardiac mass reflected by LVMV and EDV augmentation without affecting much the cardiac performance (LVEF) referring to an exercise induced positive cardiac remodeling or most commonly described as athlete's heart (148). Finally, we concluded that cardiac hypertrophic remodeling induced by chronic forced intensity-controlled treadmill running has been observed morphologically, histologically, and functionally without evoking inflammatory or fibrosis reactions as well as affecting the ejection fraction and cardiac output.

4.5 The molecular signature of cardiac hypertrophy in endurance training

The results of our RNA-sequencing analysis showed that 8-week training hearts upregulated genes involved in cell cycle, apoptosis, fatty acid homeostasis, organ growth pathways, and cardiac developmental processes. This work, however, cannot discuss all the pertinent finding of the RNA sequencing, but will focus on a few genes as examples.

Adult cardiomyocytes are traditionally viewed as not proliferating cells. Most cardiac cells could alter their size (hypertrophy) in postnatal time due to certain stimuli but not the numbers (hyperplasia). The cardiac cells are normally not able to regenerate following injury for example after myocardial infarction due to limitation of reentry to cell cycle for division (149). However, some other studies stated differently that mammalian cardiomyocytes have not yet reached their terminal differentiation and might have the potential to reprogram to proliferate using the right stimuli (150).

In our top 20 differentially expressed annotated genes between training and sedentary groups, at least five are involved in regulating cell cycle showing a probable contribution to the observed phenotypic changes in response to endurance training. Several important genes which served as an inhibitor of apoptosis and checkpoint for cell cycle progression towards mitosis such as *bcl2l1*, *ccn2*, and *cdkn1a* were both downregulated in training hearts. However, their role in protein homeostasis to promote adult cardiomyocytes reentry to the cell cycle or even apoptosis remained controversial. The mice which performed voluntary running wheel for 3 weeks have shown to downregulate cell cycle inhibitors and apoptosis regulator (p16, p53, and cell-cycle-checkpoint-kinase 2) in vascular endothelial cells by almost to half amount (42-57%) of baseline. Furthermore, previous publication has shown that the microRNAs in endurance training athlete might have a crucial role as a mediator to target downstream products of cell cycle proteins cyclin dependent kinases in skeletal muscle biopsies (152).

There are only limited number of reliable previous publications in basic science research which show the alteration in cardiomyocytes cell cycle regulator expression in response to endurance training. Several studies in the past managed to show that endurance training both voluntary wheels running and forced running on a treadmill of 4-8 weeks in rats might be responsible to enhance the regeneration capacity of cardiomyocytes. This study used ^{15}N-Thymidine multi-isotope imaging mass spectrophotometry to quantify the increased number of resident endogenous cardiac stem cell progenitors indicating cardiomyogenesis (153, 154). This long debate need to be finally solved but always faces a huge number of technical difficulties due to limitation of reliable methods to truly inspect cardiomyocytes proliferation and regeneration activities especially *in vivo* in post-fetal period (155).

Several genes pertaining to cardiac hypertrophy during endurance training were found to be upregulated in our RNA sequence analysis. The A-kinase anchoring proteins (AKAP) are important scaffolding proteins involved in subcellular MAPK signal transduction cascades leading to compensatory cardiac hypertrophic in response to stress. These proteins act also epigenetically by modifying the PKD1 associated HDAC5 activation resulting in expression of MEF-2 nuclear transcription factor and re-expression of cardiomyocytes specific developmental genes leading to hypertrophy. Previous studies showed that the deletion of AKAP in mice exhibited an accelerated progression to heart failure, increased collagen deposition, apoptosis, and attenuated compensatory cardiac hypertrophy response after angiotensin II administration as well as transverse aortic ligation. Recent genome wide expression analysis in mice indicated also the essential role of *in vivo* AKAP13-PKD1 signaling circuits in regulating cardiomyocytes contraction, apoptosis, and energy substrate metabolism during physiological response of cardiac hypertrophy (156, 157).

Both *Myh6* and *Myh7* expresses sarcomeric contractile proteins α- and β-myosin heavy chains respectively, are importantly upregulated in the cardiac hypertrophy response pertaining to environmental stress stimuli. One study indicated that the depletion of both *Myh6* and *Myh7* expression using CRISPR/Cas9 technology attenuates the cardiac hypertrophy in mice undergone transverse aortic constriction (158). The *Myh7* was however expressed mainly on the developing heart during the fetal period, the *Myh6* on the other hand produces the majority myosin contractile proteins in the adult mammals. The increased expression of α-myosin heavy chains by *Myh6* is associated with improved left ventricular contractility in healthy adults who performed high intensity interval training. The balance between these two isoform proteins is important to maintain proper physiologic cardiac contraction during adulthood and the ratio of *Myh6/Myh7* might change slightly depending on the source of culprit stimulus. The *Myh7* expression is mostly negligible in the postnatal period and re-expression of embryonal β-myosin heavy chain in adult hearts is associated with cardiac hypertrophy in response to muscle injury and remodeling indicating that *Myh7* could serve a potential target of cardiac hypertrophy reversal in the future (159). Our results suggested that *Myh7* was upregulated and *Myh6* was oppositely downregulated in training heart. The increased ratio of *Myh7/Myh6* is normally associated with pathological cardiac hypertrophy in heart failure, thus these results require a further validation in the future by analyzing the gene expression on protein levels.

Our RNA sequencing results on the training hearts also indicated activation of several other pathways in response to growth stimulus such as FGF, PDGF, and TGF-β/BMP/Smad. The exact role of these pathways in cardiac hypertrophy is currently still under extensive research. The physiological cellular response to TGF-β receptor activation might differ depending on the cell types as well as spatio-temporary factor. In heart tissues, the TGF-β plays a very important role in cardiac morphogenesis during the early life phase, but its activation at the later point of life may lead to

epithelial-mesenchymal transition after cardiac injury or inflammation and promoting the fibroblast to deposit extracellular matrix leading to organ stiffness (166). The ligands for TGF-β receptor are also varied, however they work mostly through serine-threonine kinases cascade and act canonically with other Smad proteins which activate several important transcription factors in the nucleus. The TGF-β superfamily receptors work also synergistically with bone morphogenic and growth differentiation factors-11 (GDF-11) proteins which may participate in cell growth, differentiation, and regeneration, suggesting the important role of these molecular pathways in cardiomyogenesis (167, 168).

The TGF-β pathway might also contribute to re-expression of several fetal gene proteins which alter the cellular program towards remodeling after endurance training. Prolonged endurance training on running rats for 6 weeks might potentially stimulate the mRNA expression of TGF-β in skeletal muscle, but not in cardiomyocytes without affecting their tissue protein levels (169). Moreover, this pathway could have been switched on in timely manner in response to myocardial hypoxic injury during infarction which is important for tissue repair response. Several recent experimental *in vitro* and *in vivo* studies in zebrafish model pointed out the visionary modulatory role of TGF-β in cardiomyocytes regeneration and differentiation, indicating a cross-talks between the downstream response and other crucial proteins of cell cycle and proliferation. The inhibition of TGF-β/Smad3 signaling pathway has been shown to probably limit cardiomyocytes proliferation and migration by disrupting the cell cycle checkpoint as well as epithelial-mesenchymal transition response impacting zebra fish's heart regeneration ability (170, 171). Unfortunately, there are very limited number of publications exploring these interconnecting pathways *in vivo* in mammals. Furthermore, recent advances in heart failure research showed a possible connection between the TGF-β activation and the diminished systolic function, cardiac fibrosis, and cardiomyopathies indicating the negative effects of TGF-β activation in pathological cardiac hypertrophy and remodeling after cardiac injury. It seems that the overlap between physiological and pathological cardiac hypertrophy is still controversial and need to be clarified in the future (172).

4.6 Conclusion

We observed the morphometric alterations attributable to cardiac and skeletal muscle hypertrophy due to chronic forced intensity-controlled endurance training. These detected phenotypic changes were subsequently examined microscopically, showing the enlargement of cardiomyocytes and skeletal myocytes cross-sectional area without detection of inflammatory or fibrotic responses. A consistent morphometric characterization and histology pertaining to cardiac hypertrophy could be observed in mice as early as 8 weeks of endurance training for 120 minutes/day. The training hearts maintained their volumes and normal pump function, while no significant alterations in the cardiac volumetric and functionality assessment were measured in the PET/CT-scan quantification. Finally, the running mice expressed the genes involved in the signaling pathways, which are participating in the cellular proliferation, apoptosis, contractile protein synthesis, extracellular matrix deposition, glucose transport, lipid homeostasis, and organ growth on the RNA level. Nevertheless, this observed discovery requires further clarification and validation on the protein level.

There have been no previous publications corresponding to the application of such extensive and innovative approaches to investigate endurance training-induced cardiac hypertrophy, underlining the added value of our study to the existing literature. The results could serve as a fundament of further studies to dissect the effects of endurance training on the heart physiology and cardiac

hypertrophy using genetically modified experimental animals or disease model. Moreover, further advancement in the molecular research could lead to a possible new discovery of the responsible gene signatures involved in cardiac hypertrophy during endurance training and their downstream interconnections both in physiological and certain pathologies, therefore opening the way to the new therapeutic concepts in the future.

References

1. Dabbagh A, Imani A, Rajaei S. Cardiac physiology. Postoperative Critical Care for Adult Cardiac Surgical Patients: Springer; 2018. p. 25-74.

2. Oberman R, Bhardwaj A. Physiology, Cardiac. StatPearls [Internet]: StatPearls Publishing; 2021.

3. Vives M. Cardiovascular Physiology. Cardiac Anesthesia and Postoperative Care in the 21st Century: Springer; 2022. p. 21-45.

4. Jönsson S, Agic MB, Narfström F, Melville JM, Hultström M. Renal neurohormonal regulation in heart failure decompensation. American Journal of Physiology-Regulatory, Integrative and Comparative Physiology. 2014;307(5):R493-R7.

5. Shimizu I, Minamino T. Physiological and pathological cardiac hypertrophy. Journal of molecular and cellular cardiology. 2016;97:245-62.

6. Dorn GW. The fuzzy logic of physiological cardiac hypertrophy. Hypertension. 2007;49(5):962-70.

7. Mone SM, Sanders SP, Colan SD. Control mechanisms for physiological hypertrophy of pregnancy. Circulation. 1996;94(4):667-72.

8. Hartupee J, Mann DL. Neurohormonal activation in heart failure with reduced ejection fraction. Nature Reviews Cardiology. 2017;14(1):30-8.

9. Bayes-Genis A, Morant-Talamante N, Lupón J. Neprilysin and natriuretic peptide regulation in heart failure. Current heart failure reports. 2016;13(4):151-7.

10. Morita H, Rehm HL, Menesses A, McDonough B, Roberts AE, Kucherlapati R, et al. Shared genetic causes of cardiac hypertrophy in children and adults. New England Journal of Medicine. 2008;358(18):1899-908.

11. Marian AJ. Genetic determinants of cardiac hypertrophy. Current opinion in cardiology. 2008;23(3):199.

12. Gibb M, Burton RA, Bollensdorff C, Afonso C, Mansoori T, Schotten U, et al., editors. Resolving the three-dimensional histology of the heart. International Conference on Computational Methods in Systems Biology; 2012: Springer.

13. Litviňuková M, Talavera-López C, Maatz H, Reichart D, Worth CL, Lindberg EL, et al. Cells of the adult human heart. Nature. 2020;588(7838):466-72.

14. Pearlman E, Weber K, Janicki J, editors. Quantitative histology of the hypertrophied human heart. Federation proceedings; 1981.

15. Gohda ZA. Histological architecture of cardiac myofibers composing the left ventricle of murine heart. Journal of Histology & Histopathology. 2015.

16. Bensley JG, De Matteo R, Harding R, Black MJ. Three-dimensional direct measurement of cardiomyocyte volume, nuclearity, and ploidy in thick histological sections. Scientific reports. 2016;6(1):1-10.

17. Tan WCC, Nerurkar SN, Cai HY, Ng HHM, Wu D, Wee YTF, et al. Overview of multiplex immunohistochemistry/immunofluorescence techniques in the era of cancer immunotherapy. Cancer Communications. 2020;40(4):135-53.

18. Grogan T, Reinhardt K, Jaramillo M, Lee D. An update on" special stain" histochemistry with emphasis on automation. Advances in anatomic pathology. 2000;7(2):110-22.

19. Ganesan J, Ramanujam D, Sassi Y, Ahles A, Jentzsch C, Werfel S, et al. MiR-378 controls cardiac hypertrophy by combined repression of mitogen-activated protein kinase pathway factors. Circulation. 2013;127(21):2097-106.

20. Emde B, Heinen A, Gödecke A, Bottermann K. Wheat germ agglutinin staining as a suitable method for detection and quantification of fibrosis in cardiac tissue after myocardial infarction. European journal of histochemistry: EJH. 2014;58(4).

21. Rivera-Brown AM, Frontera WR. Principles of exercise physiology: responses to acute exercise and long-term adaptations to training. Pm&r. 2012;4(11):797-804.

22. Lavie CJ, Arena R, Swift DL, Johannsen NM, Sui X, Lee D-c, et al. Exercise and the cardiovascular system: clinical science and cardiovascular outcomes. Circulation research. 2015;117(2):207-19.

23. Lee B-A, Oh D-J. The effects of long-term aerobic exercise on cardiac structure, stroke volume of the left ventricle, and cardiac output. Journal of exercise rehabilitation. 2016;12(1):37.

24. Opondo MA, Sarma S, Levine BD. The cardiovascular physiology of sports and exercise. Clinics in Sports Medicine. 2015;34(3):391-404.

25. Williams GS, Huertas MA, Sobie EA, Jafri MS, Smith GD. A probability density approach to modeling local control of calcium-induced calcium release in cardiac myocytes. Biophysical Journal. 2007;92(7):2311-28.

26. Locatelli J, de Assis LV, Isoldi MC. Calcium handling proteins: structure, function, and modulation by exercise. Heart failure reviews. 2014;19(2):207-25.

27. Patel H, Alkhawam H, Madanieh R, Shah N, Kosmas CE, Vittorio TJ. Aerobic vs anaerobic exercise training effects on the cardiovascular system. World journal of cardiology. 2017;9(2):134.

28. Lopaschuk GD, Ussher JR, Folmes CD, Jaswal JS, Stanley WC. Myocardial fatty acid metabolism in health and disease. Physiological reviews. 2010;90(1):207-58.

29. Ruegsegger GN, Booth FW. Health benefits of exercise. Cold Spring Harbor perspectives in medicine. 2018;8(7):a029694.

30. Konopka AR, Harber MP. Skeletal muscle hypertrophy after aerobic exercise training. Exercise and sport sciences reviews. 2014;42(2):53.

31. Pal S, Radavelli-Bagatini S, Ho S. Potential benefits of exercise on blood pressure and vascular function. Journal of the American Society of Hypertension. 2013;7(6):494-506.

32. Kim JH, Baggish AL. Differentiating exercise-induced cardiac adaptations from cardiac pathology: the “grey zone” of clinical uncertainty. Canadian Journal of Cardiology. 2016;32(4):429-37.

33. Sharma S, Merghani A, Mont L. Exercise and the heart: the good, the bad, and the ugly. European heart journal. 2015;36(23):1445-53.

34. Garciarena CD, Pinilla OA, Nolly MB, Laguens RP, Escudero EM, Cingolani HE, et al. Endurance training in the spontaneously hypertensive rat: conversion of pathological into physiological cardiac hypertrophy. Hypertension. 2009;53(4):708-14.

35. Eijsvogels TM, Fernandez AB, Thompson PD. Are there deleterious cardiac effects of acute and chronic endurance exercise? Physiological reviews. 2016;96(1):99-125.

36. Gibala MJ, Little JP, MacDonald MJ, Hawley JA. Physiological adaptations to low-volume, high-intensity interval training in health and disease. The Journal of physiology. 2012;590(5):1077-84.

37. Pelliccia A, Kinoshita N, Pisicchio C, Quattrini F, DiPaolo FM, Ciardo R, et al. Long-term clinical consequences of intense, uninterrupted endurance training in Olympic athletes. Journal of the American College of Cardiology. 2010;55(15):1619-25.

38. Goodman JM, Liu PP, Green HJ. Left ventricular adaptations following short-term endurance training. Journal of applied physiology. 2005;98(2):454-60.

39. Bernardo BC, Weeks KL, Pretorius L, McMullen JR. Molecular distinction between physiological and pathological cardiac hypertrophy: experimental findings and therapeutic strategies. Pharmacology & therapeutics. 2010;128(1):191-227.

40. Hill JA. Electrical remodeling in cardiac hypertrophy. Trends in cardiovascular medicine. 2003;13(8):316-22.

41. Benito B, Gay-Jordi G, Serrano-Mollar A, Guasch E, Shi Y, Tardif J-C, et al. Cardiac arrhythmogenic remodeling in a rat model of long-term intensive exercise training. Circulation. 2011;123(1):13-22.

42. Guasch E, Benito B, Qi X, Cifelli C, Naud P, Shi Y, et al. Atrial fibrillation promotion by endurance exercise: demonstration and mechanistic exploration in an animal model. Journal of the American College of Cardiology. 2013;62(1):68-77.

43. Polyák AJ, Kui P, Morvay N, Leprán I, Ágoston G, Varga A, et al. Long-term endurance training-induced cardiac adaptation in new rabbit and dog animal models of the human athlete's heart. Reviews in Cardiovascular Medicine. 2018;19(4):135-42.

44. Tharp DL, Masseau I, Ivey J, Laughlin MH, Bowles DK. Endurance exercise training does not limit coronary atherosclerosis in familial hypercholesterolemic swine. Physiological Reports. 2019;7(4):e14008.

45. Thu VT, Kim HK, Han J. Acute and chronic exercise in animal models. Exercise for Cardiovascular Disease Prevention and Treatment: From Molecular to Clinical, Part 1. 2017:55-71.

46. Rai V, Sharma P, Agrawal S, Agrawal DK. Relevance of mouse models of cardiac fibrosis and hypertrophy in cardiac research. Molecular and cellular biochemistry. 2017;424:123-45.

47. Nakamura M, Sadoshima J. Mechanisms of physiological and pathological cardiac hypertrophy. Nature Reviews Cardiology. 2018;15(7):387-407.

48. Maillet M, Van Berlo JH, Molkentin JD. Molecular basis of physiological heart growth: fundamental concepts and new players. Nature reviews Molecular cell biology. 2013;14(1):38-48.

49. Hirt MN, Sörensen NA, Bartholdt LM, Boeddinghaus J, Schaaf S, Eder A, et al. Increased afterload induces pathological cardiac hypertrophy: a new in vitro model. Basic research in cardiology. 2012;107(6):1-16.

50. Gsell MA, Augustin CM, Prassl AJ, Karabelas E, Fernandes JF, Kelm M, et al. Assessment of wall stresses and mechanical heart power in the left ventricle: Finite element modeling versus Laplace analysis. International journal for numerical methods in biomedical engineering. 2018;34(12):e3147.

51. Gibb AA, Hill BG. Metabolic coordination of physiological and pathological cardiac remodeling. Circulation research. 2018;123(1):107-28.

52. Heineke J, Molkentin JD. Regulation of cardiac hypertrophy by intracellular signalling pathways. Nature reviews Molecular cell biology. 2006;7(8):589-600.

53. Caturano A, Vetrano E, Galiero R, Salvatore T, Docimo G, Epifani R, et al. Cardiac Hypertrophy: from Pathophysiological Mechanisms to Heart Failure Development. Reviews in Cardiovascular Medicine. 2022;23(5):165.

54. Ellison GM, Waring CD, Vicinanza C, Torella D. Physiological cardiac remodelling in response to endurance exercise training: cellular and molecular mechanisms. Heart. 2012;98(1):5-10.

55. Dorn GW, Force T. Protein kinase cascades in the regulation of cardiac hypertrophy. The Journal of clinical investigation. 2005;115(3):527-37.

56. Bass-Stringer S, Tai CM, McMullen JR. IGF1–PI3K-induced physiological cardiac hypertrophy: Implications for new heart failure therapies, biomarkers, and predicting cardiotoxicity. Journal of Sport and Health Science. 2021;10(6):637-47.

57. Molkentin JD. Calcineurin–NFAT signaling regulates the cardiac hypertrophic response in coordination with the MAPKs. Cardiovascular research. 2004;63(3):467-75.

58. Tham YK, Bernardo BC, Ooi JY, Weeks KL, McMullen JR. Pathophysiology of cardiac hypertrophy and heart failure: signaling pathways and novel therapeutic targets. Archives of toxicology. 2015;89(9):1401-38.

59. Mao K, Kobayashi S, Jaffer ZM, Huang Y, Volden P, Chernoff J, et al. Regulation of Akt/PKB activity by P21-activated kinase in cardiomyocytes. Journal of molecular and cellular cardiology. 2008;44(2):429-34.

60. McMullen JR, Sherwood MC, Tarnavski O, Zhang L, Dorfman AL, Shioi T, et al. Inhibition of mTOR signaling with rapamycin regresses established cardiac hypertrophy induced by pressure overload. Circulation. 2004;109(24):3050-5.

61. Lorenz K, Schmitt JP, Vidal M, Lohse MJ. Cardiac hypertrophy: targeting Raf/MEK/ERK1/2-signaling. The international journal of biochemistry & cell biology. 2009;41(12):2351-5.

62. Samak M, Fatullayev J, Sabashnikov A, Zeriouh M, Schmack B, Farag M, et al. Cardiac hypertrophy: an introduction to molecular and cellular basis. Medical science monitor basic research. 2016;22:75.

63. Oldfield CJ, Duhamel TA, Dhalla NS. Mechanisms for the transition from physiological to pathological cardiac hypertrophy. Canadian Journal of Physiology and Pharmacology. 2020;98(2):74-84.

64. Lerchenmüller C, Vujic A, Mittag S, Wang A, Rabolli CP, Heß C, et al. Restoration of cardiomyogenesis in aged mouse hearts by voluntary exercise. Circulation. 2022;146(5):412-26.

65. Xiao J, Xu T, Li J, Lv D, Chen P, Zhou Q, et al. Exercise-induced physiological hypertrophy initiates activation of cardiac progenitor cells. International journal of clinical and experimental pathology. 2014;7(2):663.

66. Brancaccio M, Fratta L, Notte A, Hirsch E, Poulet R, Guazzone S, et al. Melusin, a muscle-specific integrin β1–interacting protein, is required to prevent cardiac failure in response to chronic pressure overload. Nature medicine. 2003;9(1):68-75.

67. Iemitsu M, Maeda S, Jesmin S, Otsuki T, Miyauchi T. Exercise training improves aging-induced downregulation of VEGF angiogenic signaling cascade in hearts. American Journal of Physiology-Heart and Circulatory Physiology. 2006;291(3):H1290-H8.

68. Oka T, Akazawa H, Naito AT, Komuro I. Angiogenesis and cardiac hypertrophy: maintenance of cardiac function and causative roles in heart failure. Circulation research. 2014;114(3):565-71.

69. Zhu X, Yuan Y, Rao S, Wang P. LncRNA MIAT enhances cardiac hypertrophy partly through sponging miR-150. Eur Rev Med Pharmacol Sci. 2016;20(17):3653-60.

70. Bernardo BC, Gao X-M, Winbanks CE, Boey EJ, Tham YK, Kiriazis H, et al. Therapeutic inhibition of the miR-34 family attenuates pathological cardiac remodeling and improves heart function. Proceedings of the National Academy of Sciences. 2012;109(43):17615-20.

71. Zhou H, Wang B, Yang Y-x, Jia Q-j, Zhang A, Qi Z-w, et al. Long noncoding RNAs in pathological cardiac remodeling: a review of the update literature. BioMed research international. 2019;2019.

72. Hastings MH, Herrera JJ, Guseh JS, Atlason B, Houstis NE, Abdul Kadir A, et al. Animal models of exercise from rodents to pythons. Circulation Research. 2022;130(12):1994-2014.

73. Bacmeister L, Schwarzl M, Warnke S, Stoffers B, Blankenberg S, Westermann D, et al. Inflammation and fibrosis in murine models of heart failure. Basic research in cardiology. 2019;114:1-35.

74. Wang Y, Wisloff U, Kemi OJ. Animal models in the study of exercise-induced cardiac hypertrophy. Physiological research. 2010;59(5):633.

75. Feng R, Wang L, Li Z, Yang R, Liang Y, Sun Y, et al. A systematic comparison of exercise training protocols on animal models of cardiovascular capacity. Life sciences. 2019;217:128-40.

76. Diffee GM, Nagle DF. Regional differences in effects of exercise training on contractile and biochemical properties of rat cardiac myocytes. Journal of Applied Physiology. 2003;95(1):35-42.

77. Moore RL, Musch TI, Yelamarty R, Scaduto Jr RC, Semanchick AM, Elensky M, et al. Chronic exercise alters contractility and morphology of isolated rat cardiac myocytes. American Journal of Physiology-Cell Physiology. 1993;264(5):C1180-C9.

78. Fenning A, Harrison G, Dwyer D, Rose'Meyer R, Brown L. Cardiac adaptation to endurance exercise in rats. Molecular and cellular biochemistry. 2003;251:51-9.

79. Wisløff U, Helgerud J, Kemi OJ, Ellingsen Ø. Intensity-controlled treadmill running in rats: V̇ o 2 max and cardiac hypertrophy. American journal of physiology-heart and circulatory physiology. 2001;280(3):H1301-H10.

80. Kemi OJ, Loennechen JP, Wisløff U, Ellingsen Ø. Intensity-controlled treadmill running in mice: cardiac and skeletal muscle hypertrophy. Journal of applied physiology. 2002;93(4):1301-9.

81. Nabi HA, Zubeldia JM. Clinical applications of 18F-FDG in oncology. Journal of nuclear medicine technology. 2002;30(1):3-9.

82. Treglia G. Diagnostic performance of 18F-FDG PET/CT in infectious and inflammatory diseases according to published meta-analyses. Contrast media & molecular imaging. 2019;2019.

83. Anand S, Singh H, Dash A. Clinical applications of PET and PET-CT. Medical Journal Armed Forces India. 2009;65(4):353-8.

84. Gropler RJ. PET radiotracers of the cardiovascular system. PET clinics. 2009;4(1):69-87.

85. Nakazato R, Berman DS, Alexanderson E, Slomka P. Myocardial perfusion imaging with PET. Imaging in medicine. 2013;5(1):35.

86. Driessen RS, Raijmakers PG, Stuijfzand WJ, Knaapen P. Myocardial perfusion imaging with PET. The international journal of cardiovascular imaging. 2017;33(7):1021-31.

87. Basu S, Kwee TC, Surti S, Akin EA, Yoo D, Alavi A. Fundamentals of PET and PET/CT imaging. Annals of the New York Academy of Sciences. 2011;1228(1):1-18.

88. Peterson LR, Gropler RJ. Radionuclide imaging of myocardial metabolism. Circulation: Cardiovascular Imaging. 2010;3(2):211-22.

89. Khalaf S, Al-Mallah MH. Fluorodeoxyglucose applications in cardiac PET: viability, inflammation, infection, and beyond. Methodist DeBakey cardiovascular journal. 2020;16(2):122.

90. Werner RA, Chen X, Rowe SP, Lapa C, Javadi MS, Higuchi T. Moving into the next era of PET myocardial perfusion imaging: introduction of novel 18 F-labeled tracers. The International Journal of Cardiovascular Imaging. 2019;35:569-77.

91. Toyama H, Ichise M, Liow J-S, Vines DC, Seneca NM, Modell KJ, et al. Evaluation of anesthesia effects on [18F] FDG uptake in mouse brain and heart using small animal PET. Nuclear medicine and biology. 2004;31(2):251-6.

92. Jeong J, Kong E, Chun K, Cho I. The impact of energy substrates, hormone level and subject-related factors on physiologic myocardial 18F-FDG uptake in normal humans. Nuclear medicine and molecular imaging. 2013;47(4):225-31.

93. Wang Q, He Z-G, Li S-Y, Feng M-H, Xiang H-B. Application of animal and human PET in cardiac research. American journal of cardiovascular disease. 2018;8(3):24.

94. Fischer M, Zacherl MJ, Weinberger T, Weckbach L, Huber B, Schulz C, et al. Comparison of metabolic and functional parameters using cardiac 18F-FDG-PET in early to mid-adulthood male and female mice. EJNMMI research. 2021;11(1):1-9.

95. Fischer M, Zacherl MJ, Weckbach L, Paintmayer L, Weinberger T, Stark K, et al. Cardiac 18F-FDG Positron Emission Tomography: An Accurate Tool to Monitor In vivo Metabolic and Functional Alterations in Murine Myocardial Infarction. Frontiers in cardiovascular medicine. 2021;8:508.

96. Todica A, Beetz NL, Günther L, Zacherl MJ, Grabmaier U, Huber B, et al. Monitoring of cardiac remodeling in a mouse model of pressure-overload left ventricular hypertrophy with [18F] FDG MicroPET. Molecular Imaging and Biology. 2018;20(2):268-74.

97. Fischer M, Olivier J, Lindner S, Zacherl MJ, Massberg S, Bartenstein P, et al. Detection of cardiac apoptosis by [18F] ML-10 in a mouse model of permanent LAD ligation. Molecular Imaging and Biology. 2022:1-9.

98. Mula J, Lee JD, Liu F, Yang L, Peterson CA. Automated image analysis of skeletal muscle fiber cross-sectional area. Journal of Applied Physiology. 2013;114(1):148-55.

99. Gläser K, Wilke K, Wepf R, Biel S. Visualizing nuclei in skin cryosections: viable options to 4′ 6-diamidino-2-phenylindol for confocal laser microscopy. Skin Research and Technology. 2008;14(3):324-6.

100. Diffee GM, Nagle DF. Exercise training alters length dependence of contractile properties in rat myocardium. Journal of Applied Physiology. 2003;94(3):1137-44.

101. Beisvag V, Kemi OJ, Arbo I, Loennechen JP, Wisløff U, Langaas M, et al. Pathological and physiological hypertrophies are regulated by distinct gene programs. European Journal of Preventive Cardiology. 2009;16(6):690-7.

102. de Lade CG, Andreazzi AE, Bolotari M, Costa VMG, Peters VM, Guerra MdO. Effects of moderate intensity endurance training vs. high intensity interval training on weight gain, cardiorespiratory capacity, and metabolic profile in postnatal overfed rats. Diabetology & metabolic syndrome. 2018;10(1):1-9.

103. Boutcher SH. High-intensity intermittent exercise and fat loss. Journal of obesity. 2011;2011.

104. Willis LH, Slentz CA, Bateman LA, Shields AT, Piner LW, Bales CW, et al. Effects of aerobic and/or resistance training on body mass and fat mass in overweight or obese adults. Journal of applied physiology. 2012.

105. Hornberger Jr TA, Farrar RP. Physiological hypertrophy of the FHL muscle following 8 weeks of progressive resistance exercise in the rat. Canadian journal of applied physiology. 2004;29(1):16-31.

106. Farrell PA, Fedele MJ, Hernandez J, Fluckey JD, Miller III JL, Lang CH, et al. Hypertrophy of skeletal muscle in diabetic rats in response to chronic resistance exercise. Journal of applied physiology. 1999;87(3):1075-82.

107. Duncan ND, Williams DA, Lynch GS. Adaptations in rat skeletal muscle following long-term resistance exercise training. European journal of applied physiology and occupational physiology. 1998;77(4):372-8.

108. Cholewa J, Guimarães-Ferreira L, da Silva Teixeira T, Naimo MA, Zhi X, de Sá RBDP, et al. Basic models modeling resistance training: an update for basic scientists interested in study skeletal muscle hypertrophy. Journal of cellular physiology. 2014;229(9):1148-56.

109. Han G-S. Endurance exercise effects on cardiac hypertrophy in mice. Journal of Physical Therapy Science. 2013;25(12):1525-7.

110. Guski H, Meyer R, Fernandez-Britto J. Morphometric, histochemical and autoradiographic studies on myocardial cells in experimental cardiac hypertrophy and ischemia. Experimental pathology. 1991;41(2):79-97.

111. dos Santos Soares D, Pinto GH, Lopes A, Caetano DSL, Nascimento TG, Andrades ME, et al. Cardiac hypertrophy in mice submitted to a swimming protocol: influence of training volume and intensity on myocardial renin-angiotensin system. American Journal of Physiology-Regulatory, Integrative and Comparative Physiology. 2019.

112. Gunadi JW, Tarawan VM, Setiawan I, Lesmana R, Wahyudianingsih R, Supratman U. Cardiac hypertrophy is stimulated by altered training intensity and correlates with autophagy modulation in male Wistar rats. BMC Sports Science, Medicine and Rehabilitation. 2019;11(1):1-9.

113. Yan Z, Zeng N, Li J, Liao T, Ni G. Cardiac Effects of Treadmill Running at Different Intensities in a Rat Model. Frontiers in Physiology. 2021;12:774681.

114. Chavanelle V, Boisseau N, Otero YF, Combaret L, Dardevet D, Montaurier C, et al. Effects of high-intensity interval training and moderate-intensity continuous training on glycaemic control and skeletal muscle mitochondrial function in db/db mice. Scientific reports. 2017;7(1):1-10.

115. Martin-Smith R, Cox A, Buchan DS, Baker JS, Grace F, Sculthorpe N. High intensity interval training (HIIT) improves cardiorespiratory fitness (CRF) in healthy, overweight and obese adolescents: a systematic review and meta-analysis of controlled studies. International Journal of Environmental Research and Public Health. 2020;17(8):2955.

116. Seldeen KL, Lasky G, Leiker MM, Pang M, Personius KE, Troen BR. High intensity interval training improves physical performance and frailty in aged mice. The Journals of Gerontology: Series A. 2018;73(4):429-37.

117. Tsai C-L, Pan C-Y, Tseng Y-T, Chen F-C, Chang Y-C, Wang T-C. Acute effects of high-intensity interval training and moderate-intensity continuous exercise on BDNF and irisin levels and neurocognitive performance in late middle-aged and older adults. Behavioural Brain Research. 2021;413:113472.

118. Massett MP, Matejka C, Kim H. Systematic review and meta-analysis of endurance exercise training protocols for mice. Frontiers in physiology. 2021:2143.

119. Chimenti L, Morici G, Paternò A, Bonanno A, Siena L, Licciardi A, et al. Endurance training damages small airway epithelium in mice. American journal of respiratory and critical care medicine. 2007;175(5):442-9.

120. Svensson M, Rosvall P, Boza-Serrano A, Andersson E, Lexell J, Deierborg T. Forced treadmill exercise can induce stress and increase neuronal damage in a mouse model of global cerebral ischemia. Neurobiology of stress. 2016;5:8-18.

121. Natali A, Turner D, Harrison S, White E. Regional effects of voluntary exercise on cell size and contraction-frequency responses in rat cardiac myocytes. Journal of Experimental Biology. 2001;204(6):1191-9.

122. Eisele JC, Schaefer I-M, Randel Nyengaard J, Post H, Liebetanz D, Brüel A, et al. Effect of voluntary exercise on number and volume of cardiomyocytes and their mitochondria in the mouse left ventricle. Basic research in cardiology. 2008;103(1):12-21.

123. Kostrominova TY. Application of WGA lectin staining for visualization of the connective tissue in skeletal muscle, bone, and ligament/tendon studies. Microscopy research and technique. 2011;74(1):18-22.

124. Boström P, Mann N, Wu J, Quintero PA, Plovie ER, Panáková D, et al. C/EBPβ controls exercise-induced cardiac growth and protects against pathological cardiac remodeling. Cell. 2010;143(7):1072-83.

125. Wang L, Wang J, Yu P, Feng J, Xu G-e, Zhao X, et al. METTL14 is required for exercise-induced cardiac hypertrophy and protects against myocardial ischemia-reperfusion injury. Nature Communications. 2022;13(1):1-21.

126. Lu J, Liu J, Zhang L, Wang X, Zhang Y, Tang Q. Morphological and functional characterization of diabetic cardiomyopathy in db/db mice following exercise, metformin alone, or combination treatments. Biochemical and Biophysical Research Communications. 2021;584:80-6.

127. Liu Q, Chen L, Liang X, Cao Y, Zhu X, Wang S, et al. Exercise attenuates angiotensin Ⅱ-induced muscle atrophy by targeting PPARγ/miR-29b. Journal of Sport and Health Science. 2021.

128. Landim-Vieira M, Schipper JM, Pinto JR, Chase PB. Cardiomyocyte nuclearity and ploidy: when is double trouble? Journal of Muscle Research and Cell Motility. 2020;41(4):329-40.

129. McMullen JR, Jennings GL. Differences between pathological and physiological cardiac hypertrophy: novel therapeutic strategies to treat heart failure. Clinical and experimental pharmacology & physiology. 2007;34(4):255-62.

130. Yang H-L, Hsieh P-L, Hung C-H, Cheng H-C, Chou W-C, Chu P-M, et al. Early moderate intensity aerobic exercise intervention prevents doxorubicin-caused cardiac dysfunction through inhibition of cardiac fibrosis and inflammation. Cancers. 2020;12(5):1102.

131. Wright KJ, Thomas MM, Betik AC, Belke D, Hepple RT. Exercise training initiated in late middle age attenuates cardiac fibrosis and advanced glycation end-product accumulation in senescent rats. Experimental gerontology. 2014;50:9-18.

132. Fischer M, Weinberger T, Messerer D, Zacherl MJ, Schulz C, Massberg S, et al. Comparison of transient and permanent LAD ligation in mice using 18F-FDG PET imaging. Annals of Nuclear Medicine. 2022;36(6):533-43.

133. Shimada YJ, Shiota T. A meta-analysis and investigation for the source of bias of left ventricular volumes and function by three-dimensional echocardiography in comparison with magnetic resonance imaging. The American journal of cardiology. 2011;107(1):126-38.

134. Shao D, Tian R. Glucose transporters in cardiac metabolism and hypertrophy. Comprehensive Physiology. 2015;6(1):331.

135. Kolwicz Jr SC, Tian R. Glucose metabolism and cardiac hypertrophy. Cardiovascular research. 2011;90(2):194-201.

136. Cicone F, Viertl D, Quintela Pousa AM, Denoël T, Gnesin S, Scopinaro F, et al. Cardiac radionuclide imaging in rodents: a review of methods, results, and factors at play. Frontiers in medicine. 2017;4:35.

137. Thackeray JT, Bankstahl JP, Wang Y, Wollert KC, Bengel FM. Clinically relevant strategies for lowering cardiomyocyte glucose uptake for 18F-FDG imaging of myocardial inflammation in mice. European Journal of Nuclear Medicine and Molecular Imaging. 2015;42(5):771-80.

138. Hildebrandt IJ, Su H, Weber WA. Anesthesia and other considerations for in vivo imaging of small animals. ILAR journal. 2008;49(1):17-26.

139. Lee WW, Marinelli B, Van Der Laan AM, Sena BF, Gorbatov R, Leuschner F, et al. PET/MRI of inflammation in myocardial infarction. Journal of the American College of Cardiology. 2012;59(2):153-63.

140. Takeishi Y, Masuda A, Kubo H, Tominaga H, Oriuchi N, Takenoshita S. Cardiac imaging with 18F-fluorodeoxyglucose PET/MRI in hypertrophic cardiomyopathy. Journal of Nuclear Cardiology. 2017;24(5):1827-8.

141. Israel O, Weiler-Sagie M, Rispler S, Bar-Shalom R, Frenkel A, Keidar Z, et al. PET/CT quantitation of the effect of patient-related factors on cardiac 18F-FDG uptake. Journal of Nuclear Medicine. 2007;48(2):234-9.

142. Foryst-Ludwig A, Kreissl MC, Sprang C, Thalke B, Böhm C, Benz V, et al. Sex differences in physiological cardiac hypertrophy are associated with exercise-mediated changes in energy substrate availability. American Journal of Physiology-Heart and Circulatory Physiology. 2011;301(1):H115-H22.

143. Gaemperli O, Kaufmann PA. PET and PET/CT in cardiovascular disease. Annals of the New York Academy of Sciences. 2011;1228(1):109-36.

144. Lücke C, Oppolzer B, Werner P, Foldyna B, Lurz P, Jochimsen T, et al. Comparison of volumetric and functional parameters in simultaneous cardiac PET/MR: feasibility of volumetric assessment with residual activity from prior PET/CT. European Radiology. 2017;27(12):5146-57.

145. Scharf M, Brem MH, Wilhelm M, Schoepf UJ, Uder M, Lell MM. Cardiac magnetic resonance assessment of left and right ventricular morphologic and functional adaptations in professional soccer players. American heart journal. 2010;159(5):911-8.

146. Harbo MB, Nordén ES, Narula J, Sjaastad I, Espe EKS. Quantifying left ventricular function in heart failure: What makes a clinically valuable parameter? Progress in cardiovascular diseases. 2020;63(5):552-60.

147. Carter JB, Banister EW, Blaber AP. Effect of endurance exercise on autonomic control of heart rate. Sports medicine. 2003;33(1):33-46.

148. Galderisi M, Cardim N, d'Andrea A, Bruder O, Cosyns B, Davin L, et al. The multi-modality cardiac imaging approach to the Athlete's heart: an expert consensus of the European Association of Cardiovascular Imaging. European Heart Journal-Cardiovascular Imaging. 2015;16(4):353-r.

149. De Falco M, Cobellis G, De Luca A. Proliferation of cardiomyocytes: a question unresolved. Frontiers in Bioscience-Elite. 2009;1(2):528-36.

150. Anversa P, Kajstura J. Ventricular myocytes are not terminally differentiated in the adult mammalian heart. Circulation research. 1998;83(1):1-14.

151. Werner C, Fürster T, Widmann T, Pöss J, Roggia C, Hanhoun M, et al. Physical exercise prevents cellular senescence in circulating leukocytes and in the vessel wall. Circulation. 2009;120(24):2438-47.

152. Nielsen S, Scheele C, Yfanti C, Åkerström T, Nielsen AR, Pedersen BK, et al. Muscle specific microRNAs are regulated by endurance exercise in human skeletal muscle. The Journal of physiology. 2010;588(20):4029-37.

153. Vujic A, Lerchenmüller C, Wu T-D, Guillermier C, Rabolli CP, Gonzalez E, et al. Exercise induces new cardiomyocyte generation in the adult mammalian heart. Nature communications. 2018;9(1):1-9.

154. Waring CD, Vicinanza C, Papalamprou A, Smith AJ, Purushothaman S, Goldspink DF, et al. The adult heart responds to increased workload with physiologic hypertrophy, cardiac stem cell activation, and new myocyte formation. European heart journal. 2014;35(39):2722-31.

155. Walsh S, Pontén A, Fleischmann BK, Jovinge S. Cardiomyocyte cell cycle control and growth estimation in vivo—an analysis based on cardiomyocyte nuclei. Cardiovascular research. 2010;86(3):365-73.

156. Taglieri DM, Johnson KR, Burmeister BT, Monasky MM, Spindler MJ, DeSantiago J, et al. The C-terminus of the long AKAP13 isoform (AKAP-Lbc) is critical for development of compensatory cardiac hypertrophy. Journal of molecular and cellular cardiology. 2014;66:27-40.

157. Johnson KR, Nicodemus-Johnson J, Spindler MJ, Carnegie GK. Genome-wide gene expression analysis shows AKAP13-mediated PKD1 signaling regulates the transcriptional response to cardiac hypertrophy. PLoS One. 2015;10(7):e0132474.

158. Yue P, Xia S, Wu G, Liu L, Zhou K, Liao H, et al. Attenuation of cardiomyocyte hypertrophy via depletion MYH7 using CASAAV. Cardiovascular Toxicology. 2021;21(3):255-64.

159. Hsieh J, Becklin KL, Givens S, Komosa ER, Lloréns JEA, Moriarity BS, et al. Myosin heavy chain converter domain mutations drive early-stage changes in extracellular matrix dynamics in hypertrophic cardiomyopathy. Frontiers in Cell and Developmental Biology. 2022:1248.

160. Hafstad AD, Boardman NT, Lund J, Hagve M, Khalid AM, Wisløff U, et al. High intensity interval training alters substrate utilization and reduces oxygen consumption in the heart. Journal of Applied Physiology. 2011;111(5):1235-41.

161. Gupta MP. Factors controlling cardiac myosin-isoform shift during hypertrophy and heart failure. Journal of molecular and cellular cardiology. 2007;43(4):388-403.

162. Broderick TL, Poirier P, Gillis M. Exercise training restores abnormal myocardial glucose utilization and cardiac function in diabetes. Diabetes/metabolism research and reviews. 2005;21(1):44-50.

163. Takala TO, Nuutila P, Katoh C, Luotolahti M, Bergman Jr, Mäki M, et al. Myocardial blood flow, oxygen consumption, and fatty acid uptake in endurance athletes during insulin stimulation. American Journal of Physiology-Endocrinology And Metabolism. 1999;277(4):E585-E90.

164. Bo H, Jiang N, Ma G, Qu J, Zhang G, Cao D, et al. Regulation of mitochondrial uncoupling respiration during exercise in rat heart: role of reactive oxygen species (ROS) and uncoupling protein 2. Free Radical Biology and Medicine. 2008;44(7):1373-81.

165. Doenst T, Pytel G, Schrepper A, Amorim P, Färber G, Shingu Y, et al. Decreased rates of substrate oxidation ex vivo predict the onset of heart failure and contractile dysfunction in rats with pressure overload. Cardiovascular research. 2010;86(3):461-70.

166. Yoshimatsu Y, Watabe T. Roles of TGF-β signals in endothelial-mesenchymal transition during cardiac fibrosis. International journal of inflammation. 2011;2011.

167. Zi Z, Chapnick DA, Liu X. Dynamics of TGF-β/Smad signaling. FEBS letters. 2012;586(14):1921-8.

168. Kawaguchi N. Stem cells for cardiac regeneration and possible roles of the transforming growth factor-β superfamily. BioMolecular Concepts. 2012;3(1):99-106.

169. Czarkowska-Paczek B, Zendzian-Piotrowska M, Bartlomiejczyk I, Przybylski J, Gorski J. The effect of acute and prolonged endurance exercise on transforming growth factor-beta1 generation in rat skeletal and heart muscle. J physiol pharmacol. 2009;60(4):157-62.

170. Hanna A, Frangogiannis NG. The role of the TGF-β superfamily in myocardial infarction. Frontiers in cardiovascular medicine. 2019;6:140.

171. Peng Y, Wang W, Fang Y, Hu H, Chang N, Pang M, et al. Inhibition of TGF-β/Smad3 Signaling Disrupts Cardiomyocyte Cell Cycle Progression and Epithelial–Mesenchymal Transition-Like Response During Ventricle Regeneration. Frontiers in cell and developmental biology. 2021;9:632372.

172. Lim H, Zhu Y. Role of transforming growth factor-β in the progression of heart failure. Cellular and molecular life sciences CMLS. 2006;63(22):2584-96.

Affidavit

Affidavit

Simahendra, Agus

Surname, first name

I hereby declare that the submitted thesis entitled

The effect of physiological treadmill training on myocardial hypertrophy in the mouse model

is my own work. I have only used the sources indicated and have not made unauthorized use of services of a third party. Where the work of others has been quoted or reproduced, the source is always given.

I further declare that the dissertation presented here has not been submitted in the same or similar form to any other institution for the purpose of obtaining an academic degree.

München, 20.09.2024 Agus Simahendra

Place, Date Signature doctoral candidate

Acknowledgements

I would like to thank my primary supervisor, Prof. Dr. med. Stefan Brunner and the other member of the thesis advisory committee, Prof. Dr. med. Ulrich Grabmaier and Prof. Dr. med. Konstatinos Dimitriadis, as well as Prof. Dr. med. Steffen Massberg as the leader of our clinic for the comprehensive supervising steps from the beginning until end of this project.

I would like also to take this opportunity to cherish the scientific recommendations as well as constructive advice from my direct supervisors in the lab, PD Dr. med. Ludwig Weckbach and PD Dr. med. Maximilian Fischer. Thank you very much for this prestigious learning opportunity in the cardiology department at the LMU Munich University hospital and their uninterrupted supervision, thus we can successfully complete this project on time with fruitful results.

I would like also to deliver my biggest thank you to my colleagues in the lab in BMC, Dr. Bartolo Ferraro, Dr. med. Angelina Krächan, Judith Arcifa, and Bernadette Frey for the continuous support and contributions during the project so I could finish writing this dissertation on time. I am grateful to have such a fun time together with a solid team for these past two years.

Thank you very much also to all of the friends who are now completing doctoral progress at the institute of cardiovascular physiology and pathophysiology in Walter-Brendel center for experimental research. I am aware that it has been a long and tiring process, but we can do this together and the fight will be worthy at the end.

I would like to cherish the endless love and supports which are coming from my parents, brother, and sister in Bali. Without their presence, I will not be the person who I am now. Last but not least, thank you very much also to all of the members of my new family and friends here in Germany, which I could not mention one by one. A special thanks to Martin for his unlimited supports and unstoppable motivations, so that I could complete the doctoral process with a lot of excitements along the way.

List of publications

Tomsits P, Chataut R, Chivukula A, **Simahendra A**, Weckbach L, Brunner S, Clauss S. Real-Time Electrocardiogram Monitoring during Treadmill Training in Mice. Journal of Visualized Experiments: Jove. 2022(183).

Zacherl MJ, **Simahendra A**, Lindner M, Bartenstein P, Todica A, Boening G, Fischer M. The assessment of left ventricular volume and function in gated small animal 18F-FDG PET/CT Imaging: a comparative study of three commercially available software tools. EJNMMI research. 2023 Aug 12;13(1):75.